Applying laser irradiation and intelligent concepts to identify grinding phenomena

By

Arif Mohammed

Aerospace Manufacturing in the Faculty of Engineering

The University of Nottingham

Thesis submitted to the University of Nottingham for the degree of Doctor of Philosophy

September 2010

Abstract

The research discussed in this thesis explores a new method for the detection of grinding burn temperature using a laser irradiation acoustic emission (AE) sensing technique. This method is applicable for the grinding process monitoring system, providing an early warning for burn detection on metal alloy based materials (specifically nickel alloy based materials: Inconel718 and MarM002). The novelty in this research is the laser irradiation induced thermal AE signal that represents the grinding thermal behaviour and can be used for grinding burn detection.

A set of laser irradiation experiments were conducted to identify key process characteristics. By controlling the laser power, the required grinding temperatures were simulated on alloy test materials. The thermal features of the extracted AE signal were used to identify the high, medium and low temperature signatures in relation to the off-focal laser distances. Grinding experiments were also conducted to investigate burn conditions. The extracted AE data was used to identify grinding burn and no burn signatures in relation to the depth of cuts. A new approach using an artificial neural network (ANN) was chosen as the pattern recognition tool for classifying grinding burn detection and was used to classify grinding temperatures by extracting the mechanical-thermal grinding AE signal. The results demonstrated that the classification accuracy achieved was 66 % for Inconel718 and 63 % for MarM002 materials. The research established that the wheel wear has a large influence on the creation of burn within the workpiece surface. The results demonstrated that the AE signals in each grinding trial presents different levels of high, medium and low temperature scales. This type of information provides a foundation for a new method for monitoring of grinding burn and wheel wear.

Acknowledgement

I am humbly grateful to Dr Janet Folkes from the University of Nottingham and to Professor Xun Chen from the Liverpool John Moores University for their supervision and meticulous assistance in the successful completion of my doctoral studies at the University of Nottingham.

First and foremost I would like to express my deepest gratitude to my supervisor Dr Janet Folkes at the University of Nottingham who after a long battle with cancer suddenly passed away just before my final thesis submission. Dr Folkes worked tirelessly during her illness and was extremely helpful during my research period. She was an extremely kind, generous, thoughtful and friendly academic with all her students. She never allowed her terminal illness to impact on her duties towards her students. She kept to her regular routine and would come to the office and enquire about the progress of her students. I had regular meetings with Dr Folkes during the last four years of my research at the University of Nottingham. Her inspirational guidance, endless support, advice and encouragement made this thesis a practical reality as opposed to just an idea and I am deeply saddened that she will not be present at my graduation ceremony.

I would forever like to remember her as the wonderful Teacher and Engineer she was and also as my doctoral supervisor throughout.

I am also extremely grateful to a number of people who assisted me in the completion of this research. I would like to thank various colleagues for their assistance and encouragement in the dark times specifically Dr James Griffin from the University of Nottingham and Dr Jamie Mcgourley from Rolls Royce plc.

I am also very grateful for the technical support provided by Rolls-Royce plc and the assistance provided by the Nottingham University laboratory technicians specifically Mr Stuart Branston and Mr Mark Daine; for their

expertise, support and assistance during the completion of the experimental phase(s) of this research.

In particular, I most humbly acknowledge the unyielding support of my parents and close siblings; without their support over the years I would not have been presented with this opportunity.

I am indebted to all my friends and colleagues; who in various ways helped and assisted me during my study period both morally and intellectually.

I would like to thank EPSRC and my sponsoring company Rolls Royce plc for their financial support during my PhD research tenure.

Finally, I would like to thank God for giving me the physical strength and faculties of my mind to complete this research to a successful conclusion.

Abbreviations

AD	Analog-to-digital
AE	Acoustic Emission
Al_2O_3	Aluminium Oxide
ANN	Artificial Neural Network
BPNN	Backpropagation Neural Network
CBN	Cubic Boron Nitride
CNC	Computer Numerical Control
DSP	Digital Signal Processing
DAC	Data Acquisition Card
DMA	Direct Memory Access
EDX	Energy Dispersive X ray Analysis
FT	Fourier Transform
FFT	Fast Fourier Transform
Fuzzy-c	Fuzzy-c clustering algorithm
GA	Genetic Algorithm
GP	Genetic Programming
JFTA	Joint Time Frequency Analysis
LMS	Least Mean Square
LS-SVM	Least Square Support Vector Machine
LSM	Liquid state machine
ME	Maximum Entropy

ML	Machine Learning
MLP	Multi layer-perceptron
MRR	Material Removal Rate
NN	Neural Network
PSO	Particle Swarm Optimisation
PAC	Physical Acoustic Corporation
PCA	Principal Component Analysis
PCI	Peripheral Component Interconnect
PXI	PCI-extensions for instrumentation
RMS	Root Mean Squares
RMSE	Root Mean Squared Error
SLT	Statistical learning theory
SEM	Scanning Electron Microscope
SNR	Signal to noise ratio
STFT	Short Time Fourier Transform
SVM	Support Vector Machine
TCM	Tool condition monitoring
VIPER	Vitreous Improved Performance Extreme
WT	Wavelet Transform
WPT	Wavelet Packet Transform

Nomenclature

Symbol	Units	Quantity
α	Integer	Learning rate
a_p	mm	Depth of cut
δ	mm	Skin thickness (or penetration depth of laser)
λ_0	μm	Wavelength of the laser
H		Absorption coefficient
μ_o	H/m	The permeability of vacuum
μ_r	H/m	The initial permeability of metal
N		Poisson's ratio
P	kg/m^3	Material density
σ	$* 10^7/\Omega.m$	Electrical conductivity
ω_1	mm	Initial radian of laser beam
ω_2	mm	Laser spot radius
c_p	$J/kg.K$	Special heat capacity
E_0	J	Laser total energy
f_1	mm	Laser focal length

f_2	mm	Laser off-focal length
$F(\omega)$		Fourier transform function
G	mm^3/mm^3	G-ratio
I_0	$W/_{mm^2}$	Laser energy flux
K	$W/m.K$	Thermal conductivity
α	m^2/s	Thermal diffusivity
K_r		Kurtosis
P_0	Watts	Laser total power
Q_w	mm^3/min	Material removal rate
R_a	µm	Roughness
S_k		Skewness
t	s	Time
$T(0,t)$	$\circ C$	Temperature of the material surface after time t (Laser)
U_{RMS}		Root-mean-square (RMS)
V_f	m/min	Feed Rate
V_s	m/s	Spindle speed (wheel speed)
V_w	mm/min	Workpiece speed

Contents

List of Tables

Lists of Figures

Chapter 1: Introduction

1.1 Introduction

Grinding is a widely used machining process, this thesis focuses on its application within the aviation industry. By using it's bonded abrasive properties as a cutting media, high removal rates are achieved with a high quality surface finish. Grinding wheels are composed of two materials: tiny abrasive particles called grains or grits, which provide the cutting of material removal, and a softer bonding agent to hold the countless abrasive grains together in a solid structure. It has been reported that grinding is a major manufacturing process which accounts for around 20-25% of total expenditure on machining operations in industrialised countries (Malkin and Guo 2008).

To ensure high quality, efficiency and reliability in modern manufacturing industries powerful instruments are needed. Modern process monitoring takes advantage of the power increasing instruments providing an increased capacity for manufacturing condition monitoring systems. There is an increased demand for intelligent monitoring systems within the manufacturing industry (Tönshoff, Karpuschewski et al. 1998) this is due to the recent developments and trends in machining technologies such as more automation and operations towards the high end removal rates and at the same time not compromising the machined surface finish. The examples are high speed and vitreous improved performance extreme removal (VIPER) grinding. High speed grinding gives both component quality and high productivity (Jackson, Davis et al. 2001).

Rolls Royce developed VIPER grinding in collaboration with the wheel manufacturer, Tyrolit to produce engine parts instead of the creep feed grinder because the creep feed grinder is slower. The VIPER grinding process uses a vitrified Aluminium Oxide (Al_2O_3) wheel at high speed to remove hard-to-cut aerospace alloys. According to Rolls Royce, the process is capable of stock removal rates of 80 ($mm^3/mm.s$) of the chosen wheel width which is eight times the achievable rate when compared to the plated CBN wheel technology for super abrasive machining of nickel based alloys (Capes 2010).

Current real time monitoring techniques for manufacturing do not yet provide satisfactory results, particularly in terms of high sensitivity and wide bandwidth responses (Erkki Jantunen 1996). It has since been realised that grinding processes contain different levels of mechanical, thermal and fluidic dynamical actions. AE monitoring for grinding is more challengeable than for other machining due to irregular distribution of grits. Effective grinding monitoring is necessary for ensuring grinding quality and improving grinding productivity (Griffin and Chen 2007).

This research was carried out with the funding support of the Engineering and Physical Science Research Council (EPSRC) and through industrial collaboration with Rolls-Royce. The aerospace turbine engine is one of the key products manufactured by Rolls-Royce. A turbine is an assembly of discs, blades attached to turbine shafts, with nozzle guide vanes, and a casing structure. As an example, a section of a Rolls Royce gas turbine engine and the turbine blades are illustrated in Figure 1-1.

Turbine blades convert the energy of sucked in air via compression of various ratios to give output kinetic energy. The gas pressure and temperature both increase as they pass through the turbine.

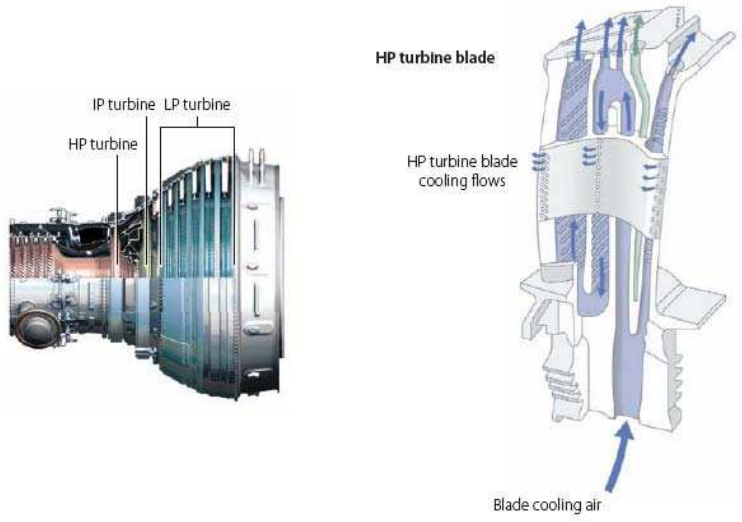

Figure 1-1: Rolls Royce gas turbine engine and a section of turbine blade which connects to the relevant disk (RollsRoyce 2007).

In most cases, many geometric features of these turbine blades are formed by the grinding process. The major problems observed after the grinding process are grinding burn, chatter giving rise to surface roughness deterioration. The plastic deformation involved in all the grinding processes has an impact on the dissipated energy converted into heat which, in turn, raises the temperature in the grinding zone. Temperature rise is an important factor and its major effects can be categorised as the following:

- Adverse effects to the surface properties, including metallurgical changes that can be catastrophic to high speed rotatives

- Temperature rises cause an increase in residual stresses on the workpiece
- Temperature gradients in the workpiece cause distortion which is due to thermal expansion and contraction of the workpiece surface, ultimately resulting in a change of dimensional accuracy.

Thermal expansion along with material burn generates a thermal elastic wave which is the source of the AE signal (Inasaki 1999; Liu, Chen et al. 2006; Kalpakjian, Schmid et al. 2009).

There are many sensing techniques used to detect material burn as it is the most common type of thermal damage in a material during the grinding process. The powerful technique of AE has become very popular in identifying grinding defects. The reason for this is that AE phenomenon is related to the elastic energy release at very high frequencies (Kwak and Song 2001). A successful AE monitoring technique relies on a better understanding of the AE in relation to grinding behaviours and more advanced intelligent signal processing techniques.

An AE sensor has a much higher sensitivity and is more responsive in terms of speed and capacity to record change when compared to other sensors such as force or power. By using just power or force sensors, it is not possible to detect signals with very high frequency ranges, The AE extracted signal can easily pick up those events that are related to grinding burn however the other mentioned sensors are less sensitive to change.

The commonly used AE extracted features can be translated in either the time or frequency domain. For example, the value of the RMS (Root Mean Squared), Kurtosis values, AE count number and the energy peak of fast Fourier transform (FFT). It is very difficult to use AE signals to target a particular grinding action with a single parameter. In order to tackle these difficulties the main tasks should be considered as follows: (a) elimination of irrelevant noise signals; (b) feature extraction in relation to the physical grinding behaviour.

The features from the AE sensor are passed through an algorithm which could be classified as defects based on associated measurements. This stage is called pattern recognition which is implemented to identify grinding defects. Neural Networks (NN) are often used for pattern recognition but there are some limitations to neural networks which are structure selection, local minima and long training times for pattern classification.

1.2 Aim and Objectives

The aims of this research are to develop a grinding process monitoring system which provides an early warning for grinding burn and wheel wear using AE signals.

In order to achieve these aims, the following objectives have been set:

- The development of a wide frequency bandwidth AE monitoring system for grinding which covers the major AE feature frequency range of aerospace alloy materials

- The identification of the AE signal features induced from different AE sources, particularly the difference between mechanical stress, thermal stress and fluid dynamic stress
- The pattern recognition of AE signal features for grinding process monitoring and defect warning
- The investigation of grinding wheel wear effects on AE signals
- The investigation of the critical AE features of grinding (material) burn in relation to surface integrity

1.2.1 Methodology

The research employed the following methods in order to achieve the aims of developing a generic grinding process monitoring system. The research program involved the design of an AE sensor system for monitoring thermal, mechanical and fluidic dynamic stress behaviours extracted from the grinding process.

A series of laser irradiation and grinding experiments were arranged in line with the research objectives. There are two AE sensors from Physical Acoustic Corporation (PAC) used to provide the extraction sources for AE signals to give the relationship of thermal, mechanical or fluid turbulence stress variables from laser irradiation and grinding tests. The integrated AE sensors from the respective experiments responded to a wide range of AE signals obtained from grinding the nickel based alloys of Inconel718 and MarM002 materials. The laser irradiation experiments consisted of simulating high temperature on Inconel718 and MarmM002 material workpieces without any grinding action.

The laser irradiation experiments were arranged in the Nd: YAG laser machine. An E-type thermocouple was placed at the centre of the laser beam spot on the front surface of the workpiece. In addition, an AE sensor was attached on the opposite side of the workpiece. By controlling the laser energy flux and irradiation time, the temperature on the workpieces could be controlled by the given off-focal distances to achieve similar thermal behaviour within the grinding process. The AE signal was able to detect thermo-elastic wave changes due to laser irradiation on these materials.

AE signals data and temperatures are measured simultaneously in the further investigation.

A series of grinding tests were arranged in a MakinoA55 machine centre to obtain both burn and no burn signatures on AE signals. The machine was used to grind workpiece materials seven times in a sequential manner using only one dressing this to provide the required burn phenomenon. The wheel wear was measured after seven passes using the razor blade technique. The surfaces' roughness are measured and recorded after each of the seven grinding passes on the workpiece materials, this was carried out in five different sections. The AE signals with burn and no burn signatures are acquired at different depth of cuts (0.02 mm to 0.2 mm) for further processing.

The Fast Fourier Transform (FFT) and the Short Time Fourier Transforms (STFT) are applied to extract features from AE signals. The FFT is suitable for extracting the frequency components at a particular finite time however the FFT does not have continuous time information when an event occurs such as when

material experiences deformation, fracture or, a combination of both. A STFT however, was developed to overcome this problem. The STFT addresses the issue of considering time as well as the frequency components and associated intensities. This technique is suitable for extracting features from non-stationary stochastic signals (James Griffin 2006).

At the end of the test the ANN were employed to assist the grinding burn identification. The ultimate goal of this research is to predict burn and no burn within the grinding zone using laser irradiation. The hypothesis is that the thermal features of AE data from laser irradiation are similar to the thermal features of AE data experienced in grinding. To validate this hypothesis the ANN was employed to identify the thermal features within the AE signal extracted from laser irradiation and trained to classify high, medium and low temperatures. The thermal features of AE data from grinding were tested in the ANN for the verification of this technique. The output neurons from an ANN are presented in the results ranging from 1 to 3 which distinguished between high, medium and low temperatures due to severe burn, normal burn and no burn phenomena.

The defects of the surface integrity were judged by surface measurement and metallurgical observation. The relationship between wheel wear and AE signals provide the foundation for AE process monitoring.

1.3 Main Contributions

Main contributions of the research are as follows:

- One of the most important contributions of this research is presented in Chapter 5. The surface temperatures on workpiece material were measured as a response of laser irradiation which was varied by changing laser off-focal distances. The measured values of surface temperatures were then compared with the surface temperatures calculated by the theoretical calculation of laser irradiation. The result showed that 34 mm, 40 mm and 46 mm produce high, medium and low temperatures. Using the STFT technique, the high, medium and low temperatures AE footprint signatures were identified through laser thermal AE signal extraction. There was no grinding in laser irradiation evaluations. Grinding burn occurs from the increased temperature of the abrasive materials coming into contact with workpiece materials. The burn was monitored using AE sensor extraction at different depth of cuts (0.02 mm to 0.2 mm) during grinding. These burn and no burn AE footprint signatures were identified through grinding producing thermal signatures identified from AE signal extraction.
- The other major contribution of this research is presented in Chapter 6, where all laser thermal AE signals and all grinding thermal AE signals are processed into a normalised format and then concatenated together to be trained and tested against the ANN network system. The method here employed a test of several cases based on laser thermal AE data seen and not seen by the ANN and several cases based on grinding thermal AE data seen and not seen by the ANN. The trained ANN was then tested against the generalised difficult to distinguish burn and no

burn phenomena. This technique provided sufficient results for the prediction of grinding burn (Inconel718 and MarM002) and defect warning.

1.4 Outlines of the thesis

- Chapter 1 is an introduction to the thesis. The aim and objectives of this research are described in this chapter. The major work and research contributions are briefly discussed. An outline of the thesis is also given at the end of this chapter.
- Chapter 2 describes the current knowledge of condition monitoring techniques, AE process monitoring for grinding and laser irradiation application in grinding and classification of the grinding conditions. This knowledge is obtained from relevant literature including books, conference papers, journals, dissertations, theses and technical reports. At the end of this chapter research gaps are outlined.
- Chapter 3 describes the AE sensing system development as the experiment setup for both laser irradiation and grinding tests. The grindability of materials along with the properties of grinding wheels are also discussed. The measured surface roughnesses are also described at the end of this chapter.
- Chapter 4 describes the feature extraction techniques in the time domain, frequency domain, and both time-frequency domain. The STFT (Griffin and Chen 2007) is discussed with a conclusion that it can be applied to the extraction of AE features.

- Chapter 5 investigates the thermal features extracted from laser irradiation and grinding experiments using energy spectrum analysis. The STFT signal processing technique was mainly used to extract sensor information. The comparison between the theoretical model and the measured models of the surface temperatures are based on laser irradiation experiments which are also discussed. The extracted laser thermal AE features are discussed where the data was obtained from three off-focal distances. The extracted grinding AE data were also discussed where the AE data was obtained from two different depths of cut.
- Chapter 6 describes the intelligent diagnostic technique where the ANN was applied to classify the burn within the tested grinding zone. The ANN has been trained for distinguishing high, medium and low temperatures when laser thermal AE data was used as the input to the ANN. The grinding thermal AE data was used to test the network, the result predicts the grinding temperatures relation to burn within the grinding zone.
- Chapter 7 draws conclusions of the research and provides suggestions and recommendations for future work.

Chapter 2: Literature Review

2.1 Introduction

This chapter surveys the current knowledge of the grinding behaviour within the grinding process, process monitoring using acoustic emission for extracting grinding signals, laser irradiation application in grinding and clarification of grinding condition through the employment of different classification techniques.

The chapter highlights the benefits and problems using current grinding process monitoring and different feature extraction techniques, feature selection and different classification techniques.

There are two major methods available in the literature for condition monitoring which can be divided into direct (Kurada and Bradley 1997) and indirect based sensor monitoring.

The indirect method for observing the condition of a cutting tool or grinding wheel are optical measurement of wear, such as the periodic observation of changes in tool/grinding wheel profile. The common reliable techniques are done by using a microscope. This requires stopping the machine for tool or grinding wheel observation.

A direct method involves programming the tool to contact a sensor after every machining cycle, this allows for the detection of broken tools.

Another direct method of observing tool conditions involves the correlation of the tool condition obtained from parameters such as cutting forces, power, temperature and accelerations which can show vibration and chatter characteristics as well as burn (Griffin and Chen 2009). A powerful technique is AE which uses a piezoelectric transducer mounted on a tool holder with a sufficient medium to ensure little signal loss from sensor to source (Kalpakjian, Schmid et al. 2009). Different signal extraction techniques are chosen by different authors to extract the key features from the signals. These are discussed in the feature extraction section of this chapter.

After extraction, key features are used to populate the classification system for the clarification of the recognised machining condition. There are different classification methods described and applied in the literature for the clarification of the various machining conditions.

Finally, based on a recent study, the conclusive remarks are mentioned and research gaps outlined at the end of this chapter.

2.2 Grinding behaviour

Grinding behaviour can be defined as grinding wheel behaviour, thermal behaviour, mechanical behaviour and the coolant effect on the grinding process.

The effect of thermal damage and wheel wear are discussed at the beginning of this chapter. The wheel life and ground workpiece quality assessment are also important issues of grinding operations.

2.2.1 Thermal effects in grinding

Thermal damage on workpiece material is one of the major problems in grinding. It can directly affect the workpiece quality and it can limit the production rates especially in machine component production in the aerospace industry. The aerospace industry often uses creep feed grinding in which the depth of cut is increased and feed rate is decreased compared with normal grinding practice which is not as dynamic for roughing and finishing operations. The creep feed grinding is used for large amounts of material removal. The grinding process requires high input energy in order to remove material from the workpiece. This high input energy leads to an excessively high temperature in the grinding zone which can cause thermal damage to the workpiece. It is important to understand the underlying factors of thermal damage which affect the workpiece quality. There are various kinds of thermal damage which could be identified on the workpiece surface such as (Malkin and Guo 2007):

- Burning
- Phase transformation
- Softening (tempering) of the surface layer with possible rehardening
- Unfavourable residual and tensile stresses
- Cracks and reduced fatigue strength

A number of researchers have investigated burn and temperature in grinding (Mayer Jr, Purushothaman et al. 1999; Chen, Rowe et al. 2000; Morgan and Rowe 2000; Rowe and Jin 2001; Jin, Rowe et al. 2002). The grinding burn is a tempered colour which is a consequence of a thin oxide layer formation on the

ground surface. The maximum temperature on the grinding zone affects the thickness of oxide layers. These layers are ferrous materials which are mainly composed of Fe_2O_3, Fe_3O_4 and FeO. When the grinding burn occurs on the workpiece surface this can be attributed to an increase in grinding force which can sharply increase wheel wear and has a direct effect on the surface roughness. There is another phenomenon which often occurs namely metals adhering between voids within a grinding wheel block during the up machining action (this state is called wheel loading). With wheel loading, the grinding process will be in an abnormal state and the grinding temperature rises to a very high level (Kwak and Ha 2004).

There are many models based on heat transfer in grinding which have been developed to study the grinding temperature. The heat transfers in grinding based on the sliding heat source model are developed by Jager and Carlshaw in 1942 (Guo, Wu et al. 1999). This model describes a heat flux distribution uniformly across the grinding contact. This model is still used by many researchers. Most thermal analysis is based on moving heat source theory as shown in Figure 2-1.

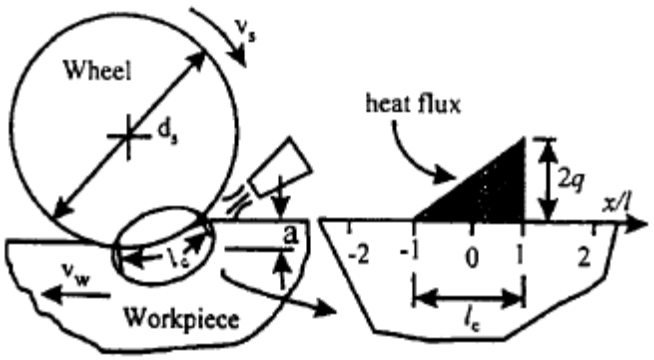

Figure 2-1: illustration of grinding and thermal model (Guo, Wu et al. 1999).

The total heat flux distribution in the grinding zone is usually modelled as being triangular, as shown in Figure 2-1, or uniform. In order to calculate the grinding temperature, it was necessary to specify the total heat flux distribution and energy partition to the workpiece at the grinding zone. The energy partitions to the workpiece and heat flux distribution within the grinding zone were estimated by matching the workpiece temperature to analytically calculated values (Kim, Guo et al. 1997; Guo, Wu et al. 1999; Rowe 2001).

Xu and Malkin (Xu and Malkin 2001) presented a comparison of methods to measure grinding temperatures. There experiments consisted of thermocouple, optical fibre with two colour infrared detectors, and a foil/workpiece thermocouple. All three methods provided comparable results where temperature responses provided reliable results with the analytical predictions of moving heat source analysis. They argued that foil/workpiece thermocouple works better than other methods and could detect a periodic peak temperature at wheel rotational frequency.

The heat generation in the grinding zone is one of the critical problems in terms of workpiece quality. The coolant has a strong effect on the chip formation process. It is building up a lubricant film in the grinding zone. This lubricant film can lower the friction, forces, and cool the workpiece material and wheel surfaces. However, too much lubrication can have a negative thermal effect as the efficiency of the cutting process is reduced and relatively more energy is used in the shearing and deformation processes (Brinksmeier, Heinzel et al. 1999).

The temperature distribution in the contact arc between the grinding wheel and workpiece in creep-feed grinding was investigated by (Kuriyagawa, Syoji et al. 2003). They realised that optimum conditions of wheel and workpiece speed could improve the cooling effect at the face. There are many investigations of temperature in the grinding arc carried out with thermocouples integrated into the workpiece (Guo and Malkin 1994). Boiling of the coolant film in the contact zone is partially responsible for thermal damage in grinding. During the film boiling, a vapour layer builds up between workpiece and coolant that strongly hinders the heat transfer. The boiling temperature of the coolant increases significantly if pressure is built up in the contact zone. This resulting delay of film boiling provides a longer period of lubrication and heat dissipation of the coolant, and helps avoid thermal damage (Brinksmeier, Heinzel et al. 1999).

2.2.2 Grinding wheel wear

Grinding is not a simple abrasion process. The grit penetrates the workpiece and ploughs the material away. To maintain a high material removal rate, the grain

needs to be constantly sharp. If a wheel is used for a long time during grinding then the wear occurs and acts like wear also seen from other tools in machining. Tonshoff et al (Tönshoff, Friemuth et al. 2002) reported that there is a thermal, mechanical and chemical effect on the contact zone in any abrasive process. When the abrasives are worn, the penetration depth is reduced and the material removal rate drops. It has a huge effect on the material removal rate, G ratio, the efficiency and, the cost of the process (Tawakoli, Westkamper et al. 2009). The G-ratio is a commonly used parameter to characterise wheel wear. It is the volume of material removed per unit divided by volume of wheel wear. The lowest wearing wheel, giving the biggest G-ratio, may not be the best as it requires larger forces and energies which leads to excessive temperatures. A better lubricating grinding fluid should increase the G-ratio, whilst also lowering the forces and temperature (Malkin and Guo 2008; Kalpakjian, Schmid et al. 2009).

The grain shape is very important because it determines the tool geometry. Figure 2-2 shows γ as the clearance angle, θ as the wedge angle, and α as the rake angle. A grinding wheel can present to the surface rake angles in the range of $+45°$C to 60 °C or greater.

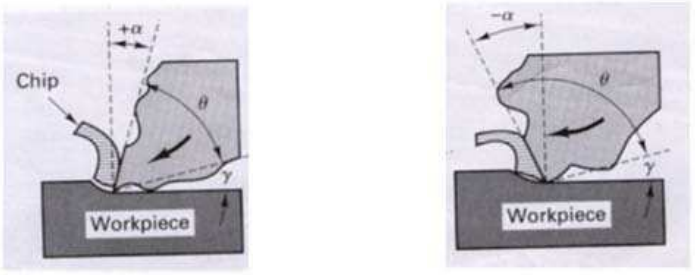

Figure 2-2: The rake angle of abrasive particles can be positive, zero or, negative(Black, DeGarmo et al. 2007).

Grits with large negative rake angles or rounded cutting edges do not form chips but will rub or plough a groove in the surface. This abrasive machining is a mixture of cutting, ploughing and rubbing, with a percentage of each being highly dependent on the geometry of the grit. The grits are continuously abraded, fractured, or dislodged from the bond, new grits are exposed that have been cut, ploughed and rubbed and are continually changing. A high percentage of the energy used for rubbing and ploughing goes into the workpiece, but when chips are found, 95% to 98% of the energy (heat) goes into the chip (Black, DeGarmo et al. 2007).

The grinding wheel wear caused by three different mechanisms were classified as: attritious wear, grain fracture, and bond fracture. These three types of wear occur simultaneously during grinding on the grinding wheel. The mechanism of wheel wear is shown in Figure 2-3.

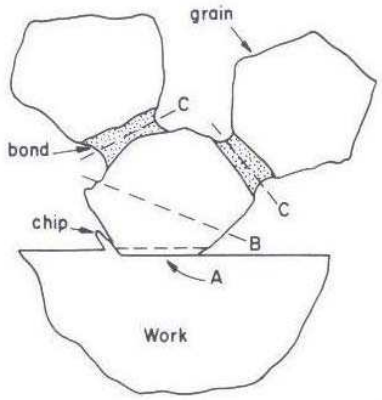

Figure 2-3: Illustration of wheel wear mechanisms: A-attritious, B-grain fracture and C-bond fracture (Malkin 1989; Lachance, Warkentin et al. 2003).

In attritious wear the cutting edges of an originally sharp grain can become dull and develop wear flat. The wear flats on active grains lead to an increase in the area of contact and frictional interactions between abrasive grain and workpiece. At the point of dulling the abrasive grain experiences a very high temperature in the area of contact that greatly enhances adhesion and chemical reaction between the two surfaces. If the grain and bond fracture does not occur during grinding then the plateau area on the grain widens and the rate of wear increases. If fracture is delayed further, as with hard grinding wheels, then the wheel become glazed and the workpiece becomes thermally damaged (Jackson, Mills et al. 2003).

Grain fracture occurs due to the removal of abrasive fragments by fracture within the grain. If the wear flat caused by attritious wear is excessive, the grain becomes dull and grinding becomes inefficient and produces undesirably high temperatures. Bond fracture, mainly for the vitrified wheels, occurs by dislodging the abrasive from the bond. This occurs due to the friction between

the chip and the wheel bond. If the bond is too strong, dull grain cannot be dislodged. This prevents other sharp grains along the circumference of the grinding wheel from contacting the workpiece to remove chips, and the grinding process becomes ineffective.

If the bond is too weak, the grains are dislodged easily, and the wear of the wheel increases. In this case, maintaining dimensional accuracy becomes difficult. The attritious wear plays a lesser part in contributing to the decrease of the wheel volume, but it could be reason for the end of the wheel life (Malkin and Guo 2008; Kalpakjian, Schmid et al. 2009).

All these wear mechanisms of attritious wear, grain fracture and bond fractures contribute to changes in the grinding wheel topography. These changes of the grinding wheel topography affect the quality of the final component. Therefore it is important to maintain the required material removal rate, cutting ability and surface integrity of the workpiece, and in order to do so, the grinding wheel should be dressed frequently.

2.2.3 The performance of grinding fluid

A number of researchers have studied the important factors that affect the performance of the grinding fluid. The basic requirements of the fluid in the grinding zone are lubrication, direct cooling and transport of debris from the cutting zone (Gviniashvill, Webster et al. 2005). They presented a fluid flow model to calculate the coolant contact zone flow rate based on the coolant pressure in the contact zone. Klocke and Baus et al (Klocke, Baus et al. 2000) introduced coolant induced forces in CBN high speed grinding with shoe

nozzles. Ebbrell et al (Ebbrell, Woolley et al. 2000) investigated the effects of cutting fluid application methods on the grinding process. They were able to show that nozzle positions affect the volume of cutting fluid passing beneath the grinding wheel. They succeeded by raising the nozzle position above the area of reversed flow and increased flow rate beneath the wheel to improve surface quality.

2.3 Acoustic emission technique for grinding monitoring

In 1955 Josef Kaiser published his thesis where he reported that engineering materials in general emit low amplitude clicks of sound when they are stressed. His work produced a new non-destructive testing technology -Acoustic emission- which started to gain momentum in the 1960s (T.Holroyd 2000). This research was mainly concerned with the extraction of an AE signal which was used to monitor the grinding process.

AE can be defined as the “transient elastic energy spontaneously released in materials undergoing deformation, fracture or combination of both” (Dornfeld and Kannateyasibu 1980).

There are various applications of the AE technique reported in the literature for example contact detection between wheel and workpiece (Dornfeld and Cai 1984; Inasaki and Okamura 1985), burn detection (Liu, Chen et al. 2006), surface integrity (Webster, Marinescu et al. 1994), metal cutting (Ravindra, Srinivasa et al. 1997), ductile/brittle (Bifano and Yi 1992) and tool wear (Pai and Rao 2002).

AE is a type of elastic energy which is released due to material particle displacement under stresses during grinding. This elastic energy generates elastic waves which can propagate through material media and are detected by acoustic emission sensors. When different external forces act on the same material or the same external force acts on different materials, the elastic waves will have different characteristics which are a good indicator for the properties of material and a feature of a processing (Liu, Chen et al. 2006).

The commonly used feature parameters for the AE are in the time domain, the frequency domain within condition monitoring or a combination of both such as the peaks of RMS values, crest factors analysis (i.e. the ratio of the peak to the RMS level of a signal), kurtosis analysis, and moving average windowing technique.

In Table 2-1, summarised is the current status of the commonly used AE feature parameters related to grinding by different authors.

Table 2-1: Current status of commonly used AE feature parameters.

Author/Year	Aim	Signal & Method
Ravindra(1997)	Tool condition monitoring	Power of the dynamic and residual of AE signal, AR parameters
De Agure,(1999)	Burn	Burn
Wang(2001)	Burn	Band Power, kurtosis and skew, and AR coefficient of AE
Kwak(2001)	grinding faults	RMS of AE
Hwang et al.(2000)	Wheel wear	RMS of AE signals, magnitude of peak frequency of AE power spectral density
Lezski(2001)	Wheel wear	AE Statisical and spectral features
Mokbel and Maksoud (2000)	generated by using different/truing speed ratios	FFT,AE spectral amplitude
Q.Liu (2005)	Grinding burn	AE, Wavelet packet transform
Liao et al. (2007)	Wheel wear	AE, discrete wavelets decomposition
James Griffin (2009)	grinding burn and chatter	AE, wavelet

Frequency domain analysis produces frequency spectrum analysis such as FFT (Fast Fourier Transform) which is widely applied to signal processing techniques in everyday engineering. These parameters are commonly used as AE feature parameters however these parameters cannot be directly related to particular behaviour in grinding. Grinding acoustic emission is the transient elastic energy spontaneously released when materials are undergoing deformation or fracture or both. For these non-stationary signals, FFT will make the frequency composition average over the duration of the signals. As a result, FFT cannot adequately describe the characteristics of the transient signals in the frequency domain (Griffin and Chen 2007). The advantage of the AE sensor is that it is easy to mount and works at a relatively low cost. There is no negative influence on the stiffness of the machine tools and it is even capable of transmitting a signal from its rotating parts (Hundt, Leuenberger et al. 1994; H.K. Tonshoff 2001).

Hundt et al, (Hundt, Leuenberger et al. 1994; Hassui, Diniz et al. 1998) states that the sources of AE signal in grinding are mainly the bond and grain fracture, grain cracks and friction between abrasive grain and workpiece. All of these attributes are directly connected to the chip formation and wheel wear.

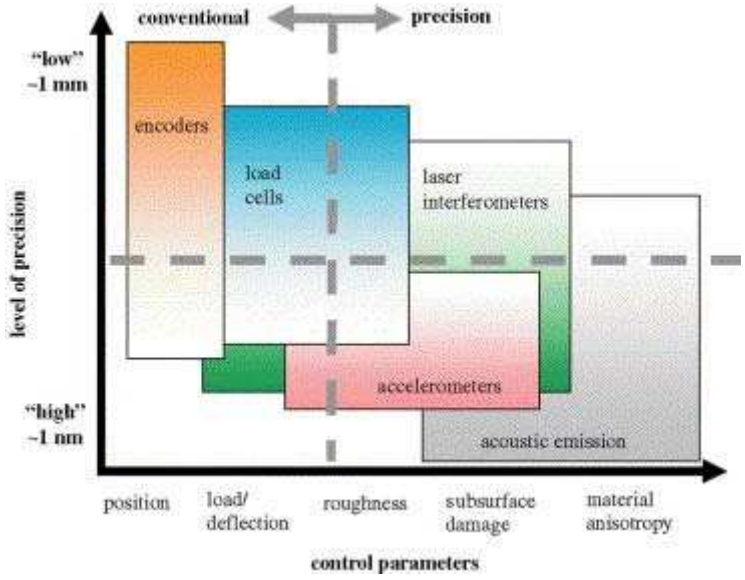

Figure 2-4: Sensor application vs. level of precision and control parameters (Lee, Hwang et al. 2006).

As shown in Figure 2-4, the acoustic emission is highly desirable due to its relatively superior signal to noise ratio (SNR) which means it compares the level of a desired signal to the level of background noise and sensitivity at the ultra precision scale when compared to load cell (power sensor) for example, with different levels of AE detectable even at extremely low depth of cut (Lee, Hwang et al. 2006).

The application of AE sensors has become very popular in many kinds of machining processes over the last three decades. Force, displacement, vibration and power sensors are commonly used to monitor the condition of the machining processes. AE has been reported to provide useful information about the condition of the operations (H.K. Tonshoff 2001).

Huang and Yin (Huang and Yin 2007) present the grinding characteristics of engineering ceramics in a high speed regime. They compared the performance

of high speed grinding with conventional speed grinding. The grinding forces (normal and tangential) and AE energy are measured in order to characterise the material removal quality of five polycrystalline ceramics based on experimentation.

The coolant supply in high speed grinding plays a more important role than conventional speed grinding. If the coolant failed to reach the grinding zone sufficiently, thermal damage would result in the workpiece. In their investigation, the flat type of nozzle was replaced by the shoe type of nozzle to bring the coolant closer to the grinding zone. The nozzle position plays an important role in high speed grinding. However, they did not show that the AE feature relates to coolant nozzle positions. They assumed that the appropriate arrangement of coolant nozzles and optimal supply of coolant flow, in terms of flow speed and rate, would avoid the thermal damage and improve the grinding quality.

Gong and Li (Gong, Li et al. 2006) have presented a paper containing the analysis and application of acoustic emission signals in accurate grinding machining. The AE signals in the grinding process were affected by many factors such as workpiece velocity, table velocity, grinding fluid quantity, the sensor position, grinding depth and workpiece material. Their experiment showed that the sensor position and workpiece material were the most influential factors in monitoring the accurate grinding on-line.

Lee et al (Lee, Hwang et al. 2006) introduced precision manufacturing process monitoring with acoustic emission. The research discusses the sensitivity of AE

at the three different manufacturing systems summarized as the Taniguchi curve; the normal/conventional, precision, and ultra-precision scales. The limitation they mentioned of the AE based monitoring solution is the oscillation of the RMS level and signal saturation.

Jayakumar et al (Jayakumar, Mukhopadhyay et al. 2005) presents the AE techniques for the on-line monitoring of various metal forming processes. The acoustic emission process monitoring gives useful information to detect die wear and cracking, frictional properties, the state of lubrication, galling and stick-slip. Process monitoring uses the AE technique to ensure high quality finish and to minimize the total cost of production when compared with other techniques.

Liao et al (Warren Liao, Ting et al. 2007) investigated the sensitivity of AE signals to the fatigue failure of ground steel samples. They determined fatigue failure in a rolling contact using the AE technique. The fatigue failure is of great concern in manufacturing machines, engines and various mechanical systems when rolling contact applications are applied. The research found that the parameters of the AE features such as amplitude, absolute energy and RMS values increase sharply when fatigue occurs and that threshold counts and average frequency components decrease sharply with the onset of fatigue. In addition, grinding induces surface integrity. The term surface integrity (finish, micro-hardness, micro-structure and residual stresses) is used to describe the quality and condition of the surface region of a machined component. The

research displays that the AE signal is the most suitable signal for monitoring fatigue.

Inasaki (Inasaki 1998) presents an application for the AE sensor for machining monitoring process. The AE signals are classified into two types of signals: continuous-type AE signals or, burst-type AE signals. The continuous-type AE signals are associated with plastic deformation in ductile materials, whilst the burst type signals are observed during crack growth in the material. The AE sensor is very sensitive to change when compared with the other sensor types mentioned previously (Lee, Hwang et al. 2006). When combined with other sensor types (for example force sensor) it could offer great advantages in the machining process if used in a sensor fusion type fashion (Griffin and Chen 2009).

Tonshoff et al (Tonshoff, Jung et al. 2000) used AE signals to monitor the production processes and describe the application of AE measurement and the monitoring method of hard turning and grinding. They focused on achieving workpiece quality during grinding and hard turning. In grinding, the researchers attempted to detect incorrect process states by using AE signals. The on-line data analysis was developed in a free configuration calculation unit. They correlated the measured values of parallel residual stresses with the RMS AE signals which are dependent on the speed ratio. This speed ratio is related to the material removal rate (MRR). They managed to improve the process and to assure the workpiece quality based on this analysis.

Hwang et al, (Hwang, Whitenton et al. 2000) presented a paper on the AE monitoring of the high speed grinding using silicon nitride. A grinding experiment was conducted at a wheel speed of 149 m/s and continued until the end of the wheel life. It is reported that the amplitude of the AE signal, collected in high speed grinding with silicon nitride using an electroplated single-layered diamond wheel. The wheel wear increased monotonically.

Inasaki (Inasaki 1999) further introduced sensor fusion for monitoring and controlling grinding processes. The system uses AE and power sensors so that most problems in the grinding process such as grinding burn, chatter vibration and deterioration due to surface roughness can be detected. These problems determine the wheel life which is closely related to the change of the grinding wheel surface at the time of grinding advances. The wheel life criteria and the sensors for detecting them are shown in Table 2-2.

Table 2-2: Wheel life criteria and sensors.

Changes of wheel surface	Wheel life criteria	Sensor
Changes in surface topography	Grinding burn	Power sensor
Changes in geometrical configuration	Deterioration of surface roughness	Acoustic emission
	Chatter vibration	

To develop an intelligent grinding system, a sensor fusion technique was established and successfully used in this research and bolsters the use for the proposed research in this thesis.

Akbari et al (Akbari, Saito et al. 1996) investigated the effect of grinding parameters on AE signals while grinding ceramic materials. This work uses a process to identify the changing AE resulting from increasing wheel depth of cut, wheel speed and table speed when used in conjunction with the workpiece.

As shown from the results, the percentages of events of high amplitude, long duration and more oscillation indicate surface cracking grows with the increasing depths of cut and table speed but decrease as the wheel speed increases.

Inasaki (Inasaki 1998) established the application for the AE sensor for monitoring machining processes. The AE signals are classified into two types of signals. These signals defined as either a continuous-type AE signal or, burst-type AE signal. It has been shown that the continuous-type AE signals are associated with plastic deformations in ductile materials, whilst the burst type signal is observed during crack growth in the material. This again provides more evidence that the AE sensor is highly sensitive to change. It is combined with the other types of sensors (for example, the force sensor) which could be a great advantage in controlling the machining process.

Dornfeld and Cai (Dornfeld and Cai 1984) investigated grinding and wheel loading using AE signals. Here they analysed the AE signals generated from the grinding zone measuring the wear-related loading of the grinding wheel and, the spark-out between wheel and work piece surface. In addition, they showed that AE energy increases with the combined effects of wheel wear and loading and the signal energy is a function of the unperformed chip thickness. The signal accuracy detects work piece/wheel contact and spark-out with a higher sensitivity than that of grinding force measurement. AE from surface grinding provided measurements relating to the loading of the grinding wheel and spark-

out (or loss of contact). They showed that AE increases with the combined effects of wheel wear and loading.

To summarise the above described methods, the applications of AE sensors are very popular compared to other types of sensors used in grinding process monitoring. The reason is that AE phenomenon is related to the elastic energy release at a very high frequency range. This rich information of the grinding process gives promotion and the choice of selection when faced with precision geometries AE can also provide information about the modes of wheel wear, wheel loading and grinding surface integrities. The AE sensor is easy to mount and is relatively low cost compared to other sensor types. There are no negative effects on the stiffness of the machine tools. The AE sensor is even capable of transmitting signals from rotating parts. However, successfully applying the AE signal into an easily understandable format is far from easy. AE signal transmission is significantly dependent on the elastic wave paths, medium and the relative location of the sources. A successful AE monitoring paradigm depends on a better understanding of the AE in relation to the grinding behaviours and a better representation based on the chosen signal processing technique.

2.4 Pattern recognition and machine learning

Pattern recognition techniques are an important component of intelligent systems and these techniques are used for both data pre-processing and decision making. Pattern recognition is the science that is concerned with the description or classification (recognition) of measurements (Schalkoff 1992). A condition

monitoring system is basically a knowledge learning system. The sensor and other physical inputs are converted into signal data in the knowledge learning system. Then, the features extracted measure the signal properties that are useful to the classification system. The task of the classifier is to use the feature vector provided by the feature extractor and assign the object to a category as useful information. Subsequently, the information is then refined as knowledge (condition identification and pattern recognition) (Duda, Hart et al. 2001).

There have been many different types of classifiers as pattern recognition tools have reported in condition monitoring such as ANN (Griffin and Chen 2007), support vector machine (SVM) (Jack and Nandi 2002; Xun Chen 2006; Widodo and Yang 2007), genetic algorithm (GA) (Jack and Nandi 2002), genetic programming (GP) (Zhang, B. Jack et al. 2005; Griffin and Chen 2009), clustering (Hard and Soft clustering methods such as K–means and Fuzzy C clustering (James Griffin 2006), liquid state machines (LSM), particle swarm optimization (PSO) and chaos and maximum entropy (ME).

The pattern recognition methods are widely used to identify the condition of the machining process and tool. This technique is based on a similarity of a sample to be identified and the pattern or classes that describe the target status (H.K. Tonshoff 2001).

There are two methods commonly used in pattern recognition either supervised or unsupervised learning. In supervised learning, a teacher provides a category label or cost for each pattern in a training set, and seeks to reduce the sum of the costs for these patterns. In unsupervised learning there is no explicit teacher,

and the system forms clusters or “natural groupings” of the input patterns (Duda, Hart et al. 2001). The main tasks of pattern recognition are feature classification. First, pattern recognition can select those important features by some criterions among all features. Secondly, pattern recognition can build up a classifier to class or cluster these features and make a decision on which features represent which grinding status (Liu, Chen et al. 2005). More features and details will normally provide an explicit recognition of the event for any kind of condition monitoring. However, a huge number of features certainly contain mutual information of different events, which may create some misleading results. The question is: which features should be kept and which features should be discarded? In fact the AE features of a defect are similar to that of a normal state in some cases whilst also similar to other defects even though there are some moderate differences. Pattern recognition is widely used for these complex and uncertain issues (Fu, Hope et al. 1998). This gives rise to an intelligent clustering or classification.

Neural computing has emerged from attempts to draw on the knowledge of how the biological neural systems store and manipulate information (Schalkoff 1992). This leads to a class of artificial neural systems termed neural networks. Neural network is one of the most effective signal analysis tools for the pattern recognition during tool condition monitoring. It has been mentioned in the literature that there are various applications such as: function approximation and complex regression (Rangwala and Dornfeld 1989; Yerramareddy, Lu et al. 1993) in learning and an optimization of machining operations, data reduction,

novelty detection (Markou and Singh 2003) for image sequence analysis using neural networks in grinding process control (Govindhasamy, McLoone et al. 2005).

The main advantage of a neural network is that it has the capability of parallel processing, especially with a large amount of data processing. The feed forward neural network, multilayer perception with the back propagation learning algorithm is the most commonly used neural network model for pattern recognition in the classification for machine fault diagnostics.

The backpropagation neural network (BPNN) however have some limitations (Jardine, Lin et al. 2006):

- Difficulty in determining the network structure and the number of nodes
- Local minima
- Slow convergence of the training process

The support vector machine (SVM) is a statistical learning theory developed by Vapnik. This technique has become very popular in recent years for solving classification, regression and novelty detection this is due to its classification of mass input vectors. Vapnik initially developed SVM to solve the classification problem with separable data. Later, this was improved to handle non-separable data and also adapted to solve the regression problem (Vladimir Cherkassky 1998). The SVM has been used successfully in various applications in process monitoring, to classify tool wear (Shi and Gindy 2007), to classify burn, chatter (Chen and Limchimchol 2006) and wheel wear or tool wear in grinding (Chiu and Guao 2008; Jiuhua Xu, Xipeng Xu et al. 2008), in milling

(Kunnapapdeelert and Prakasvudhisarn 2006; Hsueh and Yang 2008; Hsueh and Yang 2009) and in drilling (De Castro, Von Zuben et al. 2007).

In SVMs, the original input data was correlated using a mapping function in a higher dimensional classification space (which is called the feature space), in such a way as to make a problem linearly separable.

The performance is hidden from the input to the output. In the feature space, an optimal separating hyper-plane is constructed in the high dimensional space. This basically involves solving a quadratic programming problem, whilst gradient based training methods of neural network architectures on the other hand, suffer from the existence of many local minima (Vladimir Cherkassky 1998; Suykens and Vandewalle 1999).

LS-SVM is a least squares modification for the Support Vector Machine (SVM). The major advantage to LS-SVM is that they are able to obtain an excellent generalisation performance and have low computational costs compared to traditional SVM (Suykens and Vandewalle 1999).

2.4.1 Feature extraction and classification of AE signals in grinding

Liao and Ting (Liao, Ting et al. 2007) presented a paper on grinding wheel condition monitoring based on AE signals. The experiments were conducted using a diamond wheel to grind aluminium type materials. The AE signals were analysed at intervals when the wheel was in “sharp” or “dull” condition respectively. The wavelet transform signal processing technique was chosen to extract features from the AE signals. They used the adaptive genetic clustering algorithm to classify the extracted features of the AE signals. The results

displayed a 97% clustering accuracy for high MRR condition, 86.7% for the low MRR condition and, 76.7% for the combined grinding conditions (Liao, Ting et al. 2007).

Liu and Chen (Liu, Chen et al. 2005) applied the fuzzy pattern recognition technique of AE signals to identify grinding burn. The wavelet packet transform is used to extract features from AE signals. The fuzzy pattern recognition technique is used to identify grinding burn. The accuracy of grinding burn recognition is more than 92%.

Kwak and Ha (Kwak and Ha 2004) presented a neural network approach for the diagnosis of the grinding operation using AE and power signals. The AE and power sensors were used to detect grinding burn and chatter. The peak RMS and peak FFT are feature parameters extracted from the AE signal. These parameters were used as input to the NN. The NN classified the burn and chatter phenomena with a 95% classification rate.

Kwak and Ha (Kwak and Ha 2004) presented the intelligent diagnostic technique of machining state for grinding. The NN based on the back propagation algorithm was used to classify the grinding burn and chatter vibration. The AE signal feature parameters RMS peak, standard deviation, FFT peak and count of over threshold were used as input to the NN. The result of classification was successful with an accuracy rate of 90%.

Ge et al (Ge, Liu et al. 2002) presented fuzzy clustering analysis of the grinding burn damage level of a workpiece surface layer. In their research, a mathematical model of fuzzy clustering analysis as a pattern recognition

technique was developed. This model was suitable for the classification of a large number of samples.

Wang et al (Wang Z, P. DeAguiar et al. 2001) investigated the NN detection of grinding burn from AE. The feature parameters include band power, kurtosis, skew and autoregressive coefficients and were extracted from the acoustic emission signal which appeared to be suitable for the input to ANN. They mentioned the frequency band power, the kurtosis and skew are informative features for AE signal representation. The kurtosis is a measure of the sharpness of the peak while skew measures the symmetry of the distribution of its mean.

Mokbel and Maksoud (Mokbel and Maksoud 2000) reviewed their work regarding condition monitoring of diamond grinding wheels using AE sensors. The grinding condition was fixed when the wheel and the workpiece contact generated AE signals. These signals can be analysed using an FFT to give the frequency components of the signal. The experiments were carried out by taking the one grinding pass on the specimens for different grinding wheel grit sizes where the surface roughness was continually measured. The results were compared to the AE signals. The variation of both AE spectral amplitude and surface roughness were found to reflect the surface condition of the grinding wheel.

Lezanski (Lezanski 2001) reviewed his work regarding an intelligent system for grinding wheel condition monitoring. The features were extracted in his work from AE, force and vibration signals. He then applied a feed forward BPNN to select eight features, which were grinding depth of cut, coolant volume rate,

standard deviation and mean of vibration, power spectrum, and range of RMS power spectrum. The eight selected features were used to train a neuro-fuzzy model for classification. The classification accuracy was reported to be 83.3% as a best performance.

2.5 Application of laser technique in grinding

The word laser stands for light amplification by stimulated emission of radiation. The source of laser is energy, which focuses optical energy on the surface of the workpiece. The highly focused, high density energy source melts and evaporates portions of the workpiece in a controlled manner. This process is used to machine a variety of metallic and non metallic materials. It is a high energy based tool used in many fields of modern manufacturing production. The advantages of laser assisted conditioning are based on the force free working principle and, the non-reliance on expensive conditioning tools (Westkämper 1995; Kalpakjian, Schmid et al. 2009). The following applications are used in grinding:

- Hardening of work surfaces before grinding
- Condition (truing, dressing or cleaning) of grinding wheels as a substitution for conventional means
- Direct support for the grinding operation through 'pre-heating' of the work pieces in order to achieve higher stock removal rates.

There are solid state (Nd: YAG) laser and gas (CO_2) lasers commonly used in industry that operate either in a continuous wave or pulse mode. Nd: YAG lasers are optically pumped using a flash lamp or laser diodes. This laser is a

solid state laser where the medium is a rod of Yttrium-Aluminium-Garnet doped with Neodymium. This laser emits light with a wavelength of 1064 nm, in the infrared electro-magnetic spectrum. The YAG laser is one of the most common high power lasers which is available up to 4 kW output power. Due to their wave length, which is 10 times shorter than that compared with the CO_2 laser, the YAG laser has the advantage of a better focusing ability and the greater absorptive properties to materials. It is used as a heat source because the relation between heating and crack propagation can be investigated more precisely than with other lasers (Majumdar, Chen et al. 1995; Ramesh Babu and Radhakrishnan 1995; Westkämper 1995; Ueda, Yamada et al. 2002).

Another investigation of grinding burn in terms of critical temperature on the nickel based alloy (CMSX4) was presented by (Liu, Chen et al. 2006). The Nd: YAG laser applied successfully to raise the temperature and obtain a pure thermal AE signal. An AE sensor and a thermocouple were used to monitor grinding burn experienced during the grinding of a nickel based alloy (CMSX4). Laser pulses focus on a given off-focal distance point on the surface of the material and are able to obtain an AE signal due to thermal expansion. This research used Wavelet Packet Transform (WPT) to convert the extracted AE signal into a time based signal, segmented into different frequency bands.

2.6 The research gaps

Grinding burn is a common phenomenon of thermal damage that has been one of the main constraints in grinding. Nickel-based alloys such as CMSX4, Inconel718 or MarM002 have very poor machinability, which can cause an

excessively high grinding temperature, and therefore, grinding burn becomes a crucial issue that hinders the improvement of surface quality, and also has an adverse effect on in-service strength and fatigue properties. To obtain the critical temperature on CMSX4 material, the features from laser irradiation and real grinding are compared. When an Al_2O_3 wheel is used to grind CMSX4 material, the critical temperature of grinding burn was determined to be around 770°C (Liu, Chen et al. 2006).

The detection of high, medium and low temperatures proposed in this thesis are due to severe, normal or no burn, by changing the laser irradiation off-focal distances. This has not yet been investigated in the grinding zone which is one of the main contributions of this research the grinding research community. The explicit features extracted from AE signals due to high, medium and low temperatures from laser irradiation, pattern recognition (classification) of grinding burn is significant justification for this research.

Chapter 3: AE sensing systems for the laser irradiation and grinding

3.1 Introduction

This aim of this chapter describes the experimental set-up for data acquisition of both laser irradiation and grinding burn experiments. A wide bandwidth AE monitoring system for laser and for grinding are presented separately to ensure the major AE feature extraction within the frequency range of the covered nickel based alloy materials (Inconel718 and MarM002).

The objective includes:

- A self made preamplifier construction for laser tests to amplify the output of the thermocouple signal for transfer to the acquisition card
- Design experiment set-up for laser irradiation with an AE sensor and a thermocouple sensor to ensure the identification of high, medium and low temperatures in given off-focal distances
- Temperature calibration through extracted data from thermocouple sensors
- Design experiment set-up for grinding with AE sensor, force, power and vibration sensors to ensure grinding monitoring and to identify burn in given depth of cuts

The laser irradiation experiment has been arranged to simulate the elevation of temperatures by changing different off-focal distances on the workpiece

materials. The grinding experiment has been arranged to acquire data of the burn signature by changing different depth of cuts on the workpiece materials. The workpieces were Inconel718 and MarM002 of nickel based alloys. The machinability of the workpiece materials and grinding wheel as a cutting tool are described at the beginning of this chapter.

This chapter presents the experimental set up for both experiments with different conditions using AE, temperature, power, force and vibration sensors. The laser irradiation sensing system was constructed using an AE and thermocouple sensor. The grinding experiment obtained the following sensor fusion of AE, force, power and vibration. In laser irradiation, the AE and temperature data are acquired using AE and a thermocouple sensor on the workpiece materials. For the experiment, different AE signals were extracted based on different temperatures (high to low) by changing off-focal distances. The grinding experiment was arranged to acquire data from the emitted burn signature at various grinding intensities on the workpiece materials based ultimately on different depth of cuts.

3.2 Grinding process

3.2.1 Nickel and Nickel based alloys

Nickel based super alloys are the most common of the super alloys, and they are available in a wide variety of compositions as shown in Appendix 1. The proportion of nickel is from 38% to 76%. They also contain up to 27% Cr and 20% Co.

The primary use for these alloys are in (Choudhury and El-Baradie 1998):

- Aircraft gas turbines, e.g. turbine disks, combustion chambers, bolts, casings, shaft exhaust systems, blades and vanes
- Steam turbine power plants, e.g. bolts, blades, stack gas repeaters
- Reciprocating engines, e.g. turbocharger, exhaust valves, hot plugs
- Metal processing, e.g. hot work tool and dies, casting dies
- Medical applications
- Space vehicles
- Heat–treating equipment
- Nuclear power systems

These super alloys can be classified as Nickel (Ni) based, Iron (Fe-Ni) based and cobalt (Co) based. Table 3-1 displays some properties with typical applications of Nickel based Super alloys (Kalpakjian, Schmid et al. 2009).

Table 3-1: Properties and typical application of selected Nickel based Super alloys at 870°C.

Alloy	Condition	Ultimate tensile strength (MPa)	Yield strength (MPa)	Elong ation in 50 mm (%)	Typical applications
Inconel718	Wrought	340	330	88	Jet engine and rocket parts
MAR-M 200	cast	840	760	4	Jet engine blades
MAR-M 432	cast	730	605	8	Integrally cast turbine wheel

Nickel based super alloys such as Inconel718 and MarM002 are specially designed for high-temperature and high stress applications. The generic names for MarM002 are MarM002 DS (Direct solidification) and MarM002 EQ

(Equaiax). MarM002 DS forms a liquid at 1370°C and becomes solid at 1300°C. It has a density of 8.55(g/cc). During casting, the material is cooled under controlled temperature such that different layers have a different breakage resistance property upon solidification while MarM002 EQ turns to Liquid at 1375°C and solidifies at 1284°C. It has the same density as MarM002 DS. The casting process is different for MarM002 DS as the material is allowed to cool down naturally. Therefore, it has an equal solidification with the same property in every direction of the material (Fisher, Datta et al. 1999).

3.2.2 Grindability of nickel based alloys

Grindability is a general indicator of how easy it is to grind a material. It includes the following considerations: the quality of the surface produced, the surface finish, the surface integrity, the wheel wear, the cycle time, and the overall economics of the operations. Machinability and grindability are very similar terms which define how easily a material can be turned, milled, drilled, reamed, slotted, or ground. The grindability is specifically applicable to the grinding of a material that can be improved by the proper selection of process parameters (wheel speed, work speed and feed rate), grinding wheels, grinding fluid, as well as machine characteristics, fixturing methods, and work holding devices (Serope Kalpakjian and Schmid 2006).

Machinability and grindability are dependent on the same physical, mechanical and chemical properties of a given workpiece. If a material has a low machinability then it will be difficult to grind and if a material has a high machinability than it will be easy to grind. This does not mean that the

difference between the machinability of two workpieces and their grindability will be exactly the same. There are differences in the chip forming process of metal removal. The chip forming process in machining is predictable, produces uniform thickness and width. On the other hand, the abrasive grains on the periphery of the grinding wheel produce very small chips of varying thickness, width and shape. The chip characteristic in grinding is due to the random arrangement of abrasive grains on the surface of the grinding wheel and how far they protrude above the wheel surface along with their negative rake characteristic (Krar and Ratterman 1990).

Nickel based super alloys have some characteristics that are responsible for poor machinability. They have an austenitic matrix, like stainless steels. In addition, this material has a tendency to "work harden". The major reason for the development of such alloys has generally been for use in aircraft engines. These alloys retain their strength at high temperatures when encountering grinding and machining in comparison to other alloys which makes them desirable for aerospace applications although not for machining. Work hardening is a characteristic which allows the strength and hardness of a metal to actually increase while it is being formed or machined. This further decreases the grindability of such alloys (Krar and Ratterman 1990). Material properties are presented in Appendix 1.

3.2.3 Properties of grinding wheels

The grinding wheel is the interface between the machine and the workpiece. Grinding wheels consist of a combination of abrasive grains and bonding agents. The most important characteristic of a wheel is its abrasive grain, bond types, grade, and hardness. A grinding wheel surface consists of abrasive grains that form the cutting edges, bond materials to retain the grains in position and surface pores that allow space for material removal from the workpiece surface (Rowe 2009).

The grinding wheel must be harder than the workpiece and must be wear-resistant due to the transferred energy from the machine into the workpiece. There are two abrasives used in grinding which could be described as conventional abrasive and super abrasives. The conventional abrasives consist of aluminium oxide (Al_2O_3), silicon carbide (SiC) while the super abrasives consist of Cubic boron nitride (CBN) and diamond. The main components of a grinding wheel are the abrasive grains and the bond materials which hold them together. In this research, Al_2O_3 wheels are used for the grinding process monitoring. This Al_2O_3 wheel is commonly used to grind high tensile strength materials such as steel, high speed steel annealed malleable iron and, tough bronze.

There are a number of aluminium oxide grain types. Aluminium oxide was first made in 1893. It is produced by fusing bauxite, iron filling, and coke. Fused Al_2O_3 are categorized as dark (less friable), white (friable) and single crystal.

Hardness is the ability of a material to scratch or indent another material which occurs during the grinding operation. It is the most important physical property of an abrasive. Moh's scale of hardness shows that the hardness of aluminium is 9. The Knoop hardness is a measure of the materials ability to indent other materials. A material with a large Knoop number is harder than a material with a small Knoop number. Aluminium (Al) has a Knoop number in the range of 2000-3000 $\left(\frac{\mathrm{Kg}}{\mathrm{mm}^2}\right)$ compared to a diamond which has a Knoop number in the range of 7000-8000 $\left(\frac{\mathrm{Kg}}{\mathrm{mm}^2}\right)$ (Serope Kalpakjian and Schmid 2006).

In addition to hardness, an important characteristic of abrasives is the friability– defined as the ability of abrasive grains to fracture. This is an important property and gives abrasives their self-sharpening characteristic, which is essential in maintaining their sharpness during use. The Al_2O_3 wheels have a good self-sharpening ability in nickel based alloy grinding, while the wheel helps to prevent wheel loading (Chen, Griffin et al. 2007).

3.3 AE sensing system development for the laser irradiation

3.3.1 Experiment set up for laser irradiation

The laser irradiation experimental set-up consists of an AE sensor, thermocouple, USB card, preamplifier, PCI-2 based signal processor and specimens of different materials. All laser irradiation experiments were carried out in the Lumonics JK704 Nd: YAG laser machine. A schematic diagram of laser irradiation and sensor arrangements illustrated in Figure 3-1. An E-type thermocouple, located at the centre of the laser beam spot, was tightly fixed on

the front surface of the workpiece and an AE sensor and placed on the opposite side of the workpiece.

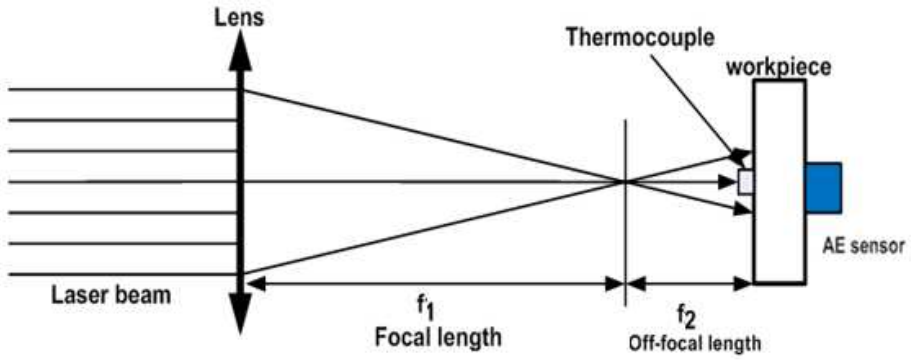

Figure 3-1: Schematic diagram of laser irradiation optical arrangement.

The E-type thermocouple consists of two dissimilar metals of Constantine (-) and Chromel (+) joined at one end so that the difference of voltage can be measured. Since voltage changes in proportion to temperature, the voltage difference indicates temperature differences. This E-type thermocouple covers a range of temperatures starting from -200˚C to +900˚C.

A self made preamplifier was constructed to amplify the output of the thermocouple signal and transfer to an acquisition card. The maximum input of the NI AT-MIO-64-3 acquisition card is $\pm$10V. If the temperature is very high due to laser irradiation on the workpiece, material provisions need to be made to ensure the maximum output of this amplifier is less than the defined limit of 10V. The temperature characteristic of type E (Constantine-Chromel) thermocouple is similar to type J, and compared to type K, therefore the AD594 is preferred for this calibration. The amplifier main circuit is AD594 which is an

amplifier and thermocouple cold junction compensator on a monolithic chip. The AD594 monolithic Integrated Circuit (IC) is shown in Figure 3-2.

The circuit has been designed to produce a temperature output proportional to 10 mV/°C. The AD594 is used to compensate the cold junction temperature with a pre-calibrated amplifier to produce an interval step level of 10 mV/ºC voltage output corresponding directly to the thermocouple output signal. Some important characteristics of the AD594 are the operation temperature range: -55 to 125 °C, Stability Vs. temperature: ±0.05 °C/°C and sensitivity 10 mV/°C. A type E thermocouple shows a Seebeck coefficient of approximately 62 μV/°C . This corresponds to a gain of 193.4 for the AD594 to realise 10 mV/°C outputs.

The AD594 is gain trimmed at the factory to match the transfer characteristic of the thermocouple at +25°C to produce a temperature proportional output of (10mV/°C), and provide an accurate reference junction over the rated operating temperature range.

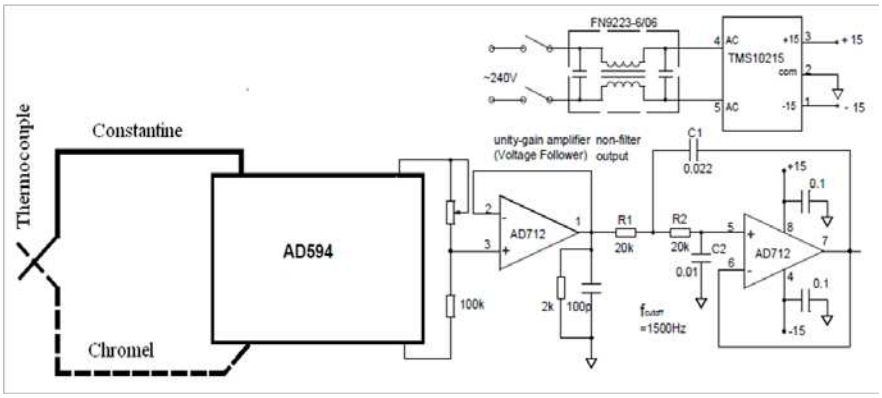

Figure 3-2 : Thermocouple preamplifier circuit.

The AD712 is a high speed, precision monolithic operational amplifier. The device has all the properties required for an ideal AC and DC amplifications and

therefore it is suitable for active filter applications. It has a slew rate of 16V/μs and it can follow the transient variance of grinding temperatures. The Integrated circuit of AD594 is connected to two, unity gain follower circuits of AD712 to maintain the signal voltage because of its isolation properties, as impedance or circuit isolation is more important than amplification while maintaining the signal voltage.

The function of the unity gain follower is to invert the signal and invert the gain to give a positive read-out. The follower circuit is only used if the thermocouple voltage continually saturates above 10V which is above what the signal acquisition board does not support (constraint to -10V to 10V).

Laser pulses focused on a point on the workpiece surface were considered as a point source to generate thermal expansion which can cause elastic AE waves.

The laser pulse on a surface of a material generates elastic waves based on two mechanisms of power density: First if enough laser power is absorbed, the material surface may be ablated or even vaporized. Secondly, when power density of the light causes no ablation, a local thermal expansion dominates over radiation pressure. Under most circumstances, the thermal behaviour of grinding is similar to the second mechanism. The issue was to control the intensity of laser power equivalent to the temperature experienced during grinding. The following condition was applied according to Table 3-2 for the laser irradiation experiment.

Table 3-2 : Laser parameters

Laser Parameter	**Conditions**
Laser	Lumonics JK704Nd:YAG
Wave length	1.06 μm
Pulse energy	1.5J
Maximum peak power	2.5 kW
Irradiation time	0.6 ms
Focal length	120 mm
Laser beam diameter	12 mm
off-focal length	34-46mm

By changing the laser irradiation off-focal distances from 34 mm to 46 mm the data was acquired from both the Thermocouple and AE sensors. Two computers were synchronised by a switch driven Data Acquisition Card and all signals (temperature and AE) were triggered through self made thermocouple amplifiers and AE amplifiers between the sensors and computers. The temperature calibration obtained from the thermocouple sensor are presented in Table 3-3 where the laser is offset by a distance of 34 mm which produces high temperatures, 40 mm offset distance equates to medium temperatures and 46 mm offset-distance, low temperatures are produced.

Table 3-3: Temperature calibration results.

Laser offset	**Inconel718**	**MarM002**	**Temperature**
(mm)	(°C)	(°C)	**scale**
34	698	493	high
40	324	318	medium
46	239	235	low

The AE sensor was placed on the back side of the workpiece. The generated AE signals were detected and processed by the PCI-2 of two channels. The

PCI-2 card consists of a signal processing unit, interface of AE data streaming storage, display and the accessories (sensor and pre-amplifier) to route a rich signal to the computer (the pre-amplifier can be selected to give the best SNR for a particular experiment based on a first test pass).

When AE is emitted which is caused by the thermal stress in the workpiece, the AE wave converts into a voltage signal which is amplified by the preamplifier and sent to the amplifier in the main processor for post processing.

3.4 The sensing system development for the grinding experiment

3.4.1 Makino A55 machine centre

The Makino A55-5XR is a horizontal 5 axes high efficiency machining centre with a Fanuc Professional 3 Computer Numerical Control (CNC) used to perform grinding amongst other machining methods. This machine affords excellent performance for milling, drilling and tapping operations when applied to aerospace manufacturing. These machines are widely used to provide different functionalities for example Rolls Royce Turbine Blade Facility in Derby use 6 to provide grinded blades for fixing to turbine disk.

This machine has a maximum spindle speed of 14000min^{-1}, power output of 22 kW and uses a taper 7/24 No.40. The spindle vibration is less than 3 μm peak to peak at 1400 min^{-1} and an AC motor is used to drive the spindle. There are two pallets in this machine with an Automatic Pallet Changer (APC) embedded in this machine. The pallet changing time is approximately seven

seconds. One of the pallets has been tailor configured for the grinding operation presented in Figure 3-3.

3.4.2 Experiment set up for grinding

The experiment set up aimed to provide a burn signature with various intensities on grinding aerospace materials by increasing the depth of cut. The research mainly looks at the grinding phenomena thorough the AE signal. The technique is based on other sensors also used to verify using the AE sensor as this is not a standardised sensor. Other sensors included force, power and vibration sensors which were used to monitor grinding phenomena. The grinding process monitoring experiment set up consisted of: a force sensor, a vibration sensor, a power sensor and an AE sensor housed in the Makino A55 machine. All these sensors were attached and situated next to the workpiece in a way that ensured maximal signal extraction. For monitoring the force, power and vibration signals an NI PXI system were connected to one computer and for monitoring AE signals a PCI2 AE system was connected to another computer. These two computers were synchronised by a switch driven Data Acquisition Card (DAC) and all signals were triggered (boosted) through a respective amplifier between the sensors and computers.

The sensor arrangement and data logging system for the grinding experiment is shown in Figure 3-3.

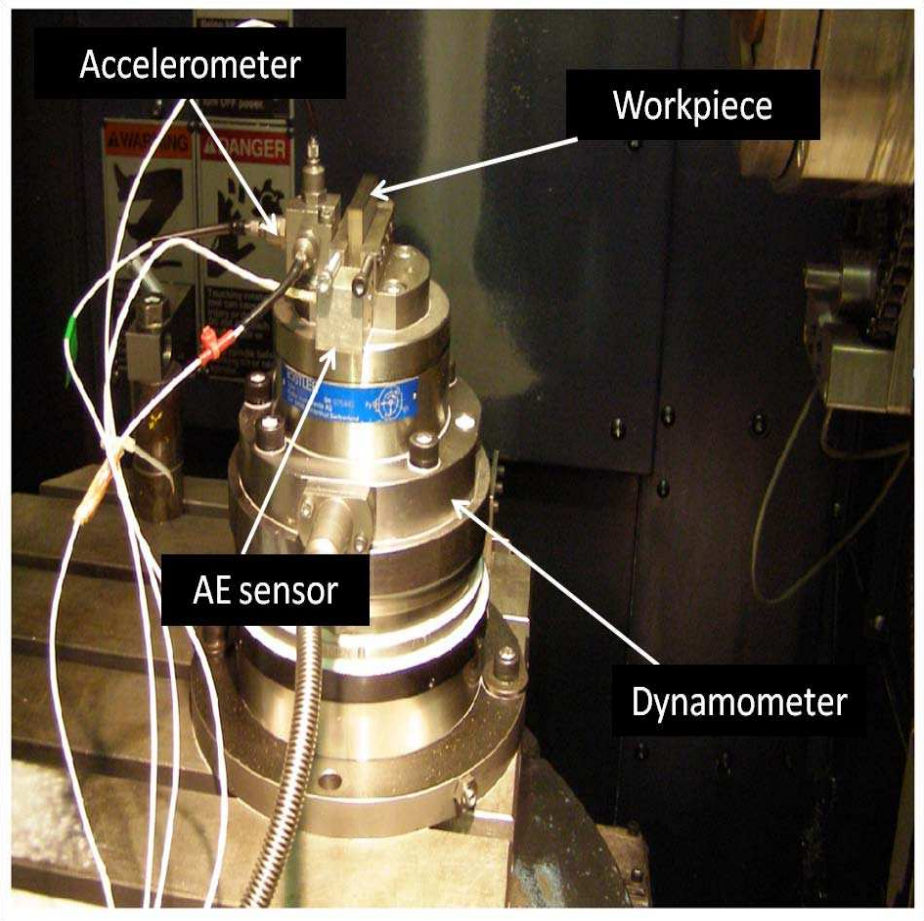

Figure 3-3: The grinding experiment set up.

There were two AE sensors of WD-AL05 and WD-AL04 supplied for the experiment however only one AE sensor was used to carry out the experiment and the other one remained on standby or was used to verify the 1st AE sensor when used in parallel for verification.

This AE sensor carefully placed within the workpiece was used to detect the responses from the grinding wheel to the workpiece interface. Grinding on Inconel718 or MarM002 samples would be carried out in sequential manner seven times in each depth of cut. The wheels would be dressed at the beginning

once just before the total seven pass (one set of cut). In Table 3-4 dressing conditions for the grinding wheel are shown.

Table 3-4 : Wheel dressing condition.

Tool	Dressing depth	Dressing lead	Dressing feed rate	Dressing ratio
Wheel	0.25 mm	3600 rpm	3 mm/min	0.8

The grinding condition used in this investigation is shown in Table 3-5.

Table 3-5: Grinding condition.

Grinding parameter	Condition
Workpiece material	MarM002, Inconel718
FeedRate	1 m/min
Wheel speed	55 m/s
Depth of cut	0.2-0.02 mm
Wheel material	Al_2O_3
Coolant	No

The burn signature on the signal would then be recorded by an AE sensor, force dynamometer, accelerometer and Power (load) sensors. The burn signatures would also be recorded by a workpiece image.

The sampling rate was set to 5MHz to ensure that there was no aliasing and a level of five times the maximum pickup frequency of the sensor giving a good resolution of material phenomenon. The main specification of these sensors is displayed in Table 3-6.

.

Table 3-6: The AE sensors specification.

Specification	**PAC WD Sensor(1)**	**PAC WD Sensor(2)**
Sensor number/date	AL04(17/11/04)	AL05(17/11/04)
Construction	Differential	Differential
Sensor drive Capability	Up to 100 m with w/RG-58 AU cable	Up to 100 m with w/RG-58 AU cable
Dimensions (dia.*ht)	17*16 mm	17*16 mm
Peak sensitivity	-63.30 (dB ref 1V/µbar)	-63.30 (dB ref 1V/µbar)
Operating frequency range	100kHz-1000kHz	100kHz-1000kHz

The generated AE signals would then be recorded by model PCI-2 with two channels providing the AE system on a card for interface to the computer.

In depth, the AE system uses the physical Acoustic, PCI-2 AE system. It has two channels, AE data acquisition and digital signal processing (DSP) system on the PCI card. It has a superior low noise and low threshold performance with 18 bit A/D conversions unit, 40 MSample/second acquisitions with sample averaging and automatic offset control (PCI-2 Based AE System User's manual, June 2003). This performance was achieved via pipelined, real time architecture, without any sacrifice in the AE performance. Through the high performance PCI (Peripheral Component Interconnect) bus and separate Direct Memory Access (DMA) architecture for each channel, significant AE data transfer speeds can be attained, assuring a wide bandwidth bus for multi channel AE data acquisition and waveform transfer. The card is built on wave mount

technology and high density ASIC (high density programmable Gate Arrays) devices; this ensures that this single AE system with the two onboard channels has a very fast acquisition capability for storing signals of interest.

This AE system has a very fast acquisition capability for storing the signal of interest. The AE system consists of a signal processing unit, interface of AE data streaming storage, display and accessories (sensor and preamplifier) for the computer.

The extracted AE signals contain both a continuous waveform and intermittent hit information. Signals are acquired based on a fixed AE threshold of 40 dB. When the grinding event occurs the AE signal exceeds the AE threshold and is called hit. These hit events would then be extracted and stored as 1024 point block information segments. These 1024 blocks would be concentrated together in order of event and with respect to time (Griffin 2008).

A preamplifier is used to amplify very weak signal as a low–level signal to line-level. The output signals from the AE sensor are very weak at high frequency (i.e. low level and high impedance). This kind of signal needs a preamplifier for transfer to an acquisition card. The preamplifiers are located very close to the sensor to make sure there is no unwanted signal and or, picks up electromagnetic interference. The output signals from the AE sensor were passed through the pre-amplifiers with a gain of 100 (40 dB). If the gain is set too high then the amplified signal will saturate. Another function of the preamplifier is to eliminate mechanical and acoustical background noises. The background noises are frequency components below 100 kHz. To control the

AE system sensitivity, the threshold set up was 30 dB (usually in a range of 10-99 dB) to obtain higher sensitivity. A low threshold produces background noise in the system.

The voltage supplying the PAC preamplifiers was 28 V_{dc} and is supplied internally via the coaxial cable from the acquisition board with no external power source present.

3.4.3 Force, power and vibration measurement

The experiment set up consisted of both the AE and other sensors being attached in a way to ensure maximal signal extraction. A kistler 3-axes Dynamometer 9272A with a 5017 amplifier selected for grinding force monitoring. Three axes force signal componentsF_x, F_y and F_z in three directions were measured. The range of this type of dynamometer is between 5-20 kN which should be enough for grinding force monitoring. The measured signals are amplified by a dynamo amplifier. The signals are separated as separate channels and are connected to the data acquisition system based on a PXI system and LabVIEW package.

Three Piezoelectric Accelerometers 8704B with a 4-channel Coupler 5134A1 were used to monitor chatter. The measured signals were amplified by an acceleration coupler. The signals were also separated and connected to the data acquisition system based on PXI system and LabVIEW package. The sensitivity of the accelerometer devices is less than that of the AE sensors.

The Makino A55 machining centre has an inbuilt Hall-effect current sensor. The Hall-effect sensor operates as an analogue transducer that varies its output voltage in response to changes in the magnetic field. The power is estimated by vector multiplications between current and voltage samples sensed by Hall-effect sensors. The sensor is suitable for measuring power consumption with the spindle of an A55 machine centre in the grinding process due to the consideration of power factor variation with a different load. The signals are then connected through the SCB-100 100–pin shielded connector to block the data acquisition system based on NI PXI-1031 and LabVIEW package.

Power sensors (Load control) can be used for grinding gap elimination (contact detection between workpiece and tool) and used to detect dull wheel (worn grinding wheel) from decreasing power. This is due to the sharper recently dressed wheel requiring less spindle power. This is due to sharper grits providing a cutting action as opposed to a rubbing and ploughing action which inherently gives off more energy in the workpiece as opposed to the chip.

3.4.3.1 Data acquisition system and LABVIEW application software

The data acquisitions are controlled by a software program LabVIEW which is a graphical interface driver system setup for the acquisition of signals. This language uses the dataflow where the flow of data determines the execution. The user interface to LabVIEW is known as the front panel where all the recording parameters should be defined.

In the front panel, the display range can be adjusted from -10 V to 10 V. The sampling rate has a maximum limit of 500 kHz and maximum number of

samples of 20000 for one channel only (this decreases the more channels that are used). A signal processing panel for play the back of the signals is also available, where the raw extracted signals can be converted to RMS values and output directly to the user. In addition, all of the extracted signals can be seen at any one time.

The hardware for the grinding test consisted of the following: LabVIEW SCB-100 shielded I/O connector block and 100 screw terminals that connect a total of eight sensory input devices in differential reference mode.

3.4.3.2 Hardware configuration

The hardware for the grinding process monitoring consists mainly of a LabVIEW SCB-100 Shielded I/O Connector and data logging card based on a National Instruments PXI (PCI extensions for Instrumentation) module.

The SCB-100 provides the connection for non-referenced or floating signal sources, differential inputs and single-ended inputs. The SCB-100 100-pin shielded connector block is a shielded board with 100 screw terminals that connect a total of 8 sensory input devices in differential reference mode to the NI PXI-1031.

PXI systems consists of NI PXI-1031 chassis, 3.0 GHz Pentium 4 Rack-mounted PXI controller and 16-Bit NI PXI-6251 with 16 analogue inputs and 24 digital I/Os.

The PXI based data acquisition system offers excellent performance in terms of high speed compared to the industry-based PCI bus which was modelled on

older architecture. This system has advanced timing and synchronisation features. The main advantage is the PXI system which can provide a high-level of integration between different modules.

3.5 Wheel wear measurement

The razor blade method was employed to measure grinding wheel wear. In this method one half of a grinding wheel ground a workpiece, while the other half remained fresh. Immediately after the grinding experiments were performed, the razor blade lowered them into the grinding position with the grinding wheel touching the blade. The wheel had a step between the work half and the fresh half. Then, the wheel ground a razor blade and the topography (step) of the wheel was copied onto the razor blade. After grinding the blade, the wear of the grinding wheel was measured using a surface profilometer (Liu, Chen et al. 2007).

3.6 Summary

This chapter has described the experimental set up for the laser irradiation and for the grinding. The laser irradiation experiment setup consisted of acoustic emission and thermocouple sensors to simulate high, medium and low temperature on the workpiece material under the given condition of laser irradiation (without grinding).

The laser thermal data is acquired using an AE sensor and thermocouple sensor by changing the laser off-focal distance to simulate high, medium and low temperatures on the workpiece.

The grinding experiment set up consisted of AE, force, power and vibration sensors to monitor burn signature under the given grinding condition.

The grinding thermal data is acquired using AE, force, power and vibration sensors by changing the depth of cut to monitor severe burn, normal burn or no burn signatures on the workpiece.

The next step is to extract thermal features from the acquired data both from laser irradiation and grinding by using a digital signal processing techniques.

Chapter 4: Digital signal processing technique

4.1 Introduction to signal processing

There are many sensors used in this research to acquire data for measured signals, for example, AE, force, vibration, temperature and power. Most of the signals data acquired through sensors are time series data. This chapter describes the signal processing technique which must be used to process the acquired data to understand the more precise information of the machining condition.

The source of noise in grinding is the rapid release of energy which is generated by grits, workpiece materials and high pressure coolant flow. There are two main tasks when considering how to tackle these difficulties in using the signal in condition monitoring: (a) the elimination of irrelevant noise signals and (b) the feature extraction in order to analyse the grinding conditions.

Signal processing is data processing for waveform data or multi dimensional data which is acquired through extracting and formatting information from the emitted raw signal. Various signal processing techniques were developed in order to analyse and interpret waveform and multidimensional data to extract useful information for further diagnostic and prognostic purposes. This procedure of extracting useful information from raw signals is called feature extraction (Jardine, Lin et al. 2006).

This chapter describes the signal processing technique for waveform which describes how to extract features from different sensory signals which are acquired through the sensing instrument. The feature extractions from the raw signals are very sensitive to the machining condition. Thus, it requires a better signal processing technique to extract features. The Fast Fourier Transform (FFT) is widely applied as a signal processing technique in engineering. The limitation is its inability to handle high frequency and non-stationary stochastic signals which are very common when machining faults occur. The time frequency uses time-frequency distribution, which represents the energy or power of waveform signals in two dimensional functions of both time and frequency such as Short-time Fourier Transform (STFT), to better reveal faults and patterns for more accurate diagnostics.

Primarily, in this research energy spectral distribution of AE signals is studied in relation to grinding burn in particular.

4.1.1 Signal properties and representation

Signals could be defined as a fundamental physical quantity, for example, voltage, pressure or electromagnetic field which changes over time. There are four main reasons for frequency analysis or spectral analysis mentioned in the Time-frequency analysis by Leon Cohen (Cohen 1995).

- To learn the source of a signal by spectrally analyzing the wave form
- To study the propagation through a frequency dependent medium, the signal is decomposed into its different frequency components. To analyse for each component and reconstruct the signal to obtain the resulting waveform

- To simplify our understanding of the waveform
- To provide solutions for ordinary and partial differential equations

The most important classification concerns deterministic and non-deterministic signals (Ruhm 2008). The deterministic signals and events can be described as analytical expressions for all times (past, present, future). They are also predictable for arbitrary times and these signals can be reproduced identically, arbitrarily and with frequency. These signals are not able to carry new information, since everything is already fixed (deterministic, predetermined).

A hierarchical roadmap of common classifications of signals is presented in Figure 4-1. A deterministic signal can be divided into periodic and aperiodic. Periodic signals are ones which repeat themselves after a specific interval of time. These signals can be decomposed into a fundamental sine wave and a set (finite or infinite) of harmonically related sine waves in Fourier series analysis. Mostly periodic signals are ones composed of sine waves but which include components not harmonically related. Aperiodic signals are ones which do not have a repetitive form and are usually transient in nature, they are sometimes called transient signals.

On the other hand, the non-deterministic signals functions cannot be determined explicitly using mathematical equations and in this case probabilistic and statistical descriptions will need to be used.

It is frequently considered that non-deterministic, random events are disturbing. In order to make results of investigations (examination, observation, measurement analysis, diagnosis) representative, it is possible to reduce the random character by systematic procedures (design of experiments).

The future values of non-deterministic signals cannot be accurately predicted and can usually only be guessed based on the average sets of signals (Baraniuk 2009). The signal can also be divided into continuous signals (analog signal) and discrete signals (digital signal) according to the time and the amplitude of the signal.

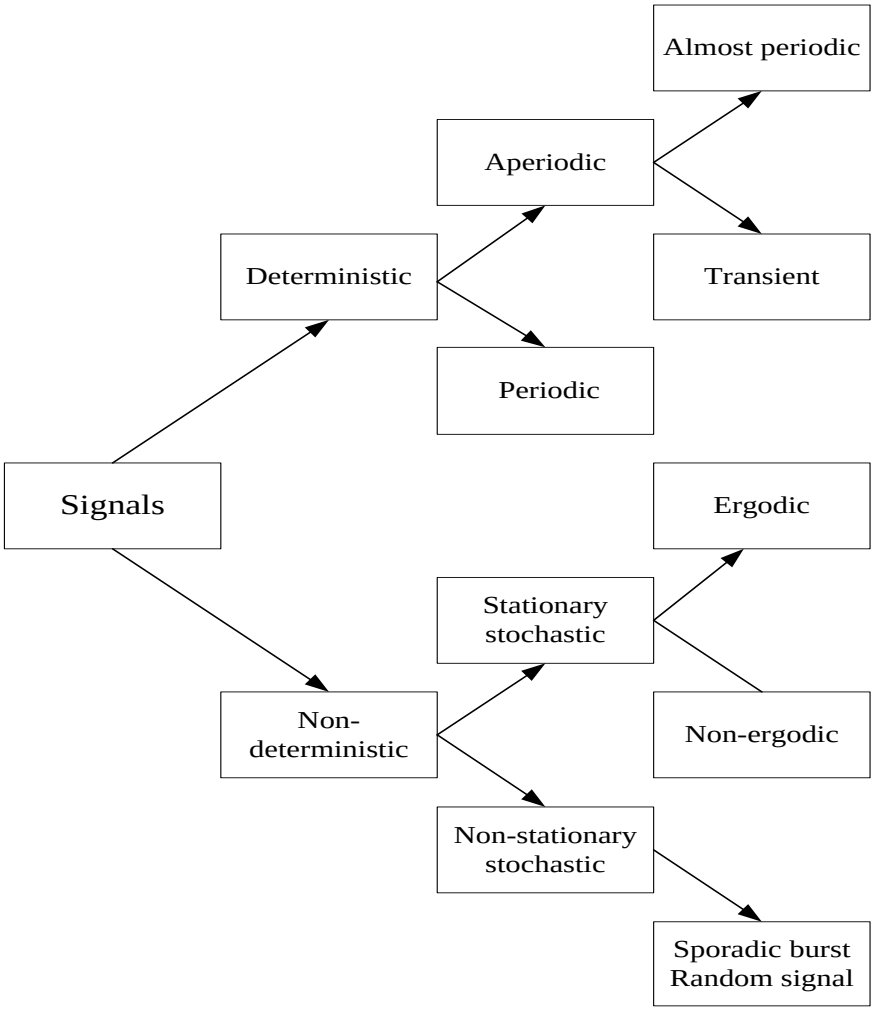

Figure 4-1: Classification of the signal.

This research mainly concentrates on the high frequency, non-stationary stochastic signal (AE signal) which is shown in Figure 4-1.

The analogue time series signal is generally used to convert digital values through the AD (analogue-to-digital) converter. The AD converter consists of three internal stages:

- Sample-and-Hold circuit
- Quantizer
- Coder

The sample-and-hold circuit consists of a switch and capacitor in its simple form. In the sample mode the switch is closed for an interval of $(T - \tau)$ seconds thereby allowing the capacitor to charge up to the voltage value of the analogue input. In the hold mode the switch is opened, and the capacitor holds the instantaneous voltage values acquired at the end of the sample mode for an interval of τ seconds, thereby allowing the A/D conversion to take place. The time interval between successive sample values,T, is called the sampling period.

The important parameters of the analogue to digital conversion are the input range, the number of digits of conversion, the sampling time, and the total number of sampled data (Moriwaki 2008).

The most important factor in sampling is the sampling time, which provides the time interval for the successful AD conversion. The AD converter equally divides the voltage of the input range into the given digits and gives the corresponding number to the input voltage at a given sampling interval. This requires more than 1 MHz sampling rate (5 MHz used in this research for AE) for acoustic emission signals. Other signals such as force, power and vibrations require less than 2kHz sampling rate (1kHz is used in this research). Another point is the accuracy of an A/D converter.

The sampling time Δt is the time interval to give the successive AD conversion. A sampling time of 1 ms means that the signal is converted at a sampling rate of 1000 samples per second, or a sampling frequency of 1 kHz. If the sampling time is shorter or the sampling frequency is higher, the original signal can be better represented as a digital form but the total number of digital data for a given time period becomes larger and may require a longer processing time.

The sampling time Δt gives the upper limit frequency f_{max} of the digitized signal to be analyzed, or

$$f_{max} = \frac{1}{2\Delta t} \qquad (4\text{-}1)$$

This means that the frequency range of the digitalised signal is limited to below $\frac{1}{2\Delta t}$ Hz. In addition, the original analogue signal beyond this frequency is included in the frequency components of the digitalised signal which is lower than f_{max}. This is called Shannon's sampling theorem (Moriwaki 2008).

If the quantity $\frac{1}{2\Delta t}$ is smaller than the frequency limit f_{max}, then overlapping of the output periodic spectra will result. It means that if the analogue voltage signal is not sampled frequently enough the high frequency input signal will appear as a low frequency signal output. These phenomena are called aliasing and cause signal deformation. In order to avoid this problem, the sampling interval should be selected according to Shannon's sampling theorem. This means that the signal must be sampled at least twice as fast as the highest frequency component.

The quantiser performs an amplitude discretistion operation by converting the discrete-time continuous–amplitude signal to a discrete-time discrete amplitude

(digital) signal, by representing the continuous amplitude range with a finite number of quantization levels (discrete levels).

The coder assigns the binary numbers to normalise with respect to the full scale – voltage of the quantiser, where full scale voltage is referred to as the maximum amplitude of the analogue input voltage. When the grade difference or interval (difference between two consecutive quantization levels) between two neighbouring quantified voltages Δx is $\frac{E}{2^b}$, the maximum of the quantified error e is $\pm 2^{-(b+1)}$ (E is the input range). The quantified error is a random noise. Increasing the A/D bit will reduce the quantified error but increase the cost in terms of time and materials (Liu 2005; Griffin 2008).

4.2 Features in time, frequency or time-frequency domains

The aim of signal processing is to extract features from sensory signals which are carried out in the time domain, frequency domain or the combination of time-frequency domain.

4.2.1 Features in time domain

The signal analysis used extracts some of the useful/rich information of the signal via the mean value, root mean square, standard deviation, root mean square (rms) value, skewness, kurtosis and power. These features of the signal can be represented as mathematical functions in the time domain as follows in Table 4-1.

.

Table 4-1: Partial feature presentations in the time domain

Feature	Formula	Note
Mean	$\mu = \frac{1}{N}\sum_{i=1}^{N} x_i = \frac{1}{\omega}\int_0^{\omega} \lvert x \rvert \delta t$	The origin moment of order 1 where x is sensory signal
STD (Standard deviation)	$\sigma = \sqrt{\left(\frac{1}{N-1}\right)\sum_{1}^{N}(x_i - \mu)^2}$	The centre moment of order 2
Skewness	$S_k = \frac{1}{N}\frac{1}{\sigma^2}\sum_{i=1}^{N}(x_i - \mu)^3$	The centre moment of order 3
Kurtosis (Kr)	$K_r = \frac{1}{N}\sum_{i=1}^{N}\frac{(x_i - \mu)^4}{\sigma^2}$	The centre moment of order 4
RMS (root-mean-square)	$U_{RMS} = \sqrt{\frac{1}{N}\sum_{i=1}^{n} x_i^2} = \frac{1}{\sqrt{N}}\left(\sum_{i=1}^{n} x_i^2\right)^{1/2}$	A discrete/continuous distribution where U_{RMS} is voltage after RMS processing.
Power	$P = \frac{1}{N}\sum_{i=1}^{N} x_i^2$	The power representation of signal

4.2.2 Feature in the frequency domain

The discrete-time or discrete-frequency Fourier transforms is usually known as Discrete Fourier Transform (DFT). The Fourier Transform (FT) can be seen in the following equations:

$$X(j\omega) = \int_{-\infty}^{\infty} x(n) e^{-j\omega nT}\, d(n\omega T) \qquad (4\text{-}2)$$

$$x(n) = \int_{-\infty}^{\infty} X(j\omega) e^{j\omega nT}\, d(\omega T) \qquad (4\text{-}3)$$

Equation (4-2) the Fourier Transform of x(n) is multiplied with an exponential term, at some certain frequency f and then integrated over all times.

There are two problems associated with the limit which extends $-\infty$ to $+\infty$ and the second problem which is associated with the frequency

variable ω which is continuous. It requires an infinite time in computation to produce the results.

4.2.3 Frequency analysis

Frequency domain analysis presents a transformed signal in a frequency domain. The advantage of frequency-domain analysis compared to time-domain analysis is its ability to identify and isolate certain frequency components of interest. The most widely used spectrum analysis is undertaken using FFT. The main idea of spectrum analysis is that it looks at certain frequency components of interest and extracts features from the signals.

In the frequency spectrum analysis of acoustic emission signals, it takes the discrete Fourier transform (DFT) in the time domain and transforms the signal into the discrete frequency domain. The problem with DFT is that the computing time is very high because it involves a large number of multiplications, addition and trigonometric operations. To reduce the computing time in the frequency spectrum analysis the FFT was developed.

FFT became popular after the publication of the Cooley-Tukey FFT algorithm in 1965 which reinvented the algorithm and described how to perform it on a computer. It opened a new area in digital signal processing by reducing the order of complexity of some computational tasks like Fourier Transform and convolution from N^2 to $N \log_2 N$, where N is the problem size (Cooley, Lewis et al. 1967; Duhamel and Vetterli 1990).

FFT uses smart algorithms in computing by calculating the average of the duration of the extracted signal in less time compared to DFT. The FFT is used for condition monitoring. The disadvantage of FFT is that it does not have any time information which means at what times these frequency components occur when material undergoes deformation or fracture or a combination of both in the condition monitoring (Liu, Chen et al. 2006; Feng and Chen 2007).

4.2.4 Time-frequency analysis

The time-frequency analysis is able to investigate the waveform signals in both time and frequency domain. The time frequency uses time-frequency distribution, which represents the energy or power of waveform signals in two dimensional functions of both time and frequency to better reveal fault and patterns for a more accurate diagnostics. Short–time Fourier Transforms (STFT) and Wigner-Ville distributions are the most popular time frequency distributions (Cohen 1989; Wang and McFadden 1993; Andrade, Esat et al. 1999). Cohen (Cohen 1989) reviewed a class of time frequency distributions which includes the spectrogram, Wigner-Ville distributions and Choi-Willams.

Most of this research uses AE signals for analysis of thermal features related to burn due to laser irradiation or grinding. The STFT is suitable to use for extracting non-stationary AE signals because it can break up the signal in small time segments and apply Fourier analysis for each time segment to determine the frequencies that existed in the segments.

The short-time Fourier transform of a signal is obtained by sliding a window and taking the Fourier transform of the windowed signal. It is assumed that the signal is stationary during the duration of the window. The STFT of a signal

$x(t)$ is obtained by calculating the spectrum of the modified signal $x(\tau)h(\tau - t)$ (more details about modified signal see equation (4-5)), where $h(\tau - t)$ is the window function $h(t)$ centred at t. It is defined by (Malik and Saniie 1993; Cohen 1995),

$$STFT(t, \omega) = \frac{1}{\sqrt{2\pi}} \int x(\tau)h(\tau - t)e^{-j\omega\tau}d\tau \qquad (4\text{-}4)$$

Equation (4-4) is shown more detailed presenting both the time and frequency analysis. To analyse the properties of the signal at time t, the emphasis is made at that time and the signal is suppressed at other times. The signal is multiplied by a window function $h(t)$, centred at t which produces the modified signal:

$$x_t(\tau) = x(\tau)h(\tau - t) \qquad (4\text{-}5)$$

The modified signal is a function of two times, the fixed time of interest t and the running time τ. The window function is chosen to leave the signal more or less unaltered around the time t and suppress these signals from other times to this time slice of interest.

$$x_t(\tau) \sim \begin{cases} x(\tau) & \text{for } \tau \text{ near } t \\ 0 & \text{for } \tau \text{ far away from } t \end{cases} \qquad (4\text{-}6)$$

The term "window" comes from the idea that we are seeking to look at only a small piece of the signal similar to when we look out a real window and see only a relatively small portion of the scenery. In this case we want to see only a small portion at any one time.

Since the modified signal emphasizes the signal around the timet, the Fourier transform will reflect the distribution of frequency around this time,

$$x_t(\omega) = \frac{1}{\sqrt{2\pi}} \int e^{-j\omega\tau}x_t(\tau)d\tau \qquad (4\text{-}7)$$

Since we are interested in analyzing the signal around the time t, we chose the window function that is peaked around t. Hence the modified signal is short and its Fourier transform is called the short-time Fourier transform.

$$\mathrm{STFT}(t,\omega) = x_t(\omega) = \frac{1}{\sqrt{2\pi}}\int e^{-j\omega\tau}x(\tau)h(\tau - t)d\tau \qquad (4\text{-}8)$$

The energy density spectrum at time t is therefore,

$$P_{sp}(t,\omega) = \left|\frac{1}{\sqrt{2\pi}}\int e^{-j\omega\tau}\, x(\tau)\, h(\tau - t)d\tau\right|^2 \qquad (4\text{-}9)$$

For each different time step, it is possible to get the different spectrum and the totality of these spectra is the time-frequency distribution, P_{sp}. The spectrogram is used to see the frequency bands occurring at specific time intervals across the extracted time domain signal. A range of FFT from STFT would be used to signify burn and no burn phenomena. The FFT segments can then be used to describe phenomenon/event occurring at a specific time in space (Cohen 1995; Griffin 2008).

Each new frame of the windowed sequence incorporates a percentage of samples from the previous frame. Typical overlaps could be found from 10% to 25% or more (Terrell and Shark 1996). To smooth the overlap, a number of so called “window functions” have been developed.

There are many popular window functions such as: Hamming, Hanning, Bartlett, or Kaiser window. A large window width provides good resolution in the frequency domain, but a poor resolution in the time domain, and vice versa (Kim, Lee et al. 2007). If a suitable window function is chosen to fully represent the non-stationary stochastic signal such as AE then STFT can provide quick and accurate results. The Kaiser Window function was chosen for its optimal

ability to compute the STFT. The Kaiser window has an additional ripple parameter β compared to other fixed windows which enable the designer to trade off the transition and ripple. In more details the Kaiser Window function is presented in Appendix 2.

The research in this thesis utilises the STFT as it is less computationally expensive than other time-frequency analysis techniques already discussed. In addition, STFT provides a good trade-off in terms of resolution in both frequency and time domains. The nature of the work carried out is not required to look into minuet phenomenon such as that described by Griffin (Griffin 2008) who utilises WPTs for micro phenomena such as the classification of cutting, ploughing and rubbing however for more macro phenomena utilises STFT to distinguish burn/no burn/chatter/no chatter and therefore this technique is acceptable for distinguishing varying levels of burn (grinding and laser irradiation).

4.3 Conclusion to signal processing

This chapter has presented the signal processing techniques which will be employed for feature extraction from sensored signals. The signal and its representation and the common classifications of the signal that appear during the grinding process were discussed at the beginning of this chapter. Before feature extraction, the signal should be normalised so that there is a uniform standard for comparison of the different features. The research focused on AE signals which are non-stationary stochastic signals. In the frequency spectrum analysis the FFT is very important but the limitation of it is that it does not have any time information about when the event occurred which is very important in

understanding the released elastic energy when material undergo deformation or fracture or, both.

The STFT technique is the most suitable tool to analyse non stationary stochastic AE signal in the time and frequency domains. The STFT uses the time-frequency distribution which represents the energy and power of waveform signals in two dimensional functions of both time and frequency which reveal the fault phenomenon and pattern for condition monitoring giving more accurate diagnostics. There is another signal processing technique conducted by using wavelet packets to extract features in time and frequency domains which has not been described in this chapter. By using wavelets, the original signal can be transformed into scale and wavelet coefficients. Such a series of coefficients represents almost all features of the original signal in terms of pattern recognition (Kiymik, Guler et al. 2005; James Griffin 2006).

Chapter 5: Investigation of thermal features of the AE signals

5.1 Introduction

This chapter aims to identify the thermal features of AE footprint signatures through laser thermal AE signal extraction and, grinding thermal AE signal extraction.

The objectives are as follows:

- Calculate the surface temperature on the alloy materials (Inconel718 and MarM002) due to laser irradiation
- Compare the surface temperature due to laser irradiation by both theoretical and experimental means
- Identify the high, medium and low temperatures through thermocouple temperature signals and correlate with extracted AE signal
- Using the STFT technique, identify the high, medium and low temperatures AE footprint signatures through laser thermal AE signal extraction
- Using the STFT technique, identify the burn and no burn AE footprint signatures through grinding thermal AE signal extraction

The laser irradiation is an ideal heat source. In this research, laser irradiation was used to control the intensity of laser power to gain the required temperature which is similar to the grinding temperature. Laser irradiation experiments were merged with thermocouple and AE sensing data which was described in the last

chapter and gives the framework to follow in order to carry out this proposed research. A model of surface temperature is introduced by theoretical calculation which is based on the laser irradiation interaction in different off-focal distances of the workpiece surface. This model should compare with the measured values of surface temperatures.

This chapter however looks at the thermal features of AE signal extraction. The energy spectral analyses will first examine the extracted AE signals in relation to laser elevated temperatures. Secondly, the AE signals obtained from grinding different depth of cut, examines the relation of grinding burn. The AE signals are high frequency and non-stationary stochastic signals. The STFT is the most suitable technique for feature extraction (Feng and Chen 2007). The STFT results will be presented in both the time and frequency domains.

All acquired signals from laser and grinding experiments will be investigated and correlated to provide a richer summary for the classification system.

5.2 Investigation of thermal features from laser irradiation

5.2.1 Thermal properties of materials

5.2.1.1 Heat capacity

Heat capacity (C) is a measurable physical quantity that characterises the amount of heat that is required to change a body's temperature by a given amount. Heat capacity is expressed in units of Joules per Kelvin.

The heat capacity indicates how much thermal energy a physical body can absorb for a change in temperature.

The specific heat capacity(c): The specific heat capacity is the amount of heat required to change a unit mass of a substance by one degree in temperature.

5.2.1.2 Thermal conductivity

The thermal conductivity k is the property of material that indicates its ability to conduct heat. The Fourier law states (Winterton 1999) that the rate of heat flow (Q) is proportional to the cross-sectional area (A) available for heat transfer and to the temperature gradient ($\frac{\Delta T}{\Delta L}$).

$$Q = -kA \frac{\Delta T}{\Delta L} \quad (W)$$

The minus sign means that the heat must flow in the opposite direction to the temperature gradient. It is also regarded as a consequence of the second law of thermodynamics. The constant of proportionality,k, is the thermal conductivity. The unit of thermal conductivity is measured in Watts per meter Kelvin $(W/m.K)$. Thermal conductivity for Inconel718 varied from 11.4 to 28.7 $(W/m.K)$.

5.2.1.3 Thermal diffusivity

In heat transfer analysis, thermal diffusivity is the thermal conductivity divided by volumetric heat capacity. It has the SI unit of (m^2/s).

$$\alpha = \frac{K}{\rho c_p}$$

Where:

k: thermal conductivity $(W/m.K)$

ρ : density (kg/m^3)

c_p: specific heat capacity ($J/kg.K$)

Thermal diffusivity measures the ability of a material to conduct thermal energy relative to its ability to store thermal energy.

5.2.2 The model of surface temperature

This research looks at the surface temperature based on the interaction of laser irradiation and workpiece surface to understand the thermal behaviour of materials. If the constant laser energy flux is absorbed at the workpiece surface and there is no phase change in the material, the equation of the heat flow in one dimension could be written as follows (Steen 2003; Liu, Chen et al. 2006):

$$T(0,t) = \frac{2I_0}{k}\eta\left(\frac{\alpha t}{\pi}\right)^{\frac{1}{2}} \qquad (5\text{-}1)$$

Where, $T(0,t)$ = Temperature of the material surface after time t

I_0= the density of laser peak power

k= thermal conductivity

α= thermal diffusivity

η = absorption coefficient

This could be determined through the following equations,

$$\eta = \frac{4\pi\delta}{\lambda_0} \qquad (5\text{-}2)$$

Where, λ_0= wave length of the laser

δ = is the skin thickness (or penetration depth).

$$\delta = \left(\frac{\lambda_0}{\pi\sigma\upsilon\mu_r\,\mu_0}\right)^{1/2} \quad (5\text{-}3)$$

Where,

σ= electrical conductivity

υ= the speed of light

μ_r= the initial permeability of metal

μ_0=the permeability of a vacuum

The absorption coefficient η can be calculated approximately as 19.16 % for Nd: YAG laser for nickel based alloy (MarM002 and Inconel718).

The laser peak power density, or peak intensity I_0, is a function of the off-focal distance f_2 then the equation could be written as follows(Steen 2003; Liu, Chen et al. 2006),

$$I_0 = \frac{2P_0}{\pi\omega_2^2} = \frac{2P_0}{\pi\left(\omega_1\frac{f_2}{f_1}\right)^2} = \frac{2E_0}{\pi t\left(\omega_1\frac{f_2}{f_1}\right)^2} \quad (5\text{-}4)$$

P_0=Laser Total Power

E_0= Laser Total energy

ω_1 = Initial Radian of laser beam

ω_2 = Laser spot radius

f_1= Laser focal length

f_2= Laser off focal length

5.2.3 The theoretical and measured models of surface temperature

According to the theoretical equations (5-1) to (5-4), the temperature rise against the off-focal length can be calculated as shown in Figure 5-1. These models of the surface temperature derived by equations (5-1) to (5-4) are then compared with the measured temperature model obtained from experiments and shown in Figure 5-1.

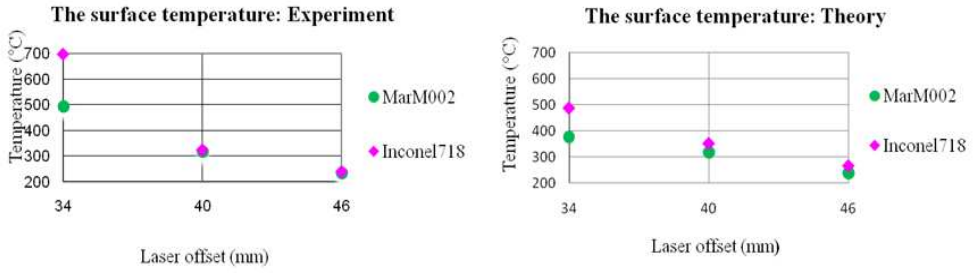

Figure 5-1: The surface temperature obtained from the experiment and theoretical calculations.

The measured values of surface temperature differ from the theoretical calculated values and off-focal distances this is due to thermal conductivity and off-focal length playing an important role in this difference. The thermal conductivity (Inconel718 and MarM02) is the property of a material that indicates its ability to conduct heat in addition with more intense heat errors that can occur as the temperature gradient rises rapidly and is difficult to control.

In addition, if the temperature of the material rises there will be an increase of electron energy exchanges through laser irradiation. The electrons are more likely to interact with the structure of those materials rather than oscillate and re-radiate (Steen 2003).

These materials (Inconel718 and MarM002) also have different absorption capacities for the radiation because they may require more energy to raise the temperature.

5.2.4 Analysis of features of AE signals from laser irradiation

The laser irradiation experiment provided a raw AE signal which was acquired in three different off-focal distances. The laser energy was 1.5 J and with a pulse width of 0.6 ms. In order to clearly observe the thermal energy distribution, the axis of the frequency is presented up to 1 MHz, which is the maximum response frequency of the AE sensor. The thermal features are extracted in terms of temperatures for analysis from the raw AE signal. Three off-focal distances are identified in laser irradiation in 34 mm, 40 mm and 46 mm which should produce high, medium and low temperatures on the workpiece materials. The features are extracted in order to analyse the high, medium and low temperatures of the AE data. The raw forms of the AE signal are extracted from 34 mm, 40 mm and 46 mm off focal distances and converted in time domain as shown in Figure 5-2 with the results obtained from Inconel718 materials. The signals were sampled at 5 MHz sampling rate.

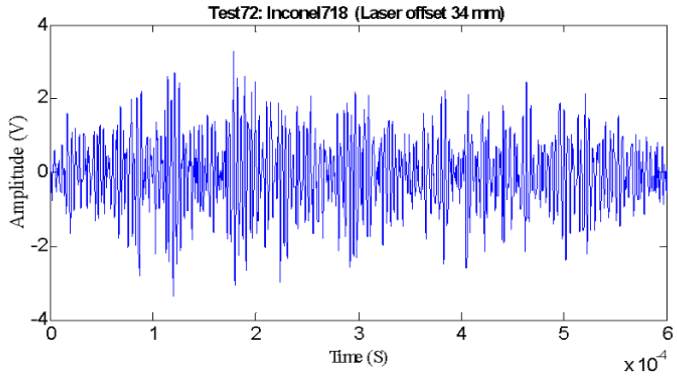

(a) Elevated temperature at 698°C (high)

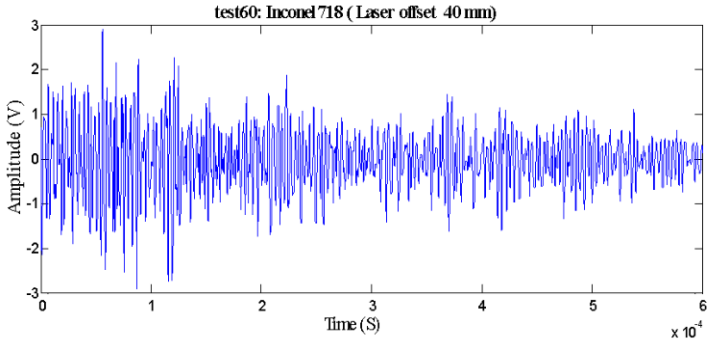

(b) Elevated temperature at 324°C (medium)

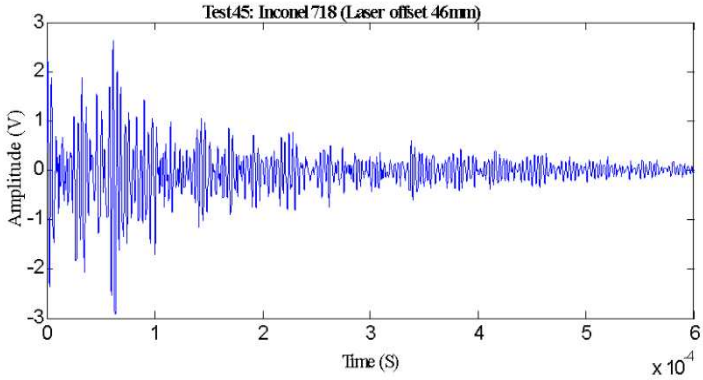

(c) Elevated temperature at 239°C (low)

Figure 5-2: Raw extracted AE signal (Materials: Inconel718).

The STFT signal processing techniques are applied to extract thermal features of AE data. The STFT is a form of joint time frequency analysis but it has a

major drawback, the window width selected is critical in determining the time and frequency resolution. The Kaiser window function was used to optimise the resolution. These raw AE signals are converted both in time and frequency domains through a STFT signal processing technique which is shown in Figure 5-3. Within the extracted AE signal from 34 mm off-focal distances to 40 mm and 46mm off-focal distances the properties were compared where both the higher and lower intensity frequency bands are much higher than others respectively from the smaller to the larger off-focal distance.

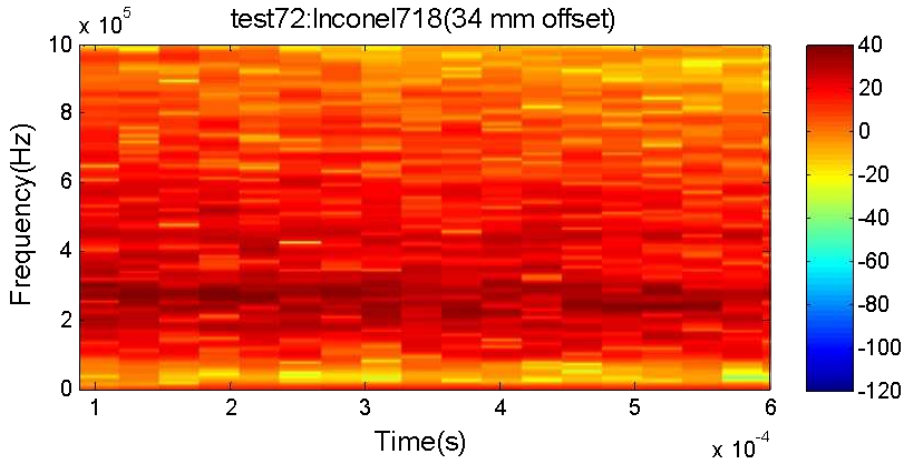

(a) Elevated temperature at 698°C (high)

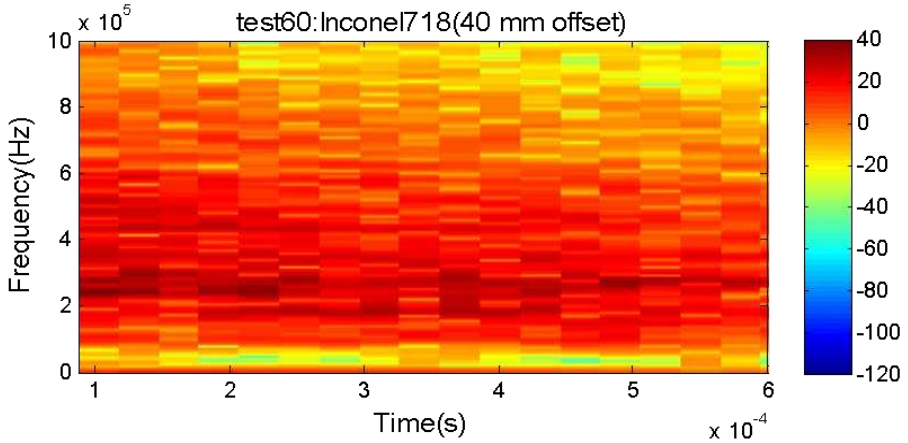

(b) Elevated temperature at 324°C (medium)

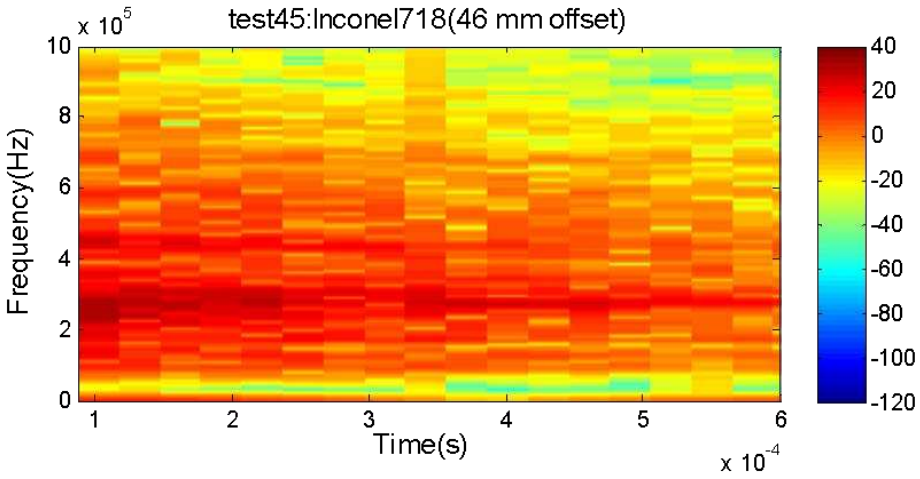

(c) Elevated temperature at 239°C (low)

Figure 5-3: The STFT of extracted AE signals (Material: Inconel718).

Figure 5-3 displays the STFT of raw extracted AE signals which have been obtained from the three off focal distances. The STFT computes the FFT peaks at periodic time intervals where varying frequency phenomenon intensities can be seen. Figure 5-3(a) displays the results of the STFT of the AE data extracted from 34mm off-focal distance whereby the intensity of frequencies are higher than in Figure 5-3 (b) and Figure 5-3 (c). High temperature changes cause the intensities in the AE signals to increase. In comparison to STFT, the FFT of extracted AE signals are presented in Figure 5-4 (a) high temperature (698°C), (b) medium temperature (324°C) and (c) low temperature (239°C).

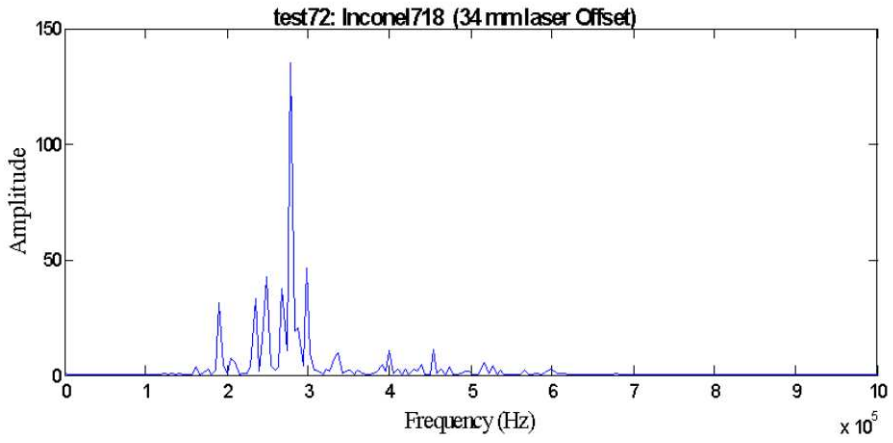

(a) Elevated temperature at 698°C (278kHz)

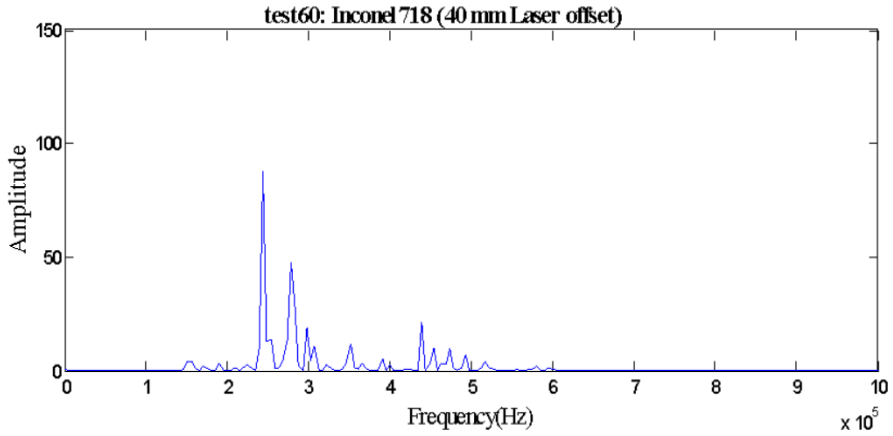

(b) Elevated temperature at 324 °C (244 kHz)

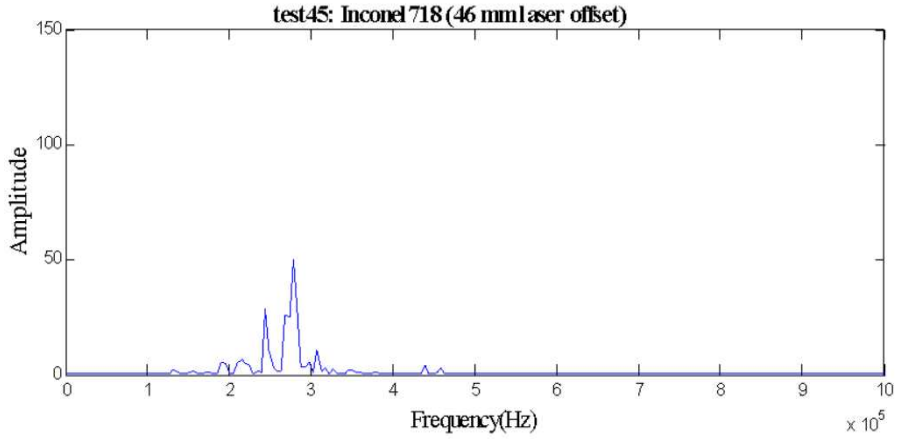

(c) Elevated temperature at 239°C (278 kHz)

Figure 5-4: The FFT of extracted AE signals (Materials: Inconel718).

Figure 5-4 shows the energy of the AE intensity of frequency component is higher due to higher temperature in (a) than in (b) and (b) is higher than (c). AE features at 34 mm laser off-focal distances presented in Figure 5-4(a). When the temperature was 698℃, the major features appeared at 190, 234, 249, 278, 297, 517 kHz and the highest peak was observed at 278 kHz.

AE features under 40mm laser off-focal distances presented in Figure 5-4(b). When the elevated temperatures were 324°C, the major features appeared at 244, 278, 351, 440, 517, 581 kHz and the highest peak was observed at 244 kHz.

AE features under laser irradiation of 46mm off-focal distances presented in Figure 5-4(c). When the elevation temperature was 239°C, the major features appeared at 244, 278 kHz and were much lower in intensity.

The laser irradiation on MarM002 materials: The raw forms of the AE signal are extracted from 34 mm, 40 mm and 46 mm off-focal distances as shown in Figure 5-5.

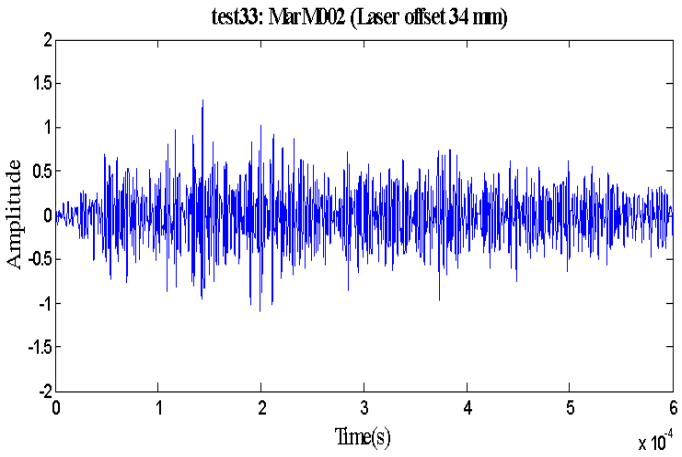

(a) Elevated temperature at 493°C (high)

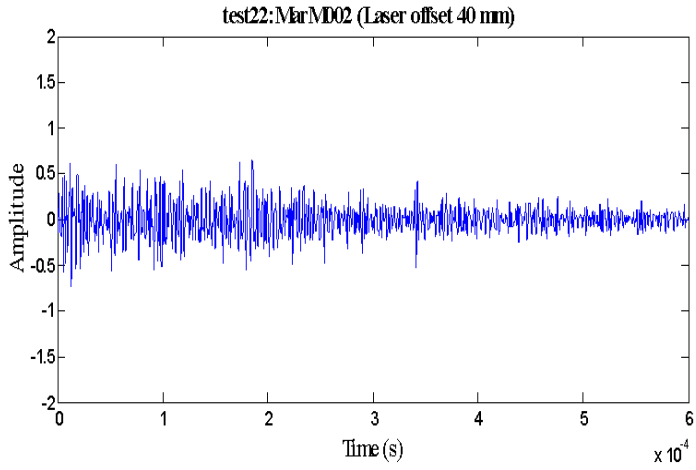

(b) Elevated medium temperature at 318°C(medium)

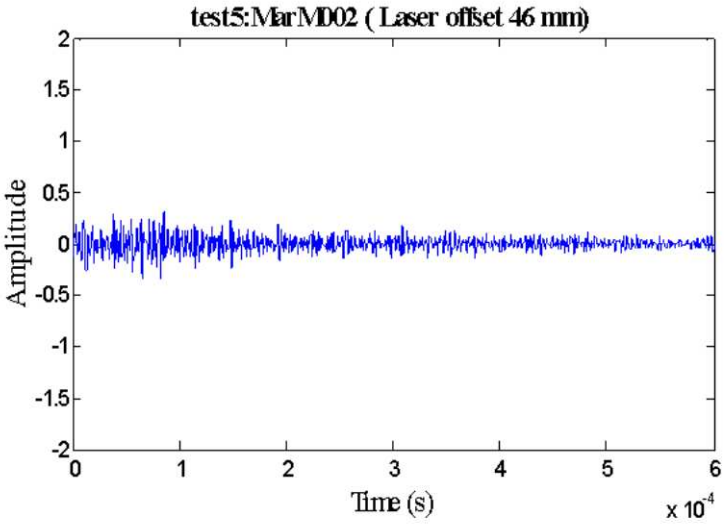

(c) Elevated low temperature at 235°C k(low)

Figure 5-5: The time series plots of raw extracted AE signals (Material: MarM002).

These raw forms of AE signals for MarM002 are converted to time and frequency components using STFT and presented in Figure 5-6. In the AE signal extracted from 34 mm off-focal distances compare to AE signal 40 mm

and 46 mm off-focal distances both the higher and lower intensity frequency bands are much higher.

The experiments using STFT clearly revealed the intensity that the AE signal, extracted from 34 mm off-focal distances compared to the AE signals of 40 mm and 46 mm for off-focal distances, both the higher and lower intensity frequency bands are much higher. The high temperature changes on the MarM002 materials caused the AE signals to have a different intensity.

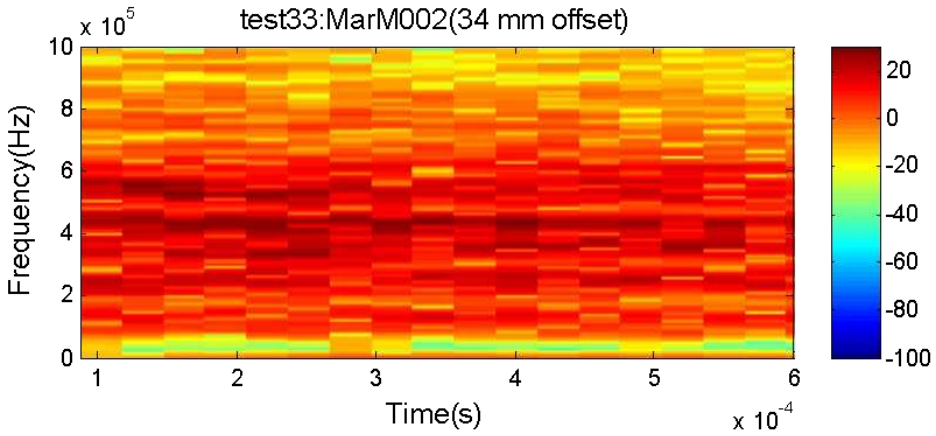

(a) Elevated temperature at 493°C (high)

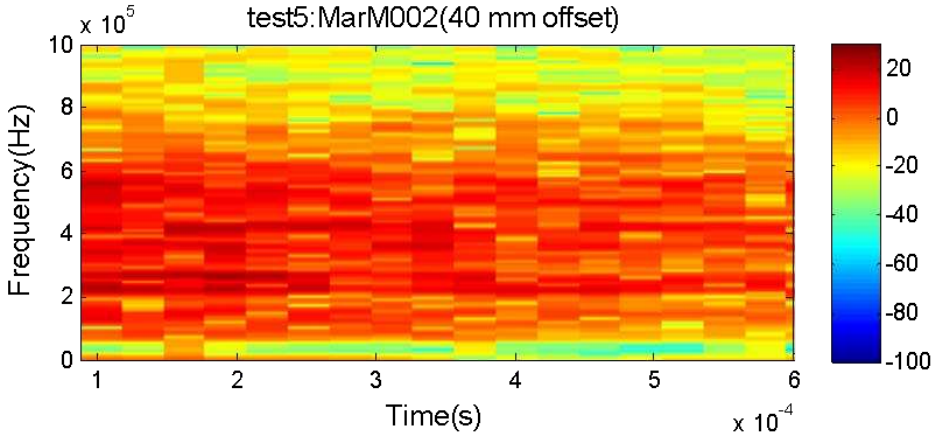

(b) Elevated temperature at 318°C (medium)

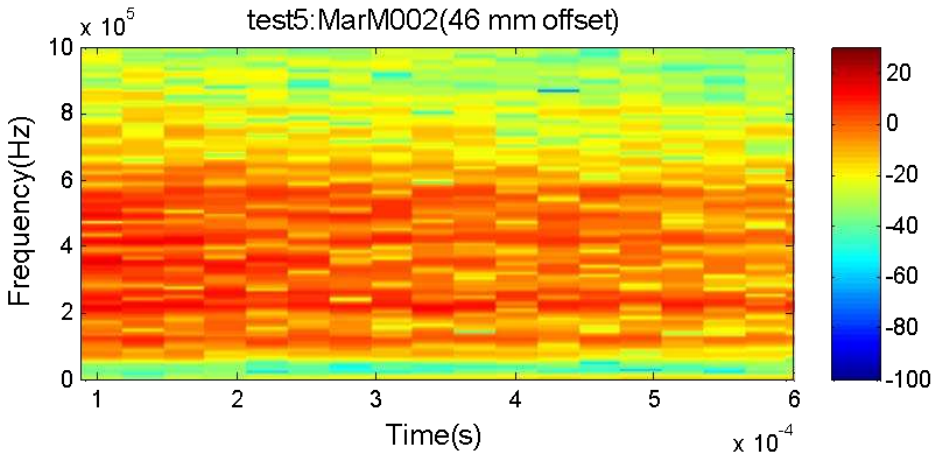

(c) Elevated temperature at 235°C (low)

Figure 5-6: The STFT of extracted AE signals (MarM002).

In comparison to STFT, the FFT of extracted AE signals in high, medium and low temperatures have been obtained from three off-focal distances are presented in Figure 5-7.

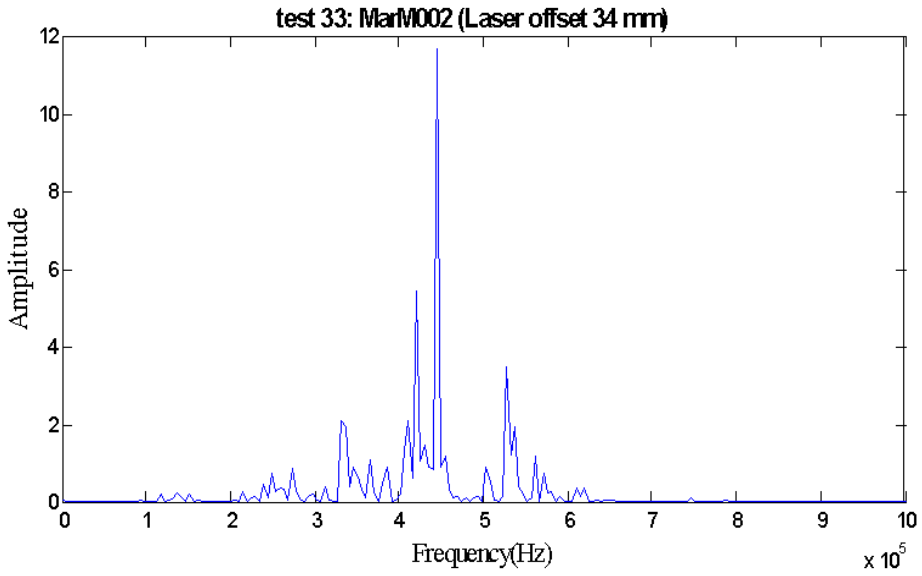

(a) Elevated temperature at 493 °C (444 kHz)

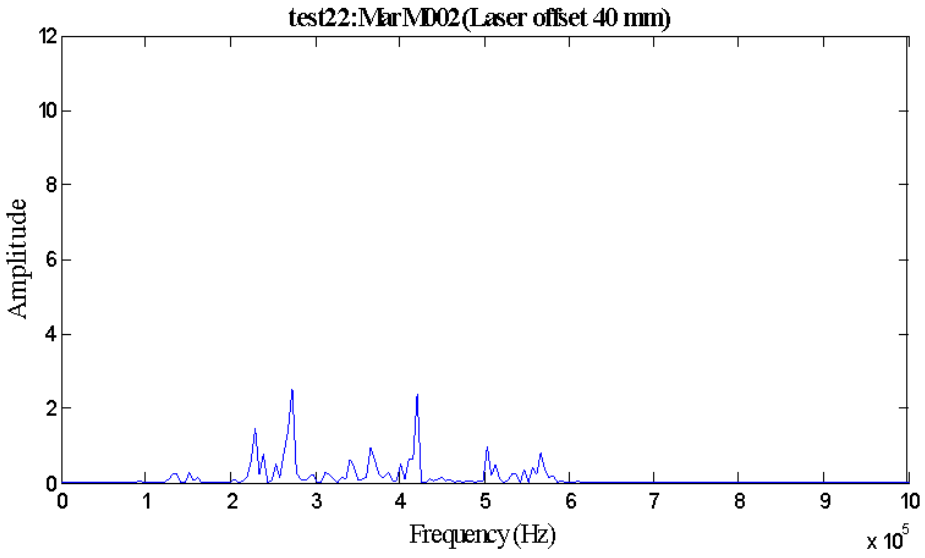

(b) Elevated temperature at 318°C (273kHz)

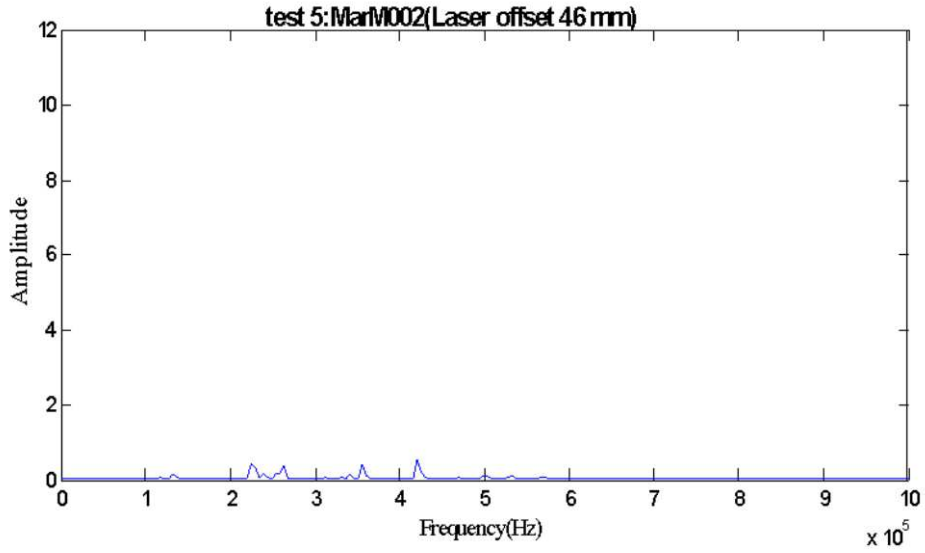

(c) Elevated temperature at 235 °C(420kHz)

Figure 5-7: The FFT of extracted AE signals (Materials: MarM002).

The FFT of AE features under 34 mm off-focal distances due to laser irradiation are presented in Figure 5-7. When the elevation temperature was 493℃ for MarM002, the major features appeared at 273, 332, 420, 444, 527 kHz frequency bands and the highest peak was observed at 444 kHz due to the high temperature.

The FFT of AE features under 40 mm laser off-focal distances due to laser irradiation is presented in Figure 5-7(b). When the elevation temperature was 318°C, the major features appeared for MarM002 at 229, 273, 502 kHz frequency bands and the highest peak was observed at 273 kHz due to the medium temperature.

The FFT of AE features under laser irradiation of 46mm off-focal distances is presented in Figure 5-7(c). When the elevation temperature was 235°C for MarM002, the major feature appeared at 356 kHz and 420 kHz with much lower intensity.

5.2.5 Discussion and analysis on laser thermal features of AE signal

In order to distinguish the intensity of energy distribution, the axis of frequency for STFT and FFT are presented up to 1000 kHz, which is the maximum response frequency of the AE sensor. The intensity of the frequency component is higher due to the off-focal points of a laser beam closer to the workpiece.

The results demonstrated that the spectra are separated in different frequency bands from high to low temperature changes. The experiments reveal that the energy distribution of the AE signal of thermal expansion under high temperatures have much higher intensities for both MarM002 and Inconel718. In the medium temperature, most of the features appeared with a lower intensity than the intensity under the high temperature conditions. In the low temperature, most of the features appear in the frequency range which has a much lower intensity than the intensity under high and medium temperature conditions.

These results of laser thermal feature should be similar to the grinding thermal feature. In order to verify this, the thermal features of the AE signal are investigated next.

5.3 Investigation of thermal features in grinding

This research looks at the investigation of extracted thermal features of AE signals from grinding. These features contain burn and no burn signatures in the form of AE signals relating to changing depth of cuts. The burn phenomenon consists of a compact burst of high amplitude which often concentrates at the end of each signal due to a deeper material change to the workpiece. According to Malkin thermal damage occurs at the end of the cut, as the wheel is about to break through, since no workpiece material remains to conduct heat downwards (Malkin 1989). In this piece of research, the workpiece materials are ground from 0.02 mm to 0.2 mm depth of cuts with the condition as shown in Table 3-5 in order to identify burn and no burn AE footprint signatures.

5.3.1 Burn and No burn analysis on Inconel718 materials

In order to analyse burn and no burn phenomena, a burn signal as an example at a 0.2 mm depth of cut and a no burn signal at 0.02 mm depth of cut for Inconel718 materials are presented in Figure 5-8. Both signals are displayed in the time domain as time series plots. Both of the signals are sampled with a sampling rate of 5 MHz.

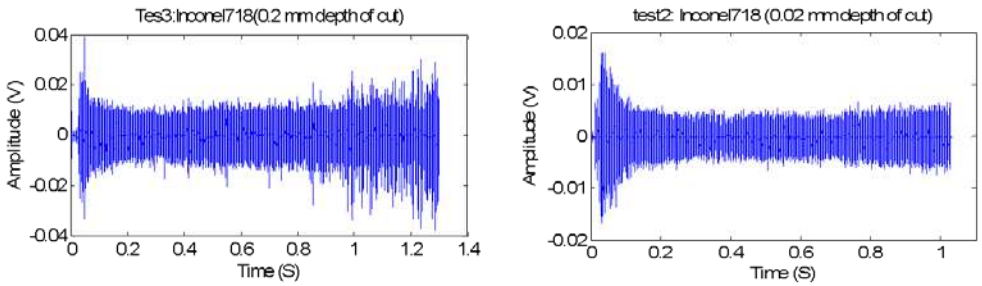

Figure 5-8: The time series plot of burn and no burn phenomena across the total extracted signal (Material: Inconel718).

The thermal features of AE data were extracted from in their raw form in the time domain relating to the different burn or no burn phenomena. The extracted AE data was then converted to both the time and frequency domains using STFT which is presented in Figure 5-9.

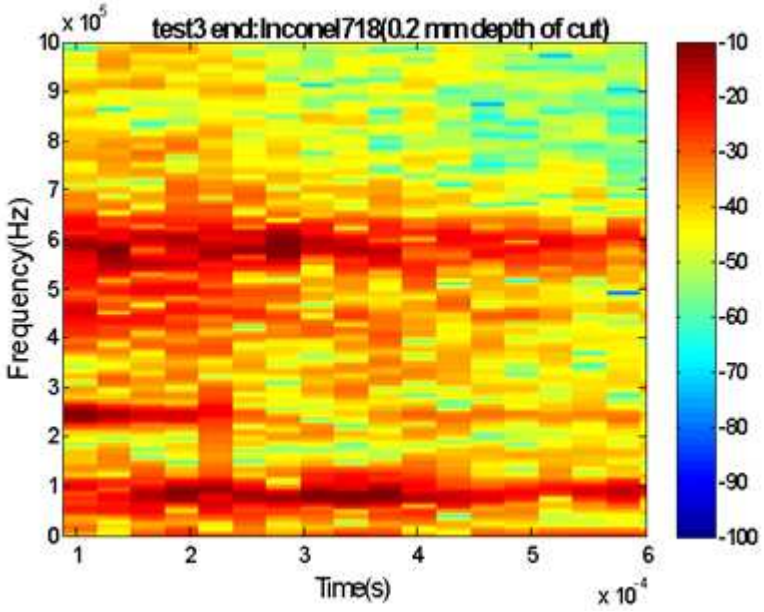

(a) With grinding burn

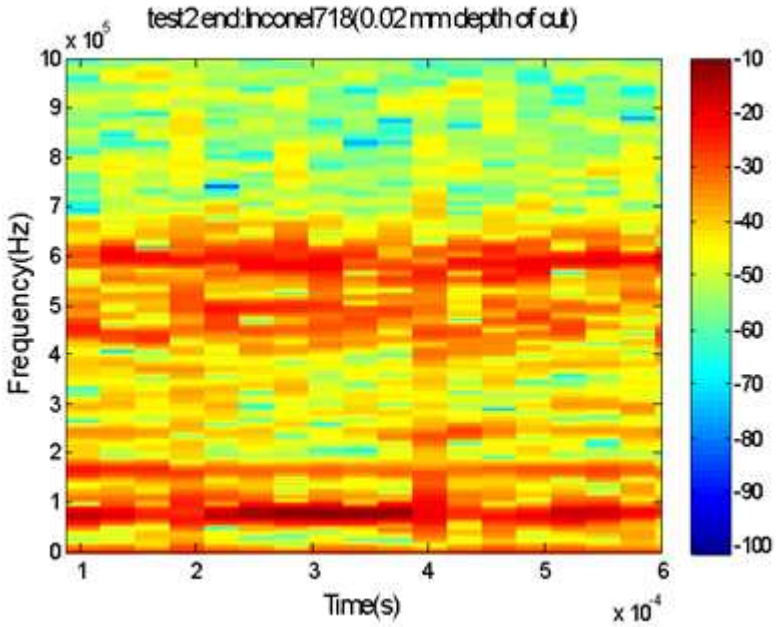

(b) Without grinding burn

Figure 5-9: The STFT of AE signal for burn and no burn phenomena (Material: Inconel718).

Looking at Figure 5-9 it is possible to see that the burn phenomena has intense amplitudes at 50 kHz to 100 kHz, 200 kHz to 300 kHz and 500 kHz to 600 kHz frequency bands. In comparison to STFT the thermal features of raw AE data were converted to frequency domain using FFT. The results obtained from FFT are presented in Figure 5-10.

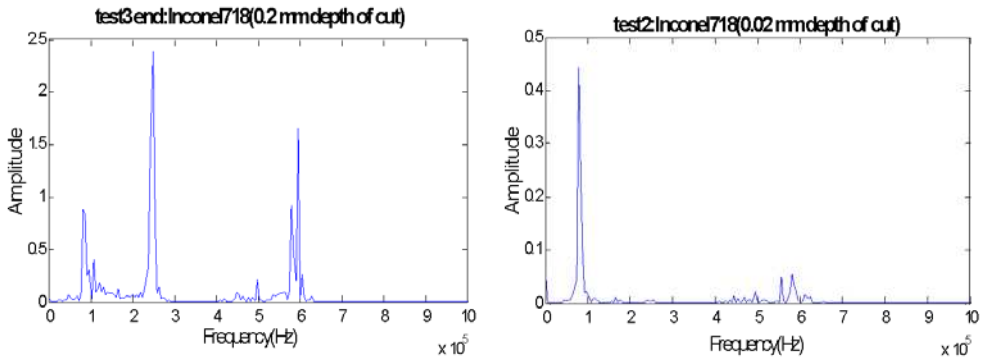

Figure 5-10: The FFT of AE signal in 0.2 mm and 0.02 mm depth of cuts. (Materials: Inconel718).

When the depth of cut was 0.2 mm, the major features appeared at 83 kHz, 249 kHz and 596 kHz. When the depth of cut was 0.02 mm, the major frequency appeared at 78 kHz, 556 kHz and 581 kHz. There was a higher energy peak at 249 kHz when the grinding burn occurred in 0.2 mm depth of cut. It was observed that the peaks in the high frequency range were generally lower than those in the low frequency range. Under the grinding burn conditions the maximum peak values in the high frequency range were only 64% of the maximum peak of the total frequency spectrum. This revealed that the thermal expansion caused by the grinding burn temperature was intense when grinding burn occurred. Under normal grinding conditions the high energy peaks do not exist in the high frequency range (> 500 kHz).

Figure 5-11 presented the scanning electron microscope (SEM) images of Inconel718 (workpiece) material after grinding. An energy dispersive X-ray (EDX) facility attached to the SEM is used for analysing the workpieces. The images are obtained from grinding experiments in 0.02 mm and 0.2 mm depth of cuts where Al_2O_3 grinding wheels are used to grind the workpiece. Figure 5-11(a) shows a SEM image of a no burn situation (0.02 mm depth of cut). Figure 5-11(b) shows a SEM image of a similar ground Inconel718 workpiece surface but also showing the burn case (0.2 mm depth of cut).

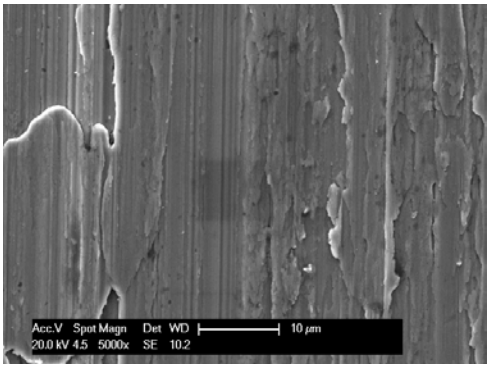

(a) Depth of cut: 0.02 mm , wheel speed:55 mm/s, feed rate: 1m/min, coolant: No. material:Inconel718

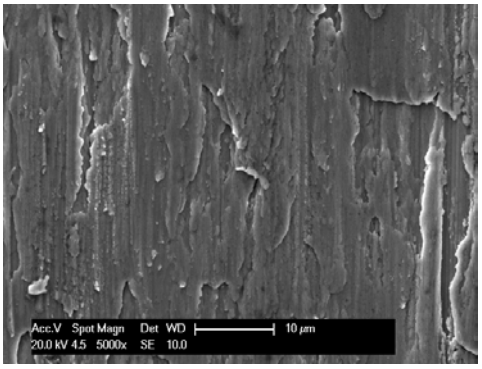

(b) Depth of cut: 0.2 mm , wheel speed:55 mm/s, feed rate: 1m/min, coolant: No. material:Inconel718

Figure 5-11: SEM images of Inconel718.

The grinding wheel abrasive (Al_2O_3) has a higher melting point (2072°C) than Inconel718 (1336°C). The microstructure of the workpiece surface changed due to the high temperature as a result of grinding burn. Some grit from the grinding wheel is fractured and leaves a portion of the grit in the surface. The fractured portion is pushed across the surface during grinding. The SEM image of Figure 5-11(b) has a higher percentage (%) of grits embedment than Figure 5-11(a) which confirmed severe burn in the burn sample.

5.3.2 Burn and no burn analysis on MarM002 materials

The thermal feature of AE data are extracted from the raw form of AE signals which are obtained during grinding MarM002 at different depth of cuts. Figure 5-12 displays a raw form of AE signals for the 0.2 mm depth of cut and no burn signals for the 0.02 mm depth of cut. In order to analyse, burn and no burn signatures are displayed in time domains as time series plots with a 5 MHz sampling rate.

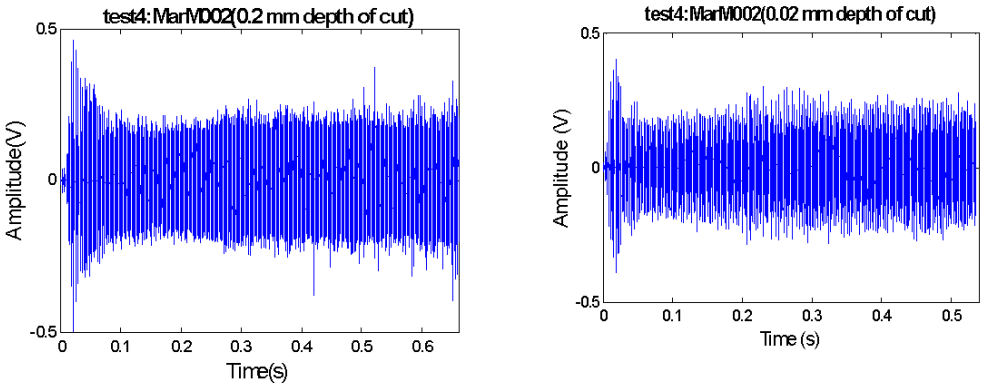

Figure 5-12: The time series plots of burn and no burn signals (MarM002 materials).

These raw forms of AE signals are extracted from the end section of the signals displayed in Figure 5-12 in order to convert into both the time and frequency domains through the use of STFT. The STFT results are presented in Figure 5-13. The STFT revealed that the AE signals from the 0.2 mm depth of cuts have higher intensity frequency bands than the intensity at the AE signals of 0.02 mm depth of cut.

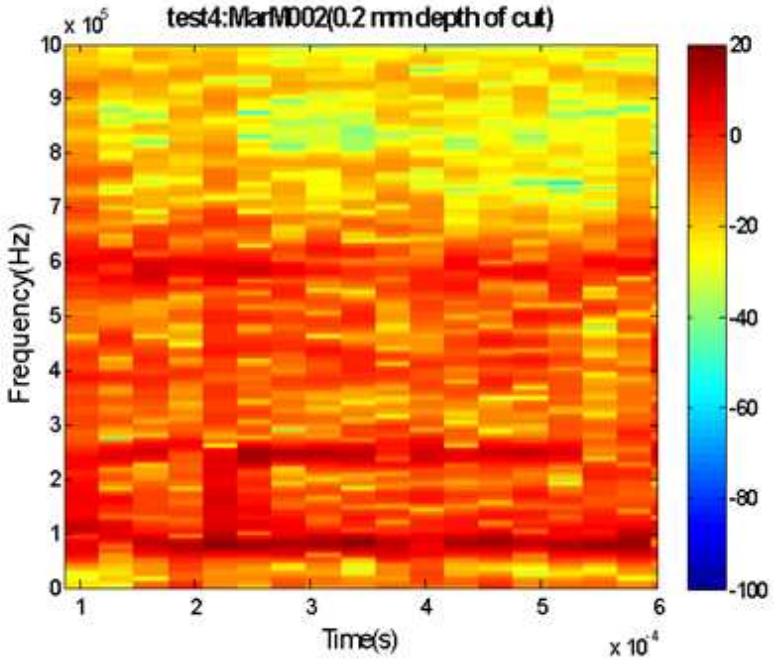

(a) With grinding burn

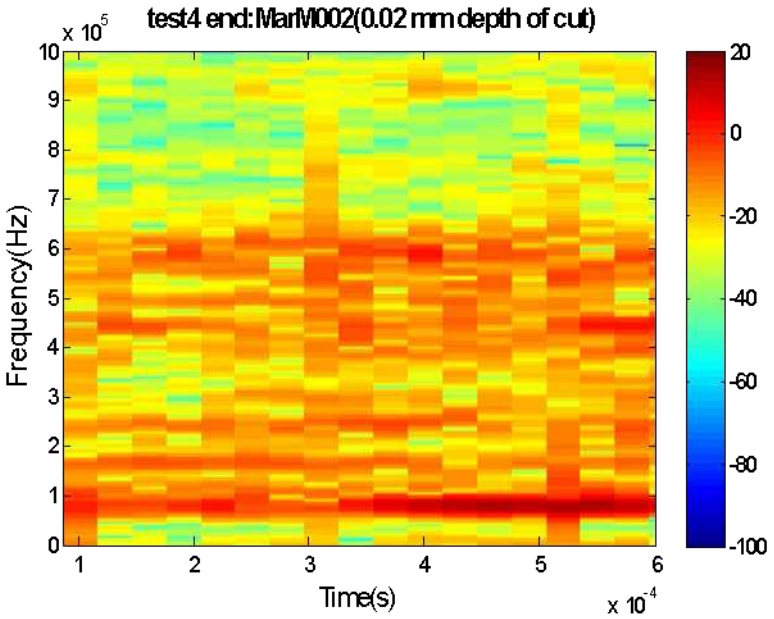

(b) Without grinding burn

Figure 5-13: The STFT of burn and no burn signatures on AE signal (MarM002 materials).

In comparison to STFT, the FFT of the extracted AE signals are shown in Figure 5-14 obtained from 0.2 mm depth of cut and 0.02 mm depth of cut respectively. The results show the energy of the AE intensity of frequency components are higher due to severe burn at the 0.2 mm depth of cut sample compared with the 0.02 mm depth of cut sample.

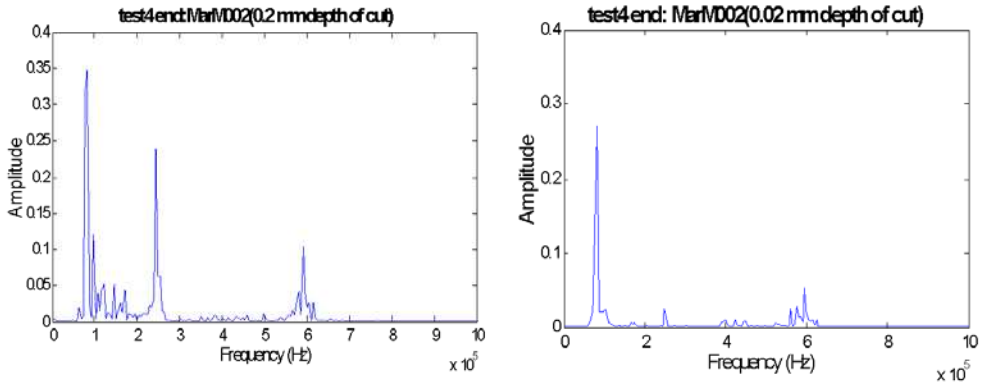

Figure 5-14: The FFT of AE signal on MarM002 materials.

AE features under 0.2 mm depth of cut concentrated between 50 to 150 kHz, 240 to 350 kHz and 550 to 650 kHz frequency range. The major features that appeared in the low frequency range were at 83 kHz, 244 kHz and in the high frequency range (> 500 kHz) were at 590 kHz. Under the grinding burn conditions, the maximum peak values in the high frequency range were 64% of the maximum peak in the total frequency spectrum. This provided evidence that thermal expansion due to grinding burn is intense in the sample of MarM002 with 0.2 mm depth of cut. When the depth of cut was 0.02 mm, the major frequency feature appeared at 83 kHz. The peaks existing in the high frequency range (> 500 kHz) were much lower, which confirmed that there was no burn or may have had slight burn within the workpiece surface during grinding of the 0.02 mm depth of cut.

In order to verify AE burn and no burn signature the SEM images of MarM002 are presented in Figure 5-15. The images were obtained from the grinding experiments at the 0.02 mm and 0.2 mm depth of cuts where Al_2O_3 grinding wheels were used.

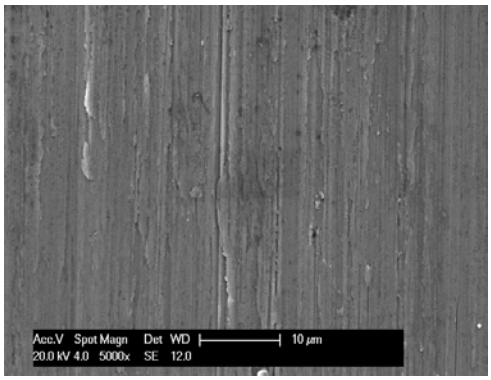

(a) Depth of cut: 0.02 mm , wheel speed:55 mm/s, feed rate: 1m/min, coolant: No. material:MarM002

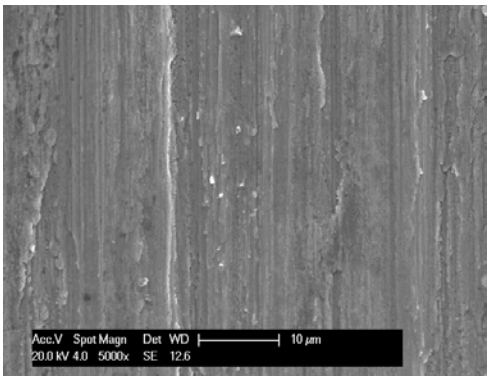

(b) Depth of cut: 0.2 mm , wheel speed:55 mm/s, feed rate: 1m/min, coolant: No. material:MarM002

Figure 5-15: SEM images of MarM002.

Figure 5-15 (a) is the image of a no burn case (0.02 mm depth of cuts). The SEM micrograph of a ground surface presented in Figure 5-15 (b) shows that the microstructure of the surface changed (melted) due to very high temperature during grinding. It is also possible to see that the grit is fractured and a portion of the grit (as white spots) is left on the surface. The wear types are known as grain fracture which is displayed in the images.

5.3.3 Discussion on grinding thermal features of burn and no burn

In the grinding burn condition, it is possible to see that the burn AE intensities were much greater than that of normal grinding AE intensities. Inconel718 and MarM008 are nickel based alloys which are very hard materials. Inconel718 hardness is known to be HRC50. It is very difficult to burn these materials due

to their hardness and heat capacity properties. The main reason for burn is the continuous high temperatures in the grinding zone due to too much material being removed at any one time. This is not the only reason for grinding burn. There may be other factors involved contributing to grinding burn. The AE waves are often mixed with other sources such as grain fracture, chatter vibration and white noise. The main challenge is how to extract thermal features of the AE signal and compare it to grinding burn for the various AE sources. The literature indicates at the onset of grinding burn, the grinding force and rate of wheel wear increases very sharply which has a direct effect on the deterioration of workpiece surface roughness (Kwak and Song 2001). The results demonstrated by using STFT from Figures 5-12 and 5-13 that when grinding burn occurred, the high frequency features of the AE signals were much stronger than those of the normal grinding condition. The FFT slice further verified the STFT signal analysis of the AE footprint burn signatures.

5.4 Results, analysis and conclusion

The main concern of this research was to control the intensity of laser power for the required temperature that is similar to the grinding zone temperature. The surface temperatures of both the calculated and measured values are demonstrated in Figure 5-1. The surface temperature obtained from 34 mm, 40 mm and 46 mm off-focal distances laser experiments produced a reasonable agreement with that obtained from theoretical calculations.

In this piece of work, the thermal features of AE signals in laser irradiation were compared with the thermal features of AE signals in grinding. The STFT was applied to extract features from the raw form of AE signals. The thermal

features of Inconel718 under 34 mm off-focal distances are concentrated due to high temperature (698°C) between 190 kHz and 600 kHz frequency bands. The thermal features of MarM002 are concentrated due to the high temperature (493°C) between 244 kHz to 581 kHz frequency band. The investigation revealed that the thermal expansions due to laser irradiation under high temperatures have the higher intensities.

AE features at 40 mm off-focal distance produce 324°C temperature (medium), the major features appeared for Inconel718 at 244 to 581 kHz frequency bands and for MarM002 at 318°C gives 229 kHz to 502 kHz frequency bands. The energy in the high frequency region reduces compared to the energy under high temperature.

AE features at 46 mm off-focal distances, the elevation temperature for Inconel718 was 239°C, the major features appeared at 244 to 278 kHz frequency bands. When the elevation temperature for MarM002 was 235°C, the major features appeared at 356 and 420 kHz. The investigation revealed that the thermal expansion due to laser irradiation under a low temperature have much lower intensities.

This investigation demonstrated that STFT is a useful technique to distinguish the frequency bands occupied by burn and no burn phenomena through thermal features of AE grinding burn. The work demonstrated that 0.2 mm depth of cut for Inconel718 under the grinding burn condition, the major features appeared in the low frequency range at 83 kHz and 249 kHz and in the high frequency range at 596 kHz. In the normal grinding condition under 0.02 mm depth of cut,

the major features appeared at 78 kHz frequency band in the low frequency range.

The work also demonstrated that with a 0.2 mm depth of cut for MarM002 under grinding burn condition, the major features appeared in the low frequency range at 83 kHz to244 kHz and in the high frequency range at 590 kHz. In normal burn conditions, using an under 0.02 mm depth of cut, the major features appeared at 83 kHz frequency band in the low frequency range (< 500 kHz).

The result concluded that the thermal features of AE signals due to laser irradiation are similar to the thermal features of AE signals in grinding irrespective of heat sources. The result demonstrated in this chapter that laser irradiation is an ideal heat source for simulating grinding temperatures. This phenomenon may instill confidence for grinding temperature identification using laser irradiation sensing techniques.

The next chapter describes the use of pattern recognition of AE signal features for grinding temperatures pattern classification through laser thermal AE features in terms of an intelligent diagnostic technique.

Chapter 6: Feature extraction using intelligent diagnostic technique

6.1 Introduction

This chapter aims to describe the use of pattern recognition of AE signal features for grinding temperature based on the pattern classification using laser thermal AE features and provide warning if burn or the onset of burn exists. The Multi-layer perceptron (MLP) neural networks with the back-propagation learning rule are chosen for classification. NN is chosen in this piece of research because it is easy to use as a pattern recognition tool and it can be confidentially used as a robust classifier with the highest correct classification rate compared with other non hybrid classifiers (Kwak and Ha 2004; Griffin and Chen 2007).

The objectives are as follows:

- Determine the neural network structure to best represent the problem space
- Design the training data set based on high, medium and low temperature signals through laser thermal AE signal extraction
- Design the testing data set based on burn and no burn signals through grinding thermal AE signal extraction
- Select the learning rate and momentum values
- Train NN to classify high, medium and low temperatures due to the phenomena provided by laser thermal features of AE signal extraction
- Test the NN results in a generalised manner to classify the grinding temperatures due to severe burn, normal burn and slight burn or no burn phenomena through grinding thermal features of AE signal extraction
- Analyse the wheel wear based on the classification results

The thermal features of AE signals due to laser irradiation and the thermal features of AE signals due to grinding are discussed for both materials in chapter 5. More signal features and more details normally provide explicit

recognition of the event for any kind of process monitoring. However, a huge number of features contain mutual information of different events, which may cause some misleading results. The question is which features should be kept and which features should be discarded? Pattern recognition is mainly used for these complex and uncertainty issues (Fu, Hope et al. 1998). The artificial neural network (ANN) is a mature proven pattern recognition tool in terms of accurate classifications for a multi dimensional data space. NN can capture domain knowledge from examples, they do not archive knowledge in an explicit from such as rules or databases and can readily handle both continuous and discrete data giving a generalisation capability (Teti, Jemielniak et al. 2010).

Every NN that is used to classify non-linear data consists of at least one hidden layer in addition to the input and output layers. These layers are inter-connected according to modifiable weights by links between the layers. The most popular methods for training such multilayer networks are based on gradient descent minimising the error, which is known as the back propagation algorithm or the generalistic delta rule (Duda, Hart et al. 2001).

Back propagation is one of the common methods for supervised learning of a multilayer neural network. Supervised NN means the use of training data for classification on the converse, unsupervised is where no training data is used and distance measures are used instead such as that seen in clustering algorithms. In unsupervised learning, it doesn't require external input. An unsupervised NN learns the data for itself using new information available. The network learns automatically to categorise them in groups of similar features (Jardine, Lin et al. 2006).

This chapter describes grinding temperature identification due to burn using pattern recognition based on a given set of parameters. A classifier model and its associated training algorithm are introduced, all are associated with pattern recognition. A NN model has been designed for the classification of high, medium and low temperatures due to burn during the grinding process. This NN model has been supervised and trained by the feed forward NN system with the back-propagation learning rule. Chapter 5 shows that the STFT of an AE signal can represent different phenomena due to high, medium and low level temperatures experienced during laser irradiation and this data is transferred into input parameters for the classification. The testing AE data consisted of the grinding thermal AE data which can represent different characteristics of burn and no burn phenomena and can be used for verification. An algorithm known as gradient descent algorithm was presented to ANN with the backpropagation learning rule to see the effect in convergence performance. Another algorithm resilient backpropgation was used to test a reasonable number of learning rules and attempt to establish an optimum network.

6.2 The basic structure of a MLP neural network

The Multilayer perceptron is a feed-forward neural network. It consists of a number of neurons which are connected by modifiable weighted links in a hierarchical structure.

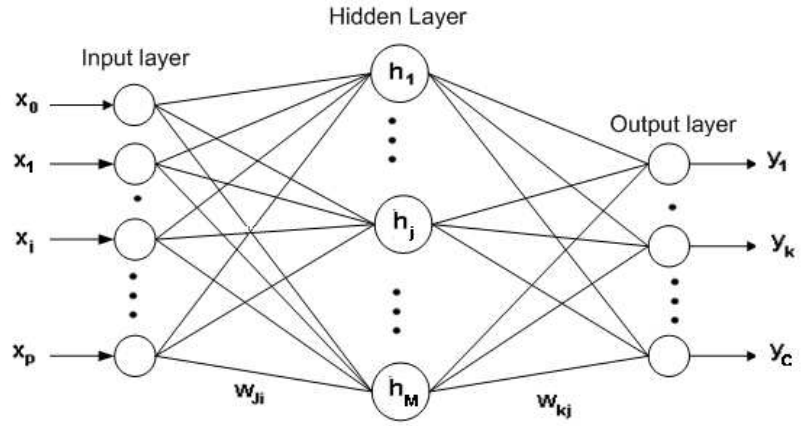

Figure 6-1: The multilayer perceptron structure (Duda, Hart et al. 2001; Zaknich 2003).

Each signal travelling along the link is multiplied by the connection weights as shown in Figure 6-1. The bias term x_0 provides a balance to the origin of the activity function which could be regarded as an extra weight term with the input fixed at one (L.H.Chiang 2001). The basic approach to learning is to start with an untrained network as shown in Figure 6-1. A training pattern is presented to the input layer, the signal travels through the net and the output is determined from the output layer. This type of supervised learning consists of presenting an input pattern and changing the network parameters to bring the actual parameter closer to the given target values. Supervised learning is essentially the user supplying training data to the recognition system to base its hypotheses on. The converse is an unsupervised network that uses input measures to base its

hypotheses on. In NN learning, these errors are compared with the desired target values. This error or criterion function is some scalar function of the weights and is minimised as the network outputs tend towards the desired outputs.

Thus the following equation is true for training, the training error of the weights E(w) linked to the input patterns is updated every gradient time step change with the sum squared difference between the desired output t_k and the actual output y_k see equation 6-1 below for mathematical representation:

$$E(w) = \frac{1}{2}\sum_{k=1}^{c}(t_k - y_k)^2 \qquad (6\text{-}1)$$

Where the network output vectors of length c and w represents all the weights in the network.

The backpropagation learning is based on gradient descent. The idea of gradient descent is to make a change in the weight proportional to the negative of the derivative of the error, as measured on the current pattern, with respect to each weight see equation 6-2 for more details (McClelland and Rumelhart 1989):

$$\Delta w = -\eta \frac{\partial E}{\partial W} \qquad (6\text{-}2)$$

Where η is the learning rate, and indicates the relative size of change in weights. Both equations above update in a step wise fashion that changes the weight space and lowers the criterion function. This iterative algorithm requires taking a weight vector at each iteration k and updating it as,

$$w(k+1) = w(k) - \eta \frac{\partial E}{\partial w} \qquad (6\text{-}3)$$

Where k indicates a particular pattern presentation (Duda, Hart et al. 2001).

6.2.1 The training data set

The training dataset should include all the data belonging to the problem space albeit some data removed and used as unforeseen cases to test the generalisation of the network. This data is used to update the weights during training of the network. The training dataset of the NN uses the laser thermal features of AE data to the neural network. The testing dataset to the NN uses the grinding thermal features of AE data. This input dataset consists of thermal features of AE signal samples extracted from 34 mm, 40 mm and 46 mm laser off-focal distances which are concatenated together in a matrix format. The input data with their respective features is realised in a matrix as $P(m \times n)$ presented in equation (6-4). This matrix is ready after normalization for input to the ANN system.

$$P(m \times n) = \begin{bmatrix} p_{11} & p_{12} & \cdots & p_{1j} & \cdots & p_{1n} \\ p_{21} & p_{22} & \cdots & p_{2j} & \cdots & p_{2n} \\ \cdots & & & & & \\ p & p_{i2} & \cdots & p_{ij} & \cdots & p_{in} \\ \cdots & & & & & \\ p_{m1} & p_{m2} & \cdots & p_{mj} & \cdots & p_{mn} \end{bmatrix} \qquad (6\text{-}4)$$

$$T(m) = [t_1 \quad t_2 \quad \cdots t_i \quad \cdots \quad t_m] \qquad (6\text{-}5)$$

Where $T(m)$ is a target vector. The target is a desired output of the given input to the network. When the learning is supervised it is presenting the given input data and changing the network parameters to bring the actual outputs closer to the desired target values. The values for the target are chosen by setting T to 3, 2 and 1 relating to high, medium and low temperatures. Each element (column) of the target vector is defined as a class which corresponds to an individual training sample case when the test samples are input into the network this will

then relate to a target output case of ANN (if the desired output is the same as the actual then this is termed as a correct classification).

AE data extracted in 34 mm off focal distances defined as the class of high temperatures and is associated with the target value of 3, AE data extracted in 40 mm off-focal distance is defined as a class of medium temperatures and is associated with the target values of 2 and finally, the AE data extracted in 46 mm off-focal distance is defined as a class of low temperatures and associated with the target value of 1. The AE data signals are extracted to signify the features from laser irradiation and grinding experiments. To signify the features and avoid misclassification in NN presentation, the AE data should be normalised. The MATLAB's subroutines **prestd** is used before training ensuring all input values to the NN are normalised so that the mean is 0 and the standard deviation is 1.

The normalization matrix (see equation 6-6) could be written after normalization using the following syntax which is ready for training the NN.

$$X(m \times n) = \begin{bmatrix} x_{11} & x_{12} & \cdots & x_{1j} & \cdots & x_{1n} \\ x_{21} & x_{22} & \cdots & x_{2j} & \cdots & x_{2n} \\ \cdots & & & & & \\ x_{i1} & x_{i2} & \cdots & x_{ij} & \cdots & x_{in} \\ \cdots & & & & & \\ x_{m1} & x_{m2} & \cdots & x_{mj} & \cdots & x_{mn} \end{bmatrix} \quad (6\text{-}6)$$

6.3 Training with backpropagation

The most popular method of training the feed forward neural network is to use the backpropagation learning rule. The objective of the training process is to minimise the mean sum-squared error using the backpropagation learning rule which tends towards correlating the training data and their output neuron values.

Considerations of the MLP structure are shown as an example in Figure 6-1. To achieve this objective of the training process the two sets of network weights need to be minimised simultaneously: the output layer weights w_{jk} and hidden layer weights w_{ji}.

Equation (6-7) shows that each hidden unit computes its sigmoidal activation function based on its inputs. This can be written:

$$h_j = f_j(\sum_{i=1}^{p} w_{ji} \, . \, x_i) = f_j(net_j) \qquad \text{for} \quad j=1,2.....M \qquad (6\text{-}7)$$

Each output unit computes its sigmoidal activation function based on the hidden unit signals as

$$y_k = f_k(\sum_{j=1}^{M} w_{jk} \, . \, h_j) = f_k(net_k) \qquad \text{for} \quad k=1,2.....c \qquad (6\text{-}8)$$

Network outputs y_k are a function of hidden outputs h_j and the weights w_{kj} between the hidden layer and the output. The output h_j are a function of the inputs x_i and the weights between the inputs and the hidden layer.

The summation of weights and bias values are multiplied by a log sigmoid transfer function in this research to give a neuron output. The log sigmoid and linear transfer functions used in the network are displayed in Figure 6-2.

(a) Log-Sigmoid Transfer Function (b) Linear Transfer Function

Figure 6-2: Displays the transfer functions used in the multi-layer ANN classifier (Demuth, Beale et al. 1994).

When using gradient descent, the local gradient of the error function is computed and the weights are then adjusted in the opposite direction of the gradient. This is the direction of the total weight changes which inherently makes the overall network error smaller. The partial derivatives and chain rule are used to calculate the contribution of each of the weights.

Change in error due to Output layer weights: Considering, first the hidden-to-output weights of w_{kj} because the error of w_{jk} is not explicitly dependent upon (Duda, Hart et al. 2001). The gradient of the error function with respect to each weight in the network is computed first over the change in error due to output layer. To compute the partial derivative of $\frac{\delta E_x}{\delta w_{kj}}$, the chain rule is applied repeatedly to calculate the contribution for each weight in the network:

$$\frac{\delta E_x}{\delta w_{kj}} = \frac{\delta E_x}{\delta y_k}\frac{\delta y_k}{\delta net_k}\frac{\delta net_k}{\delta w_{kj}} \qquad (6\text{-}9)$$

The backpropagation error to the hidden layer can be calculated easily through partial derivatives and if the error functions equation is submitted into the equation (6-9). The partial derivative of the error function with respect to the output layer weights can be expressed as

$$\frac{\delta E_x}{\delta w_{jk}} = -(t_k - y_k)y_k(1 - y_k)h_j \qquad (6\text{-}10)$$

$$\frac{\delta E_x}{\delta w_{jk}} = \delta y_k h_j \qquad (6\text{-}11)$$

Where,

$$\delta y_k = -(t_k - y_k)y_k(1 - y_k) \qquad (6\text{-}12)$$

Equation (6-12) represents the back propagating error related to the hidden layer.

Change in error due to hidden layer weights: The NN use the same procedure as propagating the error back through the network the weights between the input and the hidden layer are updated. The error pattern of the hidden layer weights when back propagated through to the input layer weights do not have "desired output" as the target for the hidden layer this is in order to correct the error. The partial derivative of the error index of input-to-hidden units to the weight vector using chain rule again can be written as follows:

$$\frac{\delta E_x}{\delta w_{ji}} = \frac{\delta E_x}{\delta h_j}\frac{\delta h_j}{\delta net_j}\frac{\delta net_j}{\delta w_{ji}} \quad (6\text{-}13)$$

The learning rule for the input-to-hidden weights can be written after working on each term explicitly as,

$$\frac{\delta E_x}{\delta w_{ij}} = -\sum_{k=1}^{c}(t_k - y_k)y_k(1-y_k)w_{jk}.h_j(1-h_j).x_i \quad (6\text{-}14)$$

$$\frac{\delta E_x}{\delta w_{ij}} = \delta h_j.x_i \quad (6\text{-}15)$$

Where

$$\delta h_j = -\sum_{k=1}^{c}(t_k - y_k)y_k(1-y_k)w_{jk}.h_j(1-h_j).x_i \quad (6\text{-}16)$$

This equation (6-16) represents the backpropagation of the error from the output layer to the hidden layer.

This algorithm is called backpropagation because during training an error must be propagated from the output layer back to the hidden layer in order to perform the learning of the input-to-hidden weights by equation (6-16). In order to minimise the error, all the weights must be adjusted incrementally in the opposite direction to the error gradient each time a training input/output vector

pair is presented to the network. The weight update equation can be written as follows:

$$\Delta w_{jk}{}^{new} = \Delta w_{jk}{}^{old} - \eta \delta y_k . h_j \qquad (6\text{-}17)$$

$$\Delta w_{ij}{}^{new} = \Delta w_{ij}{}^{old} - \eta \delta h_j . x_i \qquad (6\text{-}18)$$

Where η is the learning rate ($0 < \eta < 1$). The learning rate sets the step size during gradient descent which has a trade-off in value to ensure it is small enough to gain a true convergence but large enough to separate the data space in adequate time (James Griffin 2006).

The problem with the gradient descent algorithm is that it can stop at a local minimum instead of a global minimum.

When the network weights approach a minimum solution, the gradient becomes small and step size reduces, resulting in very slow convergence. In order to prevent this problem, a momentum factor is added to the weights update equations where the weights can be updated with some component of past updates. Adding the momentum factor to the gradient descent learning equations modifies them towards the global set of targets (Duda, Hart et al. 2001).

Gradient descent uses differentiation to tend towards the desired output for training data, if there is no momentum the local minima for the set of data may not be the global minima just the first minima it settles on. With momentum set to 0.9 this is a good compromise and most of the data space is explored giving no/less local minima results (if the problem data space is separable) and more

minimum results towards the global minima and if possible the exact required global minima.

Another algorithm used 'RProp' which stands for 'resilient backpropagation' and is an efficient new learning system that is used to perform a direct adaption of the weight step based on local gradient information. The `trainrp` (see Appendix 5) is a network training function that updates weight and bias values according to the resilient backpropagation algorithm (RProp). The basic principle of RProp is to eliminate the harmful influence of the partial derivative size on the weight step (Riedmiller and Braun 1993). The partial derivatives are already implemented in the normal back-propagation algorithm (see in equation 6-15).

As a consequence, the size of the derivative considered indicates the direction of the weight update. The size of the weight change is exclusively determined by weight specific update values $\Delta_{ij}^{(t)}$.

$$\Delta_{ij}^{(t)} = \begin{cases} -\Delta_{ij}^{(t)}, & \text{if } \frac{\delta E^{(t)}}{\delta w_{ij}} > 0 \\ +\Delta_{ij}^{(t)}, & \text{if } \frac{\delta E^{(t)}}{\delta w_{ij}} < 0 \\ 0, & \text{else} \end{cases} \qquad (6\text{-}19)$$

If the $\Delta_{ij}^{(t)}$ is too big, the algorithm could jump over a local minimum based on the partial derivative of the weight change $\Delta w_{ij}{}^{t}$ which changes sign and so the update value $\Delta_{ij}^{(t)}$ shifts according to the appropriate increase/decrease factor, η. If there is no change in the weights value, the derivative retains its sign and the update value is automatically increased to increase the speed of convergence in shallow regions. The new update value is shown as follows:

$$\Delta_{ij}^{(t)} = \begin{cases} \eta^{+} \cdot \Delta_{ij}^{(t)}, & \text{if } \frac{\delta E^{(t+1)}}{\delta w_{ij}} \cdot \frac{\delta E^{t}}{\delta w_{ij}} > 0 \\ \eta^{-} \cdot \Delta_{ij}^{(t)}, & \text{if } \frac{\delta E^{(t+1)}}{\delta w_{ij}} \cdot \frac{\delta E^{t}}{\delta w_{ij}} < 0 \\ 0, & \text{else} \end{cases} \quad (6\text{-}20)$$

Where: $0 < \eta^{-} < 1 < \eta^{+}$ indicates the decrease and increase factor respectively.

To summarise, the basic principal of 'RProp' is the direct adaptation of the weights update values. It modifies the size of the weight-step directly by introducing the concept of resilient update values. Using 'RProp', the size of the weight step is only dependent on the sequence of signs, not on the magnitude of the derivative. For this reason, learning is equally spread all over the entire network and the weight(s) near the input layer have an equal chance to grow and learn as weights for the output layer (Riedmiller and Braun 1993).

6.3.1 The testing data set

The testing input data set consists of grinding thermal AE data as extracted from the grinding experiment. There was one test set of AE signals consisting of 7 tests at the 0.2 mm depth of cut and other test sets consisting of 7 tests at the 0.02 mm depth of cut. Then, from the start to the end, a total of 30 features for the AE signal were extracted from each test signal. The STFT signal processing technique has been applied to extract the features from the total of 210 AE signals from each test set. The test set in 0.2 mm depth of cuts where thermal AE data and the test set in 0.02 mm depth of cuts of thermal AE data were concatenated together as a matrix format. To signify the features and avoid misclassification in NN presentation, the AE data of testing input are also normalised the same way as training input (see Equation (6-21) and (6-22)).

$$X_{test}(m \times n) = \begin{bmatrix} x_{t11} & x_{t12} & \cdots & x_{t1j} & \cdots & x_{t1n} \\ x_{t21} & x_{t22} & \cdots & x_{t2j} & \cdots & x_{t2n} \\ \cdots & & & & & \\ x_{ti1} & x_{ti2} & \cdots & x_{tij} & \cdots & x_{tin} \\ \cdots & & & & & \\ x_{tm1} & x_{tm2} & \cdots & x_{tmj} & \cdots & x_{tmn} \end{bmatrix} \quad (6\text{-}21)$$

$$T_{test}(m) = [t_{t1} \quad t_{t2} \quad \cdots t_{tj} \quad \cdots \quad t_{tm}] \quad (6\text{-}22)$$

Both X_{test} and T_{test} are presented to the ANN as test input vectors.

The NNs size was based on two hidden layer structures with the input layer having 256 inputs (length of the STFT vector inputs) and the hidden layer having one and half times the input neuron amount (James Griffin 2006). The result for the two hidden layer structures are presented in Table 6-1 however the levels of confidence were very low for a successful monitoring system and therefore more experimentation based on increasing the hidden layers provided best network structure with the six hidden layers producing the most accurate classifier. Various hidden layers with different neurons are investigated to identify the most optimum architecture for the analysis and the performances are presented in Table 6-1.

Table 6-1: Various ANN structure with performances.

ANN Structures	Number of layers	input layer	1st hidden layer	2nd hidden layer	3rd hidden layer	4th hidden layer	5th hidden layer	Output layer	Performance (mse)
1st	3	256	384					256	Bad
2nd	4	256	384	576				256	Bad
3rd	5	256	384	576	864			256	Bad
4th	6	256	384	576	864	1296		256	Bad
5th	7	256	384	576	864	1296	1944	256	**Best**

The following parameters are used based on trial and error as shown in Table 6-2 for training the network.

Table 6-2: Neural network parameters.

The NN Parameters	
Learning rule	Backpropagation
Hidden Layers	6
Input size	STFT: 256 neuron
Transfer function for layer 1-7	Log sigmoid
Transfer function for output layer	pure-linear
Epochs	600
Learning rate	1e-9
Momentum	0.9
Training	STFT:35 different high, medium & low temperatures cases

The training process determines the best set of weight and biases for the given data set of AE data which can be classified according to given target values of 3 associates to high temperatures, 2 associates to medium temperatures and 1 associate to low temperatures. The result is displayed in Figure 6-3, with the straight line relating to the desired results passing through the points of circles. Where the straight line is defined as the predicted output and the points of circles are defined by the actual output. The high temperature must have a value of 3 while the medium temperature must have a value of 2 and the low temperature must have a value of 1 and is defined as the target vector to the network. The result shows after training the output in the following figure is concentrated at the values of 1, 2 or 3 giving 100% trained accurately classified data.

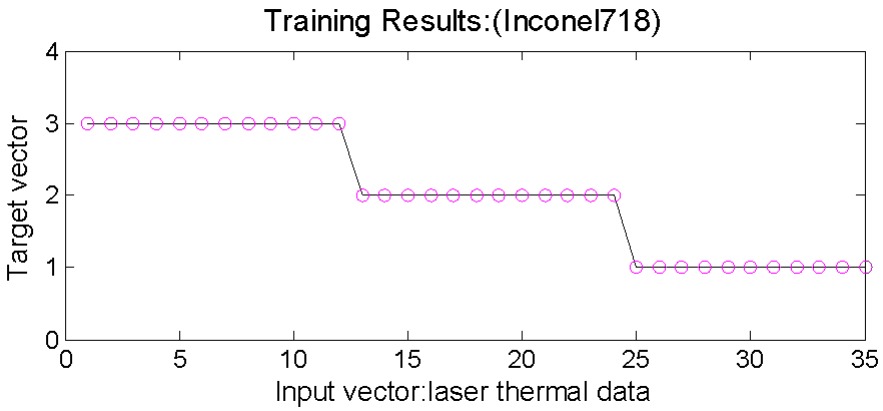

Figure 6-3: The learnt training set for a NN classification system (laser thermal AE data).

The result shows that after training, high temperatures are concentrated at the value 3, medium temperatures at 2 and low temperatures at the value of 1.

6.4 Performance evaluation

6.4.1 NN classification results on Inconel718 material

Once the training is complete, its generalisation performance needs to be evaluated in testing the data (unseen data) to estimate its true performance for the memorised data. X_{test} and T_{test} are 'mn' dimensional matrix for grinding thermal AE data against learnt weights from laser thermal AE data of both P (input data) and T (output data). The testing part will understand whether the testing data obtains a good balance between accuracy and generalization of the network. When the network has been tested then the result displayed by Figure 6-4 can be related to Figure 6-3 where thermal AE data extracted from grinding is used as the testing input. The result should predict burn and no burn phenomena within the grinding zone.

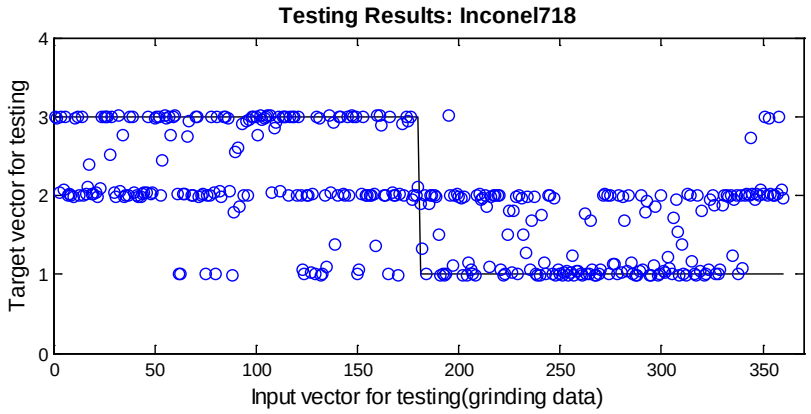

Figure 6-4: The testing output of NN.

In looking at Figure 6-4 it is possible to see high temperature due to severe burn is concentrated at values tending towards 3 and low temperature due to no burn concentrated at values tending towards 1. The result also shows the normal burn between 1 and 3 are concentrated at values around 2. The NN Mean Squared Error (MSE) for the burn and no burn classification was $2.11e^{-32}$ and the number of training epochs was 600. This research gives a confident milestone for the classification between all severe burn, medium burn and no burn in grinding. The results are very encouraging and obtain 65.56% classification accuracy (Inconel718).

6.4.2 NN classification results on MarM002

To validate this research the experiment was carried out on MarM002 materials. The AE data extracted for the 34 mm, 40 mm and 46 mm off-focal distances from laser irradiation is used for training. The neural network has been applied to identify high, medium and low temperatures in relation to grinding burn. During the ANN training process, the STFT AE data were used as inputs and

outputs for high, medium and low temperatures. The structural parameters of the ANN are presented in Table 6-3.

Table 6-3: NN Parameters for MarM002 Experiment.

The NN Parameters	
Learning rule	Backpropagation
Hidden Layer	6
Input size	STFT: 256 neuron
Transfer function for layer 1-7	Log sigmoid
Transfer function for output layer	pure-linear
Epochs	1200
Learning rate	1e-9
Momentum	0.9
Training	STFT:36 different high, medium & low temperatures cases

When the network has been designed and trained by laser thermal AE data, the results, as shown in Figure 6-5, depict a straight line which relates to the passing through of the points of circles where the straight line defined is the predicted output and points circles are defined as the actual output.

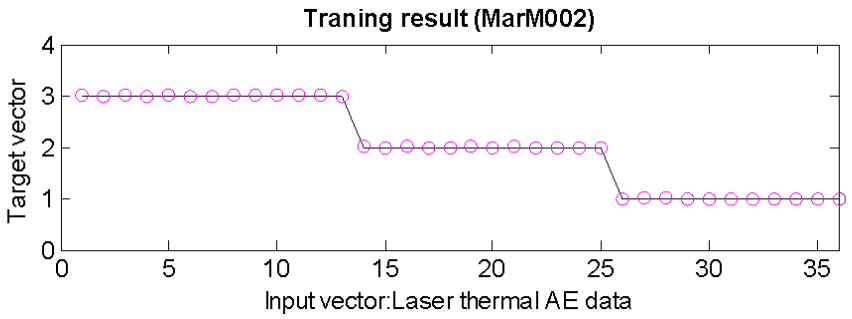

Figure 6-5: The training result of MarM002 using neural network.

When training is completed, the network can be tested with the AE data extracted from the grinding experiment. All feature extraction and pattern recognition methods on MarM002 materials were the same as on Inconel718

materials. The testing AE data consisted of grinding thermal AE data extracted from grinding MarM002 in 0.2 mm and 0.02 mm depth of cuts. The result from testing is displayed in Figure 6-6.

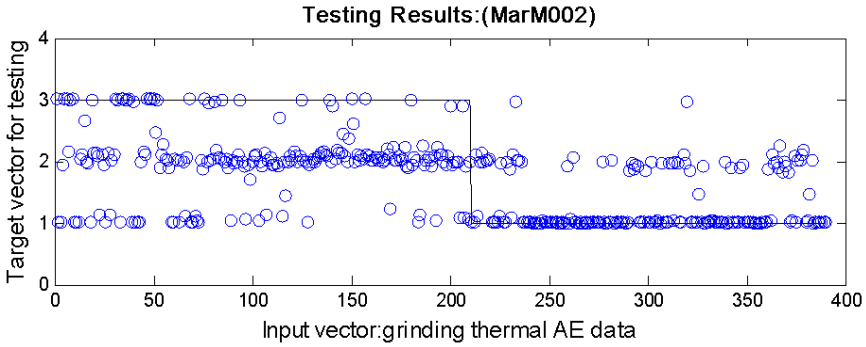

Figure 6-6 : The testing result from NN.

The result should predict severe burn due to high temperatures and no burn due to low temperatures in the grinding zone. The results show that severe burn concentrated at values in 3 and no burn concentrated at values in 1 in a similar fashion to the test results from Inconel718 material. Again, this result was very encouraging with a classification accuracy of 63% for MarM002. The classification accuracy is based on correct classification against misclassification. The value in terms of correct classification obtained from MarM002 is very close to the value obtained from the research on Inconel718 material. Looking at the results of all NN outputs for both materials (Inconel718 and MarM002) a conclusion can be drawn that this research is successful even in terms of validation.

From looking at the test results of MarM002 for the 0.02 mm depth of cut (no burn sample) using Figure 6-6, it is possible to classify high, medium and low grinding temperatures for each and every cut. For instance, 3 is associated with

high temperature, 2 with medium temperature, 1 with low temperature. These results are shown in Table 6-4.

Table 6-4: Classification of burn on MarM002 in 0.02 mm depth of cut.

Material :MarM002	1st cut	2nd cut	3rd cut	4th cut	5th cut	6th cut	7th cut
Depth of cut: 0.02	30 set	30 set	30 set	30 set	30 set	30 set	30 set
ANN output value = 3	0	x	0	0	3.33%	0	0
ANN output value = 2	53.33%	x	10%	10%	40.00%	16.67%	63.33%
ANN output value = 1	46.67%	x	90%	90%	56.67%	83.33%	36.67%

ANN output value: 1 – low temperature; 2 – medium teperature; 3 – high temperature

Grinding on this MarM002 sample in 0.02 mm was carried out in a sequential manner 7 times. The wheel was dressed only once just before being ground. Due to the random nature of grit positions on the wheel surface, the instant grinding temperature in relation to individual grit may vary significantly. Therefore the AE signals in each grinding trial may present different proportions of thermal features that represent different temperatures. Information of this type is particularly useful for grinding wheel wear monitoring. Looking at Table 6-4, it can be seen that 53.33% of the AE data are classified as medium temperature and 46.67% of data are classified as low temperature in the first cut. This proportion of the AE signals i.e 53.33% illustrated as medium temperature features. This may be due to some multi-edge grits that may act in a blunt manner right after wheel dressing. In the 2nd cut AE data was lost during data acquisition due to a computer problem (operator error). After initial wheel wear stage, these grits will dislodge and the wheel surface will become stable as it can be seen in the 3nd and 4th cuts. The newly dressed wheel wears quickly as the sharp edges of the grits are quickly worn away. As grinding continues, the wheel will keep its sharpness because of its self-sharpening ability. The mechanism of self-sharpening ability obviously

reduces grinding zone temperatures and even prevents wheel loading (Jackson, Mills et al. 2003; Liu, Chen et al. 2007). As grinding continues, the attritious wear of the grit tip will be accumulated leading to a higher temperature. In the 5th cut, ANN has classified 40% medium temperature and a minute proportion (3.33%) of very high temperatures. The result revealed that there was increased wheel attritious wear in the 5th cut. In the 6th cut, the grinding temperature decreased which may indicate the grain and bond fracture mechanism leading to self-dressing actions.

In the 7th cut, ANN has classified 63.33% grinding temperatures are at medium level. The grinding temperature in the 7th cut is higher than the previous cuts, which means the rate of wheel wear increased again in this cut. In general, the grinding temperature has a tendency of increase in a wheel redress life cycle as the result of wheel wear.

6.5 Conclusion

This piece of research has successfully demonstrated the use of ANN the AE signal features for grinding temperature based on the pattern classification using laser thermal AE features and provides warning if burn or the onset of burn exists.

The results demonstrated in Figure 6-3 and Figure 6-5 the trained neural network can distinguish between high, medium and low temperatures on Inconel718 and MarM002 materials due to laser irradiation in 34 mm, 40 mm and 46 mm off-focal distances. By using thermal AE data extracted from grinding 0.02 mm and 0.2 mm depth of cuts, the ANN can monitor grinding burn. The classification accuracy achieved with a rate of 66% for Inconel718

and 63% for MarM002. This result confirmed that thermal AE signal signature features in laser irradiation can be used for grinding burn monitoring.

The wheel wear has a large influence on the creation of burn within the workpiece surface. In order to monitor wheel wear, a closer inspection of the sample on MarM002 at 0.02 mm depth of cut was undertaken and the wheel wear mechanisms were studied.

As mentioned previously, the instant grinding temperature in relation to individual grit may vary significantly due to the random nature of grit positions on the wheel surface. The bond fracture results in a rapid loss of the grinding wheel while the grain fracture mechanism results in a comparable scale with the un-cut chip thickness which generates sharp cutting edges and is known as the 'self-dressing action'(Jackson, Mills et al. 2003). The Al_2O_3 has a good self-sharpening ability in nickel based alloys grinding (Chen, Griffin et al. 2007). Therefore the AE signals in each grinding trial may present different proportions of thermal features that represent different temperatures. The result displayed in Table 6-4 confirmed that the AE signal in each grinding trial may present different proportions of thermal features that represent different temperatures. This provides a foundation for a new method that utilises an ANN trained from laser irradiation AE data for the monitoring of grinding burn and wheel wear. This may provide a reliable tool for industrial application.

Chapter 7: Conclusion and Future work

7.1 Conclusion

Thermal damage to the workpiece in nickel based alloys is a significant problem during grinding. Grinding burn occurs from the increased temperature of the abrasive material coming into contact with workpiece material.

The high temperature in the grinding zone produces different levels of thermal damage to the workpiece of nickel based alloy (Inconel718 and MarM002). The levels of thermal damage can be categorised as either severe, normal and slight or no burn. These alloys (Inconel718 and MarM002) are designed to maintain a high level of strength even at very high temperatures and are therefore difficult to grind (Krar and Ratterman 1990).

The direct measurement of the grinding zone temperature is a very difficult task and it is also time consuming because the calibration of the (temperature) models need a large number of trials (in order to gauge the degree of accuracy achieved). This research has explored a new method of monitoring grinding burn using a laser irradiation with an AE sensing technique which provides early warning for grinding burn and wheel wear using AE signal extraction. This method using laser irradiation with an AE sensing technique can be applicable to the grinding process in terms of process monitoring.

The laser irradiation experiments in this research are arranged mainly to simulate high temperatures by changing different off-focal distances on the workpiece materials. A schematic diagram of laser irradiation experiments and

optical arrangements are demonstrated in Figure 3-1 in chapter 3. Using AE and thermocouple sensors, it is possible to detect the thermo elastic wave changes due to laser irradiation on the alloys (Inconel718 and MarM002). The result of calibration temperatures due to laser irradiation on the materials are presented in Table 3-3 in chapter 3. It was noticed during the experimental phase that the variation of surface temperature with lower off focal length is larger than that with longer off-focal length. This could be due to the material property changes at high temperature.

A model of surface temperature due to laser irradiation under high, medium and low temperatures is compared by theoretical and experimental means. The results of surface temperatures of both the calculated and measured values are demonstrated in Figure 5-1 in chapter 5. The surface temperature obtained from the following off-focal distances of 34 mm, 40 mm and 46 mm collated from the laser experimental results were in a reasonable agreement with that obtained from theoretical calculations. The result showed in Figure 5-1 in chapter 5, the measured values of surface temperature differ slightly from the theoretical values of surface temperature. This may be due to thermal conductivity (Steen 2003).

A hierarchical roadmap of common classification of signals is discussed in Figure 4-1 in chapter 4. The AE signals that appear in grinding or laser irradiation are non-stationary stochastic in nature. The signal processing technique STFT is less computationally expensive than other time-frequency analysis techniques, as discussed in chapter 4. In addition, STFT provides a good trade-off in terms of resolution in both frequency and time domains.

For more macro phenomena it is necessary to utilise STFT to distinguish either burn or no burn and therefore this technique is suitable for use in order to distinguish between varying levels of burn for grinding and temperature for laser irradiation.

The research in this thesis uses both STFT and FFT for features extraction from the raw AE signals. The thermal features of extracted AE for Inconel718 under 34 mm off-focal distances are concentrated due to high temperature (698°C) between 190 kHz and 600 kHz frequency bands. The thermal features of MarM002 are concentrated due to the high temperature (493°C) between 273 kHz to 527 kHz frequency band. The thermal expansion due to laser irradiation under high temperatures have a higher intensity than the extracted signals under medium and low temperatures.

AE features at 40 mm off-focal distance produce 324°C temperature (medium), the major features appeared for Inconel718 at 244 to 581 kHz frequency bands and for MarM002 at 239°C gives 229 kHz to 502 kHz frequency bands. The energy in the high frequency region reduces compared to the energy under high temperature.

AE features at 46 mm off-focal distances, the elevation temperature for Inconel718 was 239°C, the major features appeared at 244 to 278 kHz frequency bands. When the elevation temperature for MarM002 was 235°C, the major features appeared at 356 to 420 kHz.

From the above discussions one can conclude that the AE frequency features are shifted to a higher frequency range when temperatures increase.

In order to compare grinding burn with the thermal expansion by laser irradiation, a series of grinding experiments were carried out.

Figure 5-9 and Figure 5-13 in chapter 5 demonstrated that the STFT of AE features relation to grinding burn, where larger depths of cut present high AE amplitude (represents the higher temperature) at a higher frequency range. The result showed in Figure 5-9 under the grinding burn condition in 0.2 mm depth of cut for Inconel718, the major features appeared in the low frequency range at 83 kHz to 249 kHz and in the high frequency range at 596 kHz. In the normal grinding condition under 0.02 mm depth of cut, the major features appeared at 78 kHz frequency band.

In Figure 5-13 in the same chapter for MarM002 in 0.2 mm depth of cut under grinding burn condition, the major features appeared in the low frequency range at 83 kHz to 244 kHz and the high frequency range at 590 kHz. The result presented in the normal burn condition under 0.02 mm depth of cut, the major features appeared at 83 kHz frequency band in the low frequency range (500 < kHz).

From the above discussions about the feature extraction technique(s) one can conclude that thermal induced AE signals in a material have similar features irrespective of heat sources from the laser irradiation or grinding process.

When looking at the classification results, it was possible to further understand the ANN classification after training to distinguish between high, medium and low temperatures on the materials due to laser irradiation through the extracted AE emitted signals. During the ANN training process, the STFT of AE data

from laser irradiation tests were used as inputs with the outputs being high, medium and low temperatures.

The thermal AE data extracted from grinding in different depth of cuts (0.2 mm and 0.02 mm) were used for testing the network (ANN).

The NN result presented in Figure 6-4 in chapter 6 for Inconel718 provides a confidence milestone for the classification of severe burn, normal burn and no burn in grinding. The results of NN on MarM002 are presented in Figure 6-5 to Figure 6-6 in the same chapter. The results showed that the classification accuracy achieved for Inconel718 was 66% while 63% was produced for MarM002 in terms of correct classification. From the above results one can conclude that grinding performance can be monitored by using the thermal AE feature identified from laser irradiation.

The results of this research rely on a hypothesis that the extracted AE signals of laser irradiation are similar to the extracted AE signal in grinding under given conditions. The conditions are elaborated upon in Table 3-2 and Table 3-5 in chapter 3 for both grinding and laser irradiation. The results of this research can assist the manufacturing industry by understanding the AE signal features in relation to grinding performance.

The AE monitoring system provides critical information of grinding zone temperatures to indicate the occurrence of grinding defects. Critical information concerning the grinding zone temperature can help engineers adjust to the grinding conditions to achieve the best coolant delivery and optimal grinding results. The research offers significant benefits to the broad industrial

community and partners who are expected to benefit through the application of knowledge in condition monitoring resulting from this research.

Wheel wear is one of the principal causes of burn on the workpiece surface. The grinding temperatures for the material MarM002 were studied in section 6.4.2 in chapter 6 in order to monitor wheel wear. The instantaneous grinding temperature in relation to individual grit may vary significantly due to the random nature of the grit positions on the wheel surface. The feasibility of using thermal AE features learnt by NN to monitor grinding wheel wear has been demonstrated in Table 6-4 in chapter 6. The results in Table 6-4 show that the AE signal in each grinding trial present different proportions of thermal features that represent different levels of high, medium and low temperature scales. This type of information provides a foundation for a new method that utilises an ANN trained from laser irradiation AE data for the monitoring of grinding burn and wheel wear.

Understanding wheel wear mechanisms can influence the development of new wheel structures which can benefit the wheel manufacturing industry.

7.2 Future work

The problems with the acoustic emission technique of thermal stress are merged with other AE signals of other sources such as mechanical stress and fluidic dynamic stress. The main challenge is how to distinguish these AE signal features from different AE sources, particularly the difference between mechanical stress, thermal stress, fluid dynamic stress and white noise. Future work should look at the identification of the AE signal features induced from different AE sources, particularly the difference between thermal, mechanical

and fluid turbulence stresses. In order to identify the different acoustic emission sources the fluid turbulence and mechanical stresses need to be investigated based on physical experiments with different grinding conditions.

Different grinding conditions can be applied to enable the collection or AE data for setting up a data bank that can provide stress related AE information.

Currently the temperature level is set as three (high, medium and low). If the temperature level is divided further the grinding process can be monitored more precisely.

The coolant supply in high speed grinding plays a more important role than conventional speed grinding (Huang and Yin 2007). Huang and Yin noticed that if the coolant fails to reach the grinding zone sufficiently, thermal damage will result on the workpiece. They assumed that appropriate arrangement of coolant nozzle and optimal supply of coolant flow, in terms of flow speed and rate, could avoid thermal damage. Future work should investigate this based on the nozzle position in relation to the fluid features of AE signals.

A review of more discussions and further references on the applications of wavelet transform for signal processing techniques in machine condition monitoring and fault diagnostics are given (Peng and Chu 2004). Future work should look at using wavelet packet transform (WPT) to process the signal to extract more distinguishing features which STFT or FFT may fail to provide. The limitation of STFT is in time-frequency resolution due to signal segmentation. It can provide good time resolution or good frequency resolution depending on the window function. The STFT can be used to process only non-

stationary signals with slow change in their dynamics compared to the wavelet packet transform.

The neural network has the capability of parallel processing, especially for a large amount of data processing. The backpropagation (bp) neural network has the following limitations:

- difficulty in determining the network structure
- difficulty in determining the number of nodes
- Slow convergence of the training process

Therefore, further investigation is required to select new methods for pattern recognition.

SVM is a statistical learning theory; it is one of the most powerful learning algorithms. It has been reported in the literature that the least square support vector machine (LS-SVM) is a very useful technique compared to neural network making it easy to overcome the problems of the neural network (Vladimir Cherkassky 1998; Suykens and Vandewalle 1999; Xun Chen 2006). The major advantage to LS-SVM is that it has an excellent generalization performance and low computing costs compared to the neural network (Suykens and Vandewalle 1999).

References

Akbari, J., Y. Saito, et al. (1996). "Effect of grinding parameters on acoustic emission signals while grinding ceramics." Journal of Materials Processing Technology **62**(4): 403-407.

Andrade, F. A., I. I. Esat, et al. (1999). "Gearbox Fault detection using statistical methods, time-frequency methods (STFT and Wigner-Ville distribution) and harmonic wavelet - A comparative study." Comadem '99, Proceedings: 77-85.

Baraniuk, R. (2009). Signals and Systems. Florida, University Press of Florida.

Bifano, T. G. and Y. Yi (1992). "Acoustic emission as an indicator of material-removal regime in glass micro-machining." Precision Engineering **14**(4): 219-228.

Black, J. T., E. P. DeGarmo, et al. (2007). DeGarmo's materials and processes in manufacturing. Hoboken, N.J, Wiley.

Brinksmeier, E., C. Heinzel, et al. (1999). "Friction, Cooling and Lubrication in Grinding." CIRP Annals - Manufacturing Technology **48**(2): 581-598.

Capes, P. (2010). "Flexible grinding and no grinding required." from http://www.radical-departures.net/2003/rolls-royce.asp, last visited 14/08/2010.

Chen, X., J. Griffin, et al. (2007). "Mechanical and thermal behaviours of grinding acoustic emission." International Journal of Manufacturing Technology and Management **12**(1-3): 184-199.

Chen, X. and T. Limchimchol (2006). "Monitoring grinding wheel redress-life using support vector machines." International Journal of Automation and Computing **3**(1): 56-62.

Chen, X., W. B. Rowe, et al. (2000). "Analysis of the transitional temperature for tensile residual stress in grinding." Journal of Materials Processing Technology **107**(1-3): 216-221.

Chiu, N. H. and Y. Y. Guao (2008). "State classification of CBN grinding with support vector machine." Journal of Materials Processing Technology **201**(1-3): 601-605.

Choudhury, I. A. and M. A. El-Baradie (1998). "Machinability of nickel-base super alloys: a general review." Journal of Materials Processing Technology **77**(1-3): 278-284.

Cohen, L. (1989). "Time Frequency-Distributions - a Review." Proceedings of the Ieee **77**(7): 941-981.

Cohen, L. (1995). Time-frequency analysis. Englewood Cliffs, N.J Prentice Hall PTR.

Cooley, J. W., P. A. W. Lewis, et al. (1967). "Historical Notes on Fast Fourier Transform." Ieee Transactions on Audio and Electroacoustics **Au15**(2): 76-&.

De Castro, L., F. Von Zuben, et al. (2007). Artificial Immune Systems for Classification of Petroleum Well Drilling Operations. Artificial Immune Systems, Springer Berlin / Heidelberg. **4628:** 47-58.

Demuth, H. B., M. H. Beale, et al. (1994). MATLAB: neural network toolbox, MathWorks, Inc.

Dornfeld, D. and H. G. Cai (1984). "An Investigation of Grinding and Wheel Loading Using Acoustic-Emission." Journal of Engineering for Industry-Transactions of the Asme **106**(1): 28-33.

Dornfeld, D. A. and E. Kannateyasibu (1980). "Acoustic-Emission during Orthogonal Metal-Cutting." International Journal of Mechanical Sciences **22**(5): 285-296.

Duda, R. O., P. E. Hart, et al. (2001). Pattern classification. NewYork, Wiley.

Duhamel, P. and M. Vetterli (1990). "Fast fourier transforms: A tutorial review and a state of the art." Signal Processing **19**(4): 259-299.

Ebbrell, S., N. H. Woolley, et al. (2000). "The effects of cutting fluid application methods on the grinding process." International Journal of Machine Tools & Manufacture **40**(2): 209-223.

Erkki Jantunen, H. J., Robert Milne (1996). Expert System for Automated On-Line Diagnosis of Tool Condition. Integrated Monitoring Diagnostics & Failure Prevention. T. Showcase. Alabama**:** 259–268.

Feng, Z. and X. Chen (2007). "Image processing of grinding wheel surface." International Journal of Advanced Manufacturing Technology **32**(1-2): 27-33.

Fisher, G., P. K. Datta, et al. (1999). "An assessment of the oxidation resistance of an iridium and an iridium/platinum low-activity aluminide/MarM002 system at 1100°C." Surface and Coatings Technology **113**(3): 259-267.

Fu, P., A. D. Hope, et al. (1998). "Tool wear state recognition using a neurofuzzy classification architecture." Insight **40**(8): 544-547.

Ge, P. Q., W. P. Liu, et al. (2002). "Fuzzy clustering analysis of the grinding burn damage level of a workpiece surface layer." Journal of Materials Processing Technology **129**(1-3): 373-376.

Gong, Y. D., H. Li, et al. (2006). "Analysis and Application of Acoustic Emission Signals in Accurate Grinding Machining." KEY ENGINEERING MATERIALS **VOL 315/316**: 868-871.

Govindhasamy, J. J., S. F. McLoone, et al. (2005). "Neural modelling, control and optimisation of an industrial grinding process." Control Engineering Practice **13**(10): 1243-1258.

Griffin, J. (2008). Pattern recognition of micro and macro grinding phenomenon with a generic strategy to machine process monitoring. Department of mechanical, materials and manufacturing. Nottingham, The University of Nottingham. **PhD**.

Griffin, J. M. and X. Chen (2007). "Grinding Acoustic Emission Classification in Terms of Mechanical Behaviours." Key Engineering Materials **329**: 15-20.

Griffin, J. M. and X. Chen (2009). "Multiple classification of the acoustic emission signals extracted during burn and chatter anomalies using genetic programming." International Journal of Advanced Manufacturing Technology **45**(11-12): 1152-1168.

Guo, C. and S. Malkin (1994). "Analytical and Experimental Investigation of Burnout in Creep-Feed Grinding." CIRP Annals - Manufacturing Technology **43**(1): 283-286.

Guo, C., Y. Wu, et al. (1999). "Temperatures and Energy Partition for Grinding with Vitrified CBN Wheels." CIRP Annals - Manufacturing Technology **48**(1): 247-250.

Gviniashvill, V., J. Webster, et al. (2005). "Fluid flow and pressure in the grinding wheel-workpiece interface." Journal of Manufacturing Science and Engineering-Transactions of the Asme **127**(1): 198-205.

H.K. Tonshoff, I. I. (2001). Sensors in Manufacturing. Weinheim ; Chichester, WILEY-VCH Verlag GmbH.

Hassui, A., A. E. Diniz, et al. (1998). "Experimental evaluation on grinding wheel wear through vibration and acoustic emission." Wear **217**(1): 7-14.

Hsueh, Y. W. and C. Y. Yang (2008). "Prediction of tool breakage in face milling using support vector machine." International Journal of Advanced Manufacturing Technology **37**(9-10): 872-880.

Hsueh, Y. W. and C. Y. Yang (2009). "Tool breakage diagnosis in face milling by support vector machine." Journal of Materials Processing Technology **209**(1): 145-152.

Huang, H. and L. Yin (2007). "Grinding characteristics of engineering ceramics in high speed regime." International Journal of Abrasive Technology **1**(1): 78-93.

Hundt, W., D. Leuenberger, et al. (1994). "An Approach to Monitoring of the Grinding Process Using Acoustic Emission (AE) Technique." CIRP Annals - Manufacturing Technology **43**(1): 295-298.

Hwang, T. W., E. P. Whitenton, et al. (2000). "Acoustic emission monitoring of high speed grinding of silicon nitride." Ultrasonics **38**(1-8): 614-619.

Inasaki, I. (1998). "Application of acoustic emission sensor for monitoring machining processes." Ultrasonics **36**(1-5): 273-281.

Inasaki, I. (1999). "Sensor fusion for monitoring and controlling grinding processes." International Journal of Advanced Manufacturing Technology **15**(10): 730-736.

Inasaki, I. and K. Okamura (1985). "Monitoring of Dressing and Grinding Processes with Acoustic Emission Signals." CIRP Annals - Manufacturing Technology **34**(1): 277-280.

Jack, L. B. and A. K. Nandi (2002). "Fault detection using support vector machines and Artificial Neural Networks, augmented by Genetic Algorithms." Mechanical Systems and Signal Processing **16**(2-3): 373-390.

Jackson, M., B. Mills, et al. (2003). "Controlled wear of vitrified abrasive materials for precision grinding applications." Sadhana **28**(5): 897-914.

Jackson, M. J., C. J. Davis, et al. (2001). "High-speed grinding with CBN grinding wheels -- applications and future technology." Journal of Materials Processing Technology **110**(1): 78-88.

James Griffin, X. C. (2006). "Classification of the acoustic emission signals of rubbing, ploughing and cutting during single grit scratch tests." Int. J. Nanomanufacturing **1, No. 2**.

Jardine, A. K. S., D. Lin, et al. (2006). "A review on machinery diagnostics and prognostics implementing condition-based maintenance." Mechanical Systems and Signal Processing **20**(7): 1483-1510.

Jayakumar, T., C. K. Mukhopadhyay, et al. (2005). "A review of the application of acoustic emission techniques for monitoring forming and grinding processes." Journal of Materials Processing Technology **159**(1): 48-61.

Jin, T., W. B. Rowe, et al. (2002). "Temperatures in deep grinding of finite workpieces." International Journal of Machine Tools & Manufacture **42**(1): 53-59.

Jiuhua Xu, Xipeng Xu, et al. (2008). "Monitoring and compensation of thermal error of profile grinding spindle." **Advances in Grinding and Abrasive Technology XIV** 219-223.

Kalpakjian, S., S. R. Schmid, et al. (2009). Manufacturing, Engineering and Technology SI, Pearson Education Canada.

Kim, B. S., S. H. Lee, et al. (2007). "A comparative study on damage detection in speed-up and coast-down process of grinding spindle-typed rotor-bearing system." Journal of Materials Processing Technology **187**: 30-36.

Kim, N. K., C. Guo, et al. (1997). "Heat Flux Distribution and Energy Partition in Creep-Feed Grinding." CIRP Annals - Manufacturing Technology **46**(1): 227-232.

Kiymik, M. K., I. Guler, et al. (2005). "Comparison of STFT and wavelet transform methods in determining epileptic seizure activity in EEG signals for real-time application." Computers in Biology and Medicine **35**(7): 603-616.

Klocke, F., A. Baus, et al. (2000). "Coolant Induced Forces in CBN High Speed Grinding with Shoe Nozzles." CIRP Annals - Manufacturing Technology **49**(1): 241-244.

Krar, S. F. and E. Ratterman (1990). Superabrasives: grinding and machining with CBN and diamond. the University of Michigan, Gregg Division, McGraw-Hill.

Kunnapapdeelert, S. and C. Prakasvudhisarn (2006). "Prediction of surface roughness in CNC endmilling by using support vector machines." ICIM 2006: Proceedings of the Eighth International Conference on Industrial Management: 346-351.

Kurada, S. and C. Bradley (1997). "A machine vision system for tool wear assessment." Tribology International **30**(4): 295-304.

Kuriyagawa, T., K. Syoji, et al. (2003). "Grinding temperature within contact arc between wheel and workpiece in high-efficiency grinding of ultrahard cutting tool materials." Journal of Materials Processing Technology **136**(1-3): 39-47.

Kwak, J.-S. and J.-B. Song (2001). "Trouble diagnosis of the grinding process by using acoustic emission signals." International Journal of Machine Tools and Manufacture **41**(6): 899-913.

Kwak, J. S. and M. K. Ha (2004). "Intelligent diagnostic technique of machining state for grinding." International Journal of Advanced Manufacturing Technology **23**(5-6): 436-443.

Kwak, J. S. and M. K. Ha (2004). "Neural network approach for diagnosis of grinding operation by acoustic emission and power signals." Journal of Materials Processing Technology **147**(1): 65-71.

Kwak, J. S. and J. B. Song (2001). "Trouble diagnosis of the grinding process by using acoustic emission signals." International Journal of Machine Tools & Manufacture **41**(6): 899-913.

L.H.Chiang, E. L. R. a. R. D. B. (2001). Fault detection and diagnosis in industrial systems. London, Springer.

Lachance, S., A. Warkentin, et al. (2003). "Development of an automated system for measuring grinding wheel wear flats." Journal of Manufacturing Systems **22**(2): 130-135.

Lee, D. E., I. Hwang, et al. (2006). "Precision manufacturing process monitoring with acoustic emission." International Journal of Machine Tools & Manufacture **46**(2): 176-188.

Lee, D. E., I. Hwang, et al. (2006). "Precision manufacturing process monitoring with acoustic emission." International Journal of Machine Tools and Manufacture **46**(2): 176-188.

Lezanski, P. (2001). "An intelligent system for grinding wheel condition monitoring." Journal of Materials Processing Technology **109**(3): 258-263.

Liao, T. W., C. F. Ting, et al. (2007). "A wavelet-based methodology for grinding wheel condition monitoring." International Journal of Machine Tools & Manufacture **47**(3-4): 580-592.

Liu, Q. (2005). Pattern Recognition of Grinding Defects and Assessment Strategies of Grinding. Department of Mechanical, Materials, and Manufacturing Engineering. Nottingham, The University of Nottingham.

Liu, Q., X. Chen, et al. (2005). "Fuzzy pattern recognition of AE signals for grinding burn." International Journal of Machine Tools & Manufacture **45**(7-8): 811-818.

Liu, Q., X. Chen, et al. (2006). "Investigation of acoustic emission signals under a simulative environment of grinding burn." International Journal of Machine Tools and Manufacture **46**(3-4): 284-292.

Liu, Q., X. Chen, et al. (2007). "Assessment of Al2O3 and superabrasive wheels in nickel-based alloy grinding." The International Journal of Advanced Manufacturing Technology **33**(9): 940-951.

Majumdar, P., Z. H. Chen, et al. (1995). "Evaporative material removal process with a continuous wave laser." Computers & Structures **57**(4): 663-671.

Malik, M. A. and J. Saniie (1993). Generalized time-frequency representation of ultrasonic signals. Ultrasonics Symposium, 1993. Proceedings., IEEE 1993.

Malkin, S. (1989). Grinding Technology Theory and Application of Machining with Abrasives Dearborn, Michigan, Society of Manufacturing Engineers.

Malkin, S. and C. Guo (2007). "Thermal analysis of grinding." Cirp Annals-Manufacturing Technology **56**(2): 760-782.

Malkin, S. and C. Guo (2008). Grinding technology: theory and applications of machining with abrasives, Industrial Press.

Markou, M. and S. Singh (2003). "Novelty detection: a review--part 2:: neural network based approaches." Signal Processing **83**(12): 2499-2521.

Mayer Jr, J. E., G. Purushothaman, et al. (1999). "Model of Grinding Thermal Damage for Precision Gear Materials." CIRP Annals - Manufacturing Technology **48**(1): 251-254.

McClelland, J. L. and D. E. Rumelhart (1989). Explorations in parallel distributed processing: a handbook of models, programs, and exercises, MIT Press.

Mokbel, A. A. and T. M. A. Maksoud (2000). "Monitoring of the condition of diamond grinding wheels using acoustic emission technique." Journal of Materials Processing Technology **101**(1-3): 292-297.

Morgan, M. N. and W. B. Rowe (2000). "An investigation of temperatures in form grinding." Proceedings of the 33rd International Matador Conference: 433-438.

Moriwaki, T. (2008). Fundamentals: Sensors in Mechanical Manufacturing – Requirements, Demands, Boundary Conditions, Signal Processing, Communication Techniques, and Man-Machine Interfaces, Wiley-VCH Verlag GmbH & Co. KGaA.

Pai, P. S. and P. K. R. Rao (2002). "Acoustic emission analysis for tool wear monitoring in face milling." International Journal of Production Research **40**(5): 1081 - 1093.

Peng, Z. K. and F. L. Chu (2004). "Application of the wavelet transform in machine condition monitoring and fault diagnostics: a review with bibliography." Mechanical Systems and Signal Processing **18**(2): 199-221.

Ramesh Babu, N. and V. Radhakrishnan (1995). "Influence of dressing feed on the performance of laser dressed Al2O3 wheel in wet grinding." International Journal of Machine Tools and Manufacture **35**(5): 661-671.

Rangwala, S. S. and D. A. Dornfeld (1989). "Learning and Optimization of Machining Operations Using Computing Abilities of Neural Networks." Ieee Transactions on Systems Man and Cybernetics **19**(2): 299-314.

Ravindra, H. V., Y. G. Srinivasa, et al. (1997). "Acoustic emission for tool condition monitoring in metal cutting." Wear **212**(1): 78-84.

Riedmiller, M. and H. Braun (1993). Direct adaptive method for faster backpropagation learning: The RPROP algorithm. 1993 IEEE International Conference on Neural Networks.

RollsRoyce. (2007). "Gas Turbine Technology - Introduction to a jet engine." Retrieved 19th of August, 2010, from http://www.rolls-royce.com/Images/gasturbines_tcm92-4977.pdf.

Rowe, W. B. (2001). "Temperature case studies in grinding including an inclined heat source model." Proceedings of the Institution of Mechanical Engineers Part B-Journal of Engineering Manufacture **215**(4): 473-491.

Rowe, W. B. (2009). Grinding Wheel Developments. Principles of Modern Grinding Technology. Boston, William Andrew Publishing**:** 35-58.

Rowe, W. B. and T. Jin (2001). "Temperatures in high efficiency deep grinding (HEDG)." Cirp Annals-Manufacturing Technology **50**(1): 205-208.

Ruhm, K. (2008). "Ruhm, K. H.; Classification of Signal Properties – Survey;." from www.mmm.ethz.ch/dok01/d0000800.pdf.

Schalkoff, R. J. (1992). Pattern recognition: Statistical, Structural and neural approaches. Canada, John Wiley & sons, Inc.

Serope Kalpakjian and S. R. Schmid (2006). Manufacturing Engineering and Technology. Upper Saddle River, NJ 07458.

Shi, D. F. and N. N. Gindy (2007). "Tool wear predictive model based on least squares support vector machines." Mechanical Systems and Signal Processing **21**(4): 1799-1814.

Steen, W. M. (2003). Laser Material processing. London,, Springer-Verlag.

Suykens, J. A. K. and J. Vandewalle (1999). "Least squares support vector machine classifiers." Neural Processing Letters **9**(3): 293-300.

T.Holroyd (2000). The Acoustic Emission & Ultrasonic Monitoring Handbook. Oxford, coxmoor publishing company.

Tawakoli, T., E. Westkamper, et al. (2009). "Effects of vibration-assisted grinding on wear behavior of vitrified bond Al2O3 wheel." Advances in Abrasive Technology Xii **76-78**: 21-26.

Terrell, T. J. and L.-K. Shark (1996). Digital signal processing : a student guide. Basingstoke [etc.], Macmillan Press.

Teti, R., K. Jemielniak, et al. (2010). "Advanced monitoring of machining operations." CIRP Annals - Manufacturing Technology **59**(2): 717-739.

Tönshoff, H. K., T. Friemuth, et al. (2002). "Process Monitoring in Grinding." CIRP Annals - Manufacturing Technology **51**(2): 551-571.

Tonshoff, H. K., M. Jung, et al. (2000). "Using acoustic emission signals for monitoring of production processes." Ultrasonics **37**(10): 681-686.

Tönshoff, H. K., B. Karpuschewski, et al. (1998). "Grinding process achievements and their consequences on machine tools challenges and opportunities." CIRP Annals - Manufacturing Technology **47**(2): 651-668.

Ueda, T., K. Yamada, et al. (2002). "Thermal stress cleaving of brittle materials by laser beam." Cirp Annals-Manufacturing Technology **51**(1): 149-152.

Vladimir Cherkassky, F. M. (1998). Learning from data:concepts, theory, and methods, John Wiely & Sons, INC.

Wang, W. J. and P. D. McFadden (1993). "Early detection of gear failure by vibration analysis i. calculation of the time-frequency distribution." Mechanical Systems and Signal Processing **7**(3): 193-203.

Wang Z, W., P. DeAguiar, et al. (2001). "Neural network detection of grinding burn from acoustic emission." International Journal of Machine Tools & Manufacture **41**(2): 283-309.

Warren Liao, T., C.-F. Ting, et al. (2007). "A wavelet-based methodology for grinding wheel condition monitoring." International Journal of Machine Tools and Manufacture **47**(3-4): 580-592.

Webster, J., I. Marinescu, et al. (1994). "Acoustic Emission for Process Control and Monitoring of Surface Integrity during Grinding." CIRP Annals - Manufacturing Technology **43**(1): 299-304.

Westkämper, E. (1995). "Grinding Assisted by Nd:YAG Lasers." CIRP Annals - Manufacturing Technology **44**(1): 317-320.

Widodo, A. and B.-S. Yang (2007). "Support vector machine in machine condition monitoring and fault diagnosis." Mechanical Systems and Signal Processing **21**(6): 2560-2574.

Winterton, R. H. S. (1999). Heat transfer. Oxford, Oxford University Press.

Xu, X. P. and S. Malkin (2001). "Comparison of methods to measure grinding temperatures." Journal of Manufacturing Science and Engineering-Transactions of the Asme **123**(2): 191-195.

Xun Chen, T. L. (2006). "Monitoring Grinding Wheel Redress-life Using Support Vector Machines." International Journal of Automation and Computing **3**(1): 56-62.

Yerramareddy, S., S. C. Y. Lu, et al. (1993). "Developing Empirical-Models from Observational Data Using Artificial Neural Networks." Journal of Intelligent Manufacturing **4**(1): 33-41.

Zaknich, A. (2003). Neural networks for intelligent signal processing. River Edge, NJ World Scientific.

Zhang, L., L. B. Jack, et al. (2005). "Fault detection using genetic programming." Mechanical Systems and Signal Processing **19**(2): 271-289.

Appendices

Appendix 1:

Material properties:

Property	Inconel718	MarM002	AISIB1112
Composition(WT%)	Mo:3,Cr:19,Ti:0.9,	Cr:9,W:10,Co:10,Al:5.7,Ti:1.5,	C:0.08-0.13,Mn:0.6,
	Nb:5.1,Fe:18.3,Ni:53.7	Ta:2.5,Hf:1.65%,Zr:0.06,C:0.15,	S:0.08-0.13,P:0.04
		B:0.01,bal Ni	
Density (Kg/m3)	8193	8530	7800-8030
Hardness	HRC 50		HB220
Tenislie Strength (MPa)	758-1407	840	HB220
Yield strength(Mpa=N/mm2)	150	760	279-516
Elastic Modules (Gpa)	31		190-210
Elongation in 50mm(%)	21-27	4	32.8
Melting Point (C)	1260-1336	1370-1375	
Possion's Ratio	0.284		0.27-0.3
Thermal Conductivity (W/mK)	11.4~28.7	13	60.5
Specific heat capacity(K/KgK)c	430~700		427.2
Thermal diffusivity (x1e-6mm2/2)	2.01~8.24	21	17.74

Appendix 2:

Kaiser Window: The Kaiser window is a one-parameter family of window functions used for digital signal processing. The Kaiser window has an additional ripple parameter β compared to other fixed windows which enable the designer to trade off the transition and ripple. The figure below illustrates the Kaiser window based on the Kaiser Window function.

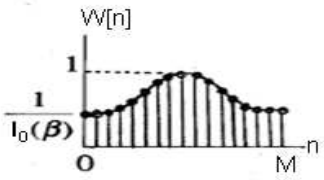

The Kaiser window is defined by the following formula:

$$W_n = \begin{cases} \frac{I_0(\pi\alpha\sqrt{1-\left(\frac{2n}{M}-1\right)^2})}{I_0(\pi\alpha)}, 0 \le n \le M \\ 0, \quad \text{otherwise} \end{cases}$$

Where:

- I_0 is the zeroth order modified Bessel function of the first kind.
- α is an arbitrary real number that determines the shape of the window. In the frequency domain, it determines the trade-off between main-lobe width and side lobe level, which is a central decision in window design.
- M is an integer, and the length of the sequence is $N = M + 1$.
- When N is an odd number, the peak value of the window is $W_{\frac{M}{2}} = 1$ and when N is even, the peak values are $W_{\frac{N}{2}-1} = W_{\frac{N}{2}} < 1$.

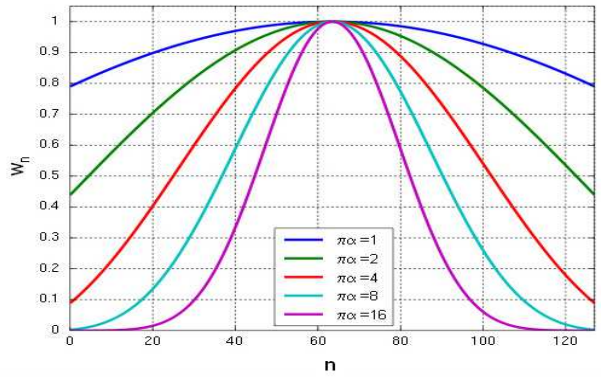

The figure above illustrates the Kaiser Window function for the argument $M = 128$ and $\pi\alpha = \beta$=1, 2, 4, 8, 16.

Appendix 3:

Matlab code: STFT of raw extracted time signal:

% data= laser thermal acoustic emission (AE) data

%or grinding thermal AE data

```
signal= data;

s_stft = specgram(signal,1024,5000000,Kaiser(1024,50),875);

specgram(signal,1024,5000000,Kaiser(1024,50),875);

% S_stft is the short time Fourier transform of the input signal

% Matrix, block size 1024

% Sampling rate 5MHz

%  Kaiser window of length 50 is used;

% Numoverlap = 875=length(window)/2

%P is the number of samples the sections of an overlap.
```

Appendix 4:

prestd pre-processes the network training set by normalizing the inputs and targets so that they have means of zero and standard deviations of 1.

prestd(p,t) takes these inputs,

p - R x Q matrix of input (column) vectors.

t - S x Q matrix of target vectors.

and returns,

pn - R x Q matrix of normalized input vectors.

meanp - R x 1 vector containing standard deviations for each P.

stdp - R x 1 vector containing standard deviations for each P.

tn - S x Q matrix of normalized target vectors.

meant - S x 1 vector containing standard deviations for each T.

stdt - S x 1 vector containing standard deviations for each T.

Appendix 5:

The matlab code for training and testing the neural network:

```
clf reset;
nntwarn off;
pausetime = 0.1;
% Example of training set.
 P_train =laser thermal AE data[];
% Example of target set.
 T_train = [3 3 3 3 3 3 3 3 3 3 2 2 2 2 2 2 2 2 2 2 1 1 1 1 1 1 1 1 1 1];
 % Plot training vector
plot(P_train,T_train,'+');
title('Training Vectors');
xlabel('Input Vector P');
ylabel('Target Vector T');
 %The structure of the neural network
% Set input vector size R, layer sizes from S1 to S7 and batch size Q.
% Initialize weights and biases.
 [R,Q] = size(P_train);
S1=256;
 S2=384; S3=576;
 S4=864; S5=1296; S6=1944; S7= 256;
[S8,Q]= size(T_train);
```

```
 % A feed-forward network is created.
% The trainrp network training function is to be used.
net = newff(minmax(P_train),[S1 S2 S3 S4 S5 S6 S7 S8],{'logsig' 'logsig'
'logsig' 'logsig' 'logsig' 'logsig' 'logsig' 'purelin'},'TRAINRP','learngdm','mse');
net = init(net) ;
% initialise NN with defined parameters
net.trainParam.epochs =600;
% maximum epoch stop condition
net.trainParam.mem_reduc = 2;
% if NN very difficult to train due to complexity
%this function ensures quicker training with approximations
net.trainParam.show = 50;
% display NN output for every 50 iterations
net.trainParam.mc = 0.95;
% Momentum set 0.9-0.95 being least random to ensure bounce
%from local minima
net.trainParam.lr = 1e-9;
% NN learning rate - lower more accurate steps
net.trainParam.goal = 1e-35;
% Mean Squared Error (MSE) goal
net.trainParam.min_grad = 1e-35;
% minimum gradient during learning
net = train(net,P_train,T_train);
[a,b]=size(P_train);
   X = [1:b];
Y = sim(net,P_train);
Y1 = Y;
```

```
figure
plot(X,T_train,X,Y,'o')
title('Traing Results');
xlabel('Input vector from laser thermal data');
ylabel('Target vector for training');

 % test the neural network
P_test=grinding thermal AE data;
 [a,b]=size(P_test);
X = [1:b];
Y = sim(net,P_test);
figure
plot(X,T_test,X,Y,'o')
title('Testing Results');
xlabel('Input vector for testing(grinding data)');
ylabel('Target vector for testing');
```

Appendix 6:

An example of high, medium and low temperatures of raw extracted laser thermal AE signal are presented in this section. Each test sets of high, medium and low temperatures concatenate together to make one training input for the NN system.

An example of laser thermal AE data (34 mm offset)

Test1	Test2	Test3	Test4	Test5	Test6
1.2137	0.9009	-0.838	-0.1404	0.5243	0.2783
1.6211	0.5777	-0.2011	-0.4007	0.0293	0.2454
1.5903	0.1807	0.4184	-0.394	-0.423	0.184
1.2253	-0.2969	0.8161	-0.1953	-0.9262	0.1175
0.7828	-0.817	1.0349	0.0909	-1.3544	0.0354
0.5039	-1.2647	1.1335	0.3397	-1.5491	-0.0824
0.4672	-1.5275	1.1628	0.4019	-1.4988	-0.2203
0.556	-1.5259	1.1289	0.191	-1.3865	-0.3381
0.5319	-1.3083	0.9977	-0.2042	-1.3257	-0.4367
0.1944	-1.026	0.7392	-0.5472	-1.1634	-0.5588
-0.4523	-0.7572	0.3674	-0.6256	-0.6467	-0.7035
-1.1829	-0.4743	-0.0693	-0.3983	0.2954	-0.7675
-1.6929	-0.0781	-0.5225	0.0238	1.4258	-0.6516
-1.7808	0.4636	-0.9558	0.4941	2.3572	-0.3635
-1.431	1.0416	-1.2561	0.9015	2.8898	-0.0198
-0.8118	1.4496	-1.2803	1.1237	2.931	0.2527
-0.1447	1.5439	-0.94	1.0404	2.4528	0.4135

0.5805	1.3105	-0.3653	0.5945	1.5143	0.5057
1.1429	0.8329	0.1566	-0.1123	0.4016	0.575
1.5525	0.2228	0.3793	-0.8466	-0.6787	0.6095
1.7637	-0.4318	0.2963	-1.3434	-1.4563	0.5628
1.7026	-1.0465	0.108	-1.4902	-1.865	0.4273
1.3337	-1.5027	0.0345	-1.3031	-1.9456	0.2673
0.7447	-1.6938	0.1602	-0.9503	-1.8314	0.1758
0.1129	-1.5567	0.4251	-0.5939	-1.6376	0.1907
-0.4328	-1.1744	0.6967	-0.3381	-1.3962	0.2457
-0.8609	-0.7233	0.8316	-0.1947	-1.0825	0.2097
-1.1933	-0.3607	0.7514	-0.1032	-0.6912	0.0107
-1.489	-0.1651	0.4654	0.0162	-0.2832	-0.2762
-1.9684	-0.1071	0.0775	0.2261	0.0528	-0.4862
-1.9214	-0.0552	-0.264	0.5429	0.2872	-0.5121
-1.5119	0.1355	-0.4605	0.9223	0.4334	-0.3836
-0.8307	0.5197	-0.4959	1.2543	0.4846	-0.2106
-0.1358	1.0144	-0.3937	1.4417	0.4004	-0.0739
0.5383	1.4179	-0.1773	1.4222	0.1852	0.0195
1.0254	1.5418	0.097	1.1682	-0.0275	0.09
1.4096	1.3068	0.3076	0.6915	-0.0436	0.1239
1.7063	0.7987	0.318	0.0534	0.2033	0.0845
1.8641	0.217	0.0732	-0.6482	0.5417	-0.0168
1.8345	-0.2792	-0.3604	-1.2714	0.6958	-0.0983
1.6446	-0.6507	-0.8356	-1.7237	0.5231	-0.0748
1.3593	-0.9156	-1.1597	-1.9327	0.1547	0.0613

0.9745	-1.0501	-1.1911	-1.8781	-0.1614	0.2368
0.3821	-0.968	-0.8881	-1.5665	-0.3073	0.3449
-0.5133	-0.604	-0.3583	-1.0327	-0.3952	0.3076
-1.6306	-0.0055	0.1956	-0.3586	-0.6027	0.1267
-2.6728	0.6543	0.5878	0.4498	-0.9311	-0.1068
-3.2395	1.139	0.7459	1.189	-1.1383	-0.2728
-3.1596	1.2961	0.6946	1.7322	-0.9717	-0.3278
-2.4827	1.135	0.5075	1.9944	-0.383	-0.3418
-1.4243	0.784	0.2667	1.9111	0.4251	-0.4114
-0.3604	0.4093	0.0589	1.4356	1.1563	-0.5255
0.5441	0.0925	-0.047	0.6055	1.6059	-0.5475
1.2449	-0.1984	-0.0299	-0.3644	1.7508	-0.3485
1.5534	-0.5573	0.0833	-1.1246	1.6266	0.0504
1.6086	-1.0248	0.2429	-1.3718	1.2613	0.4755
1.5467	-1.5171	0.3916	-1.1115	0.6903	0.7355
1.4945	-1.8711	0.4538	-0.6308	0.0293	0.7553
1.522	-1.9233	0.3571	-0.2036	-0.5658	0.6201
1.6163	-1.6782	0.1038	-0.0061	-0.9439	0.466
1.6828	-1.3001	-0.1926	0.0067	-1.0373	0.3473
1.5592	-0.9891	-0.3787	-0.0711	-0.9055	0.2225
1.0773	-0.7688	-0.3897	-0.1852	-0.6998	0.0659
0.1593	-0.5106	-0.2918	-0.3113	-0.6076	-0.0464
-1.1228	-0.0592	-0.2005	-0.3931	-0.759	-0.0208
-2.5123	0.5988	-0.1648	-0.3232	-1.1158	0.0919
-3.5768	1.2857	-0.1395	-0.0198	-1.4594	0.1041

-3.9848	1.793	-0.0708	0.4633	-1.4896	-0.1059
-3.6167	2.0524	0.0177	0.911	-1.03	-0.4331
-2.512	2.1186	0.0653	1.0569	-0.2274	-0.6226
-0.9232	2.0634	0.0787	0.7965	0.8072	-0.5124
0.622	1.8549	0.137	0.2808	1.6434	-0.1996
1.9065	1.3895	0.2994	-0.1868	2.1683	0.0519
2.6203	0.6018	0.5496	-0.3714	2.3328	0.0513
2.7976	-0.4144	0.8292	-0.2728	2.1207	-0.1752
2.4912	-1.4386	1.0541	-0.0806	1.514	-0.4782
1.8546	-2.1992	1.1225	-0.0024	0.6027	-0.7608
1.1509	-2.483	0.9195	-0.1126	-0.3784	-0.9861
0.5502	-2.2993	0.3745	-0.3211	-1.1496	-1.1066
0.17	-1.8198	-0.4816	-0.4627	-1.5339	-1.0065
-0.0842	-1.2622	-1.4856	-0.4407	-1.5726	-0.5951
-0.4346	-0.7678	-2.4125	-0.2915	-1.4277	0.0882
-1.0169	-0.3009	-2.9902	-0.119	-1.2189	0.8463
-1.7371	0.2484	-3.0689	0.0195	-0.9342	1.4014
-2.3499	0.8136	-2.5791	0.1532	-0.5393	1.5952
-2.6304	1.2683	-1.5476	0.3372	-0.1056	1.4628
-2.5001	1.4978	-0.311	0.5591	0.1941	1.1762
-1.9483	1.4811	0.8493	0.7102	0.2231	0.911
-1.0218	1.2909	1.5754	0.6421	-0.0299	0.7245
0.0436	1.0251	1.7872	0.3153	-0.4386	0.5737
1.1643	0.7517	1.7167	-0.1312	-0.7913	0.4178
1.9245	0.4746	1.6471	-0.4376	-0.8563	0.2533

2.2581	0.1379	1.7124	-0.4398	-0.5481	0.0519
2.2044	-0.3119	1.8003	-0.2512	0.0201	-0.2631
1.8815	-0.8451	1.7029	-0.206	0.6012	-0.7257
1.4487	-1.3108	1.3382	-0.5722	0.9723	-1.2131
1.0508	-1.5735	0.8264	-1.3016	1.0724	-1.5647
0.7425	-1.5806	0.3528	-2.067	0.99	-1.6568
0.4578	-1.4194	-0.0385	-2.4281	0.8875	-1.4841

An example of laser thermal AE data (40 mm offset):

Test11	Test12	Test13	Test14	Test15	Test16
-0.1889	-0.3714	0.8493	0.3388	0.7807	-0.7746
-0.6381	-0.6247	0.3122	0.0577	0.5161	-0.6882
-0.9253	-0.8246	-0.2835	-0.314	0.4929	-0.5765
-0.9946	-0.8429	-0.6952	-0.7474	0.5579	-0.4761
-0.8707	-0.6073	-0.8234	-1.1344	0.4843	-0.4425
-0.6415	-0.1447	-0.7245	-1.3727	0.1865	-0.5762
-0.4114	0.4266	-0.5261	-1.4087	-0.2295	-0.8829
-0.2387	0.9519	-0.351	-1.251	-0.5765	-1.1469
-0.1306	1.2976	-0.2625	-0.9665	-0.7321	-1.0935
-0.0595	1.4069	-0.2081	-0.6195	-0.6806	-0.6293
0.0055	1.2571	-0.0601	-0.2652	-0.4944	0.0781
0.0809	0.8521	0.2441	0.0674	-0.2643	0.766
0.1709	0.2411	0.589	0.3781	-0.0702	1.2311
0.2786	-0.4883	0.7401	0.6796	0.0278	1.4331

0.4053	-1.2076	0.5579	0.9491	0.0079	1.4396
0.5414	-1.7966	0.1685	1.1231	-0.0995	1.3498
0.6552	-2.1113	-0.1184	1.1307	-0.2286	1.2253
0.6915	-2.0423	-0.0735	0.9705	-0.3265	1.0556
0.6037	-1.5598	0.2368	0.7291	-0.3858	0.7685
0.3842	-0.7666	0.5148	0.5194	-0.4254	0.2988
0.0793	0.1157	0.4901	0.379	-0.4535	-0.3339
-0.2213	1.0974	0.1364	0.2527	-0.4541	-0.9824
-0.4291	1.7209	-0.3174	0.0693	-0.405	-1.4237
-0.5017	1.9388	-0.5844	-0.1746	-0.2759	-1.5418
-0.4587	1.7386	-0.5515	-0.4096	-0.0284	-1.3569
-0.365	1.2152	-0.3278	-0.5576	0.3491	-1.0306
-0.2994	0.549	-0.097	-0.5933	0.7981	-0.6769
-0.315	-0.0687	0.0476	-0.5533	1.1786	-0.3467
-0.4031	-0.4975	0.1227	-0.4953	1.3556	-0.0543
-0.4935	-0.6928	0.1566	-0.4566	1.225	0.1862
-0.4999	-0.705	0.1346	-0.4379	0.7477	0.3552
-0.3815	-0.6455	0.0446	-0.4257	0.0122	0.4468
-0.1639	-0.6027	-0.0583	-0.4212	-0.7797	0.4813
0.0897	-0.6055	-0.0848	-0.4431	-1.3379	0.4837
0.3262	-0.5972	-0.0119	-0.4978	-1.5201	0.4489
0.5188	-0.4971	0.0696	-0.549	-1.3334	0.3287
0.6494	-0.2683	0.0262	-0.5237	-0.9464	0.0711
0.6803	0.0436	-0.1831	-0.3589	-0.5173	-0.282
0.5802	0.3354	-0.4477	-0.0534	-0.1196	-0.5524

0.34	0.5206	-0.5835	0.3134	0.1547	-0.5445
-0.0043	0.5902	-0.4886	0.614	0.3076	-0.2478
-0.372	0.6009	-0.2344	0.7327	0.3803	0.1126
-0.6681	0.6052	0.0125	0.6284	0.4431	0.2759
-0.8069	0.5957	0.1569	0.3537	0.5484	0.184
-0.7587	0.5164	0.2451	0.0388	0.6937	0.0204
-0.5655	0.325	0.3714	-0.1624	0.8231	0.0223
-0.3116	0.0378	0.546	-0.1526	0.8811	0.2399
-0.0903	-0.2771	0.6873	0.0537	0.8332	0.4837
0.0455	-0.546	0.7047	0.3458	0.6601	0.524
0.0952	-0.7364	0.596	0.5832	0.3586	0.3378
0.1001	-0.8536	0.4321	0.6687	-0.0674	0.123
0.1154	-0.9326	0.2927	0.5716	-0.5673	0.0681
0.1837	-0.9906	0.199	0.332	-1.037	0.1636
0.3119	-1.0273	0.0821	0.032	-1.3358	0.2597
0.4563	-1.0138	-0.163	-0.2255	-1.384	0.2521
0.5307	-0.9214	-0.5509	-0.354	-1.1985	0.1602
0.4489	-0.727	-0.9189	-0.325	-0.8728	0.0482
0.1807	-0.4254	-1.0074	-0.191	-0.4886	-0.0674
-0.2121	-0.0247	-0.7181	-0.0668	-0.0699	-0.1965
-0.5933	0.4312	-0.2298	-0.076	0.3809	-0.3067
-0.8078	0.8756	0.1526	-0.2832	0.8329	-0.3458
-0.7532	1.2293	0.2521	-0.6568	1.1844	-0.3369
-0.452	1.4643	0.1645	-1.0666	1.3315	-0.3717
-0.0177	1.5781	0.1022	-1.3642	1.2253	-0.4773

0.3861	1.5629	0.1608	-1.4472	0.9153	-0.5435
0.629	1.3721	0.2481	-1.2735	0.5142	-0.4355
0.658	0.9503	0.2271	-0.8884	0.1074	-0.1425
0.4968	0.3061	0.0809	-0.3623	-0.2628	0.2155
0.2182	-0.4672	-0.0717	0.2643	-0.5686	0.4859
-0.0989	-1.1991	-0.0992	0.8817	-0.781	0.5487
-0.3787	-1.7118	0.0122	1.3999	-0.8924	0.3449
-0.553	-1.8738	0.1328	1.728	-0.9549	-0.0772
-0.5628	-1.6581	0.0906	1.8052	-1.015	-0.5313
-0.3858	-1.164	-0.1657	1.6276	-1.044	-0.7813
-0.0742	-0.567	-0.4889	1.2613	-0.9806	-0.687
0.2457	0.0403	-0.6464	0.7901	-0.7953	-0.3146
0.4282	0.5554	-0.5335	0.2875	-0.5155	0.1486
0.3879	0.9482	-0.2795	-0.2219	-0.1944	0.5014
0.1498	1.2214	-0.0937	-0.7007	0.1337	0.6449
-0.1639	1.3678	-0.0558	-1.0691	0.4501	0.607
-0.3934	1.3483	-0.0662	-1.2397	0.7462	0.5158
-0.4212	1.1206	0.0073	-1.1704	0.9952	0.4471
-0.2344	0.6699	0.17	-0.9186	1.1679	0.3696
0.0623	0.0485	0.3079	-0.6229	1.2159	0.2075
0.3012	-0.6369	0.3421	-0.4309	1.1075	-0.0394
0.3476	-1.2302	0.333	-0.4022	0.8704	-0.2777
0.1721	-1.6056	0.4062	-0.4678	0.5902	-0.4239
-0.141	-1.6675	0.6024	-0.4837	0.3385	-0.5045
-0.4447	-1.4139	0.8206	-0.3494	0.1248	-0.6186

-0.6107	-0.954	0.9189	-0.0806	-0.0955	-0.7892
-0.5905	-0.4334	0.8667	0.2216	-0.3742	-0.8798
-0.4175	0.0992	0.719	0.4529	-0.7202	-0.6983
-0.1651	0.4859	0.5133	0.5582	-1.0446	-0.1984
0.0922	0.7303	0.2039	0.5286	-1.222	0.452
0.2933	0.8567	-0.2512	0.3803	-1.1417	0.9983
0.3864	0.9116	-0.7529	0.1465	-0.824	1.2925
0.3409	0.9049	-1.0782	-0.1224	-0.4013	1.381
0.1724	0.8078	-1.1118	-0.3568	-0.0067	1.3611
-0.0458	0.5875	-0.9616	-0.4678	0.2915	1.2397

An example of laser thermal AE data (46 mm offset):

test42	test43	test44	test45	test46	test47
1.0327	0.1712	-0.231	0.3732	-0.2936	0.3211
0.7086	-0.491	-0.6568	1.1994	-1.2803	0.3659
0.3024	-1.0831	-0.8722	1.7756	-2.0408	0.3885
0.1071	-1.4737	-0.8789	2.1198	-2.4073	0.3839
0.2783	-1.6352	-0.7599	2.2489	-2.3414	0.304
0.6922	-1.6208	-0.6006	2.1931	-1.915	0.0696
1.0215	-1.5229	-0.4443	1.9639	-1.2769	-0.3613
0.9885	-1.3916	-0.2832	1.5491	-0.6494	-0.9391
0.5164	-1.2275	-0.0943	0.9604	-0.1334	-1.4957
-0.2609	-0.9723	0.116	0.2478	0.2545	-1.8546
-1.0978	-0.5683	0.2997	-0.5127	0.5316	-1.8564

-1.7338	0.0079	0.3995	-1.2256	0.82	-1.4832
-1.9413	0.6973	0.4099	-1.8189	1.1789	-0.8676
-1.5894	1.3269	0.3897	-2.2147	1.5799	-0.2152
-0.7672	1.6953	0.4178	-2.3542	1.9108	0.4178
0.1926	1.6721	0.5286	-2.2159	2.0356	0.7758
1.1863	1.2766	0.6888	-1.8061	1.8604	0.8457
1.6553	0.6873	0.8182	-1.1823	1.377	0.7144
1.5857	0.1575	0.8371	-0.4798	0.6778	0.5594
1.0334	-0.1267	0.6946	0.2499	-0.0787	0.542
0.1608	-0.1263	0.38	0.911	-0.7682	0.7212
-0.8087	0.0446	-0.0739	1.4023	-1.3361	1.0126
-1.5708	0.195	-0.5765	1.7212	-1.8348	1.2702
-1.8821	0.1627	-1.012	1.8754	-2.2861	1.3553
-1.6193	-0.0992	-1.2833	1.872	-2.6624	1.1908
-0.9577	-0.4984	-1.3599	1.7014	-2.8712	0.7862
-0.235	-0.8741	-1.2714	1.3327	-2.7943	0.2387
0.4099	-1.0849	-1.073	0.7663	-2.3484	-0.3037
0.8362	-1.1054	-0.806	0.0751	-1.5421	-0.697
1.0987	-0.9784	-0.4947	-0.6125	-0.5539	-0.8643
1.2073	-0.7559	-0.1605	-1.1386	0.4456	-0.86
1.0944	-0.4648	0.1617	-1.4145	1.4728	-0.7938
0.7239	-0.1209	0.4273	-1.4493	2.1836	-0.752
0.1999	0.249	0.6037	-1.3059	2.6124	-0.7285
-0.286	0.6073	0.6888	-1.0749	2.7497	-0.6436
-0.5924	0.9119	0.7089	-0.802	2.5904	-0.434

-0.7279	1.1167	0.7031	-0.5304	2.1741	-0.1263
-0.777	1.1695	0.69	-0.3073	1.612	0.1672
-0.766	1.0462	0.6558	-0.1639	0.9381	0.3211
-0.6427	0.7746	0.5634	-0.0781	0.2268	0.2673
-0.3629	0.4392	0.3784	0.0238	-0.5029	0.0183
0.0052	0.1215	0.1117	0.2051	-1.2027	-0.3519
0.3113	-0.1444	-0.177	0.448	-1.8174	-0.7456
0.4584	-0.3974	-0.4117	0.6516	-2.2349	-1.0504
0.4947	-0.7047	-0.5451	0.6986	-2.371	-1.1844
0.5576	-1.0727	-0.5737	0.5524	-2.2001	-1.1106
0.737	-1.438	-0.52	0.2887	-1.7438	-0.8408
0.9824	-1.6858	-0.4154	0.0485	-1.0794	-0.4407
1.1444	-1.713	-0.2994	-0.0497	-0.3394	-0.0012
1.0581	-1.5308	-0.2118	0.015	0.47	0.3903
0.6452	-1.2244	-0.1743	0.1617	1.1936	0.6882
-0.0589	-0.8618	-0.1679	0.2646	1.7377	0.8982
-0.9024	-0.4395	-0.1489	0.2231	2.0493	1.0596
-1.6382	0.0751	-0.0916	0.007	2.0923	1.2052
-2.0737	0.6693	-0.0177	-0.3351	1.8616	1.3242
-2.1195	1.2891	0.0183	-0.6885	1.3794	1.352
-1.8674	1.8476	-0.0247	-0.8884	0.7099	1.2037
-1.4554	2.2303	-0.1352	-0.8292	-0.0467	0.8261
-0.9772	2.313	-0.239	-0.5258	-0.7895	0.2356
-0.4584	2.0029	-0.2283	-0.1199	-1.4118	-0.4657
0.1761	1.3138	-0.0232	0.2045	-1.8647	-1.1252

0.7794	0.4532	0.3668	0.3348	-2.0872	-1.6007
1.2473	-0.3021	0.8304	0.2704	-2.0695	-1.8198
1.5189	-0.7327	1.1844	0.0873	-1.4103	-1.7704
1.6263	-0.8127	1.2915	-0.1199	-0.9174	-1.5101
1.6306	-0.6915	1.1124	-0.2728	-0.4425	-1.1353
1.5336	-0.5499	0.7056	-0.318	-0.0128	-0.7358
1.2748	-0.4865	0.1816	-0.238	0.2786	-0.3543
0.8176	-0.4825	-0.3656	-0.0546	0.4538	0.0235
0.2176	-0.4645	-0.8643	0.181	0.5744	0.4367
-0.4077	-0.394	-1.2336	0.4089	0.7297	0.9153
-0.9528	-0.3006	-1.4405	0.5811	0.9659	1.4209
-1.3465	-0.246	-1.4502	0.6674	1.2433	1.8671
-1.5625	-0.2658	-1.2671	0.6558	1.4411	2.1485
-1.5421	-0.3409	-0.9516	0.5591	1.4362	2.1961
-1.2702	-0.4053	-0.575	0.4065	1.182	1.9886
-0.8484	-0.3949	-0.2142	0.2258	0.727	1.5516
-0.4334	-0.3009	0.0818	0.0305	0.2078	0.9253
-0.1428	-0.1868	0.322	-0.177	-0.2506	0.1514
-0.0226	-0.1355	0.5451	-0.3854	-0.5884	-1.6608
0.04	-0.1715	0.7773	-0.5557	-0.8325	-2.4964
0.1697	-0.235	1.0007	-0.6272	-1.0285	-3.0799
0.3964	-0.2286	1.1631	-0.5518	-1.1841	-3.3317
0.6546	-0.0946	1.2006	-0.3482	-1.243	-3.2368
0.8542	0.1395	1.0617	-0.1019	-1.1341	-2.7915
0.9497	0.3735	0.7178	0.0723	-0.831	-2.0057

0.9369	0.4993	0.1914	0.098	-0.3711	-0.9723
0.8408	0.4633	-0.448	-0.0201	0.1682	0.0922
0.7083	0.2893	-1.088	-0.2057	0.6943	1.2043
0.5872	0.0452	-1.5946	-0.3571	1.1057	2.064
0.488	-0.2054	-1.8519	-0.398	1.3147	2.6261
0.3604	-0.4218	-1.7576	-0.3021	1.2873	2.8556
0.1312	-0.5716	-1.2989	-0.098	1.0385	2.7015
-0.2393	-0.6259	-0.6052	0.1444	0.6427	2.1574
-0.7199	-0.5734	0.1727	0.3354	0.1907	1.3526
-1.2	-0.4395	0.9775	0.3958	-0.2448	0.4257
-1.5781	-0.2533	1.5171	0.285	-0.6265	-0.4474
-1.7768	-0.004	1.7557	0.0232	-0.9433	-1.1551
-1.7795	0.3549	1.6651	-0.307	-1.1808	-1.698

Appendix 7:

An example of grinding thermal features of AE data in 0.2 mm depth of cut is presented (normalised). The thermal features are extracted using STFT from start, middle and end sections of an AE signal of data.

AE example of burn phenomenon (0.2 mm depth cut):

test7/part1	part2	part3	part4	part5	part6
0.0419	0.0408	0.0468	0.0257	0.05	0.0452
0.0379	0.0369	0.0427	0.0239	0.0451	0.0398
0.0276	0.0269	0.0327	0.0196	0.033	0.0266
0.0145	0.0148	0.0221	0.0156	0.0193	0.0126
0.0021	0.0053	0.0147	0.0131	0.0094	0.0034
0.0109	0.0055	0.0109	0.0109	0.0063	0.0024
0.025	0.0105	0.0089	0.0065	0.0104	0.0095
0.0431	0.0176	0.0076	0.0041	0.0208	0.0194
0.0631	0.0267	0.008	0.0145	0.0355	0.0331

0.0783	0.0349	0.0129	0.0238	0.0489	0.0522
0.0807	0.0399	0.0223	0.0267	0.055	0.0738
0.0649	0.0456	0.0366	0.0248	0.0539	0.0882
0.0344	0.0658	0.0566	0.0292	0.0545	0.0834
0.0403	0.1096	0.0844	0.0544	0.0686	0.0541
0.0912	0.1707	0.1214	0.1069	0.1073	0.0066
0.1304	0.2318	0.1635	0.1753	0.1675	0.0442
0.1343	0.2694	0.1973	0.2328	0.2266	0.0822
0.1004	0.2654	0.2052	0.2525	0.2587	0.103
0.0556	0.2198	0.1775	0.2242	0.2531	0.1113
0.048	0.1525	0.1217	0.1593	0.2184	0.1101
0.0609	0.0887	0.0614	0.0833	0.1716	0.0962
0.0631	0.0427	0.0399	0.0254	0.1252	0.0679
0.0539	0.0176	0.0586	0.0304	0.0866	0.0319
0.0387	0.0211	0.0683	0.0426	0.065	0.0085
0.0274	0.0346	0.0651	0.0405	0.0611	0.0299
0.0222	0.0447	0.0548	0.032	0.0585	0.0449
0.016	0.0476	0.0423	0.0234	0.049	0.0481
0.0086	0.0422	0.0307	0.0177	0.0365	0.0391
0.0082	0.0312	0.021	0.0154	0.0264	0.0218
0.0144	0.0201	0.0146	0.0144	0.0197	0.0036
0.0213	0.0155	0.0128	0.0127	0.0157	0.0105
0.0276	0.0194	0.0136	0.0116	0.0154	0.0164
0.0335	0.029	0.0146	0.0153	0.0182	0.0168
0.0388	0.0427	0.0147	0.0232	0.0212	0.0167
0.0415	0.0558	0.0132	0.0304	0.023	0.0187
0.038	0.0623	0.0109	0.0323	0.0235	0.0206
0.0274	0.0588	0.0111	0.0276	0.0228	0.02
0.0135	0.0473	0.0137	0.0186	0.0214	0.0173
0.003	0.0328	0.0154	0.0094	0.0192	0.0137
0.007	0.0199	0.0151	0.0029	0.0165	0.0099
0.0091	0.0092	0.0132	0.0048	0.0128	0.0073
0.0083	0.0009	0.0105	0.0104	0.008	0.0072
0.0061	0.0083	0.0073	0.0158	0.0028	0.0064
0.0035	0.0136	0.0035	0.0188	0.0018	0.0024
0.0031	0.0153	0.0014	0.0178	0.0042	0.0073
0.0047	0.0136	0.0064	0.014	0.0051	0.0155
0.0111	0.0086	0.0127	0.0142	0.0068	0.02
0.0289	0.0009	0.0205	0.0252	0.0111	0.0187
0.0576	0.0127	0.0294	0.0442	0.0171	0.0136
0.0905	0.0265	0.0388	0.0651	0.023	0.0153
0.1149	0.0373	0.0465	0.0799	0.0266	0.0255
0.1195	0.0424	0.049	0.0819	0.0274	0.0342
0.1021	0.0422	0.0444	0.0704	0.0265	0.0372
0.0713	0.0377	0.0343	0.0506	0.0238	0.0339
0.0397	0.0298	0.0234	0.0291	0.0187	0.0254
0.0174	0.0203	0.016	0.011	0.0119	0.0158
0.0158	0.0137	0.0127	0.0069	0.0051	0.0165
0.0238	0.012	0.0111	0.0146	0.0012	0.0237
0.0294	0.0122	0.0097	0.0171	0.0071	0.0267
0.0327	0.0145	0.0082	0.0133	0.0142	0.0245
0.0357	0.0193	0.0075	0.0045	0.0227	0.0204
0.0393	0.0239	0.0095	0.0062	0.0299	0.017

0.0428	0.0261	0.0128	0.0149	0.0326	0.013
0.0446	0.0255	0.0148	0.02	0.0302	0.0105
0.0442	0.0223	0.0151	0.0223	0.0258	0.0161
0.0419	0.0168	0.0137	0.0234	0.0221	0.0245
0.0384	0.0094	0.0106	0.0245	0.0179	0.0316
0.0334	0.0019	0.0061	0.0262	0.0118	0.0376
0.0272	0.0065	0.0027	0.0275	0.0077	0.0431
0.0213	0.0109	0.0066	0.0267	0.0093	0.0476
0.0182	0.0107	0.0113	0.0241	0.0111	0.05
0.0165	0.0065	0.0147	0.0235	0.0116	0.0498
0.0126	0.0078	0.0157	0.0275	0.0121	0.0469
0.0073	0.0161	0.0142	0.0322	0.0124	0.0418
0.0079	0.0229	0.013	0.0337	0.0111	0.0352
0.0115	0.0255	0.0157	0.0317	0.0076	0.0282
0.0118	0.0228	0.0197	0.0278	0.0029	0.022
0.0092	0.015	0.0206	0.023	0.0067	0.017
0.0054	0.0095	0.0173	0.0176	0.0134	0.0122
0.001	0.0194	0.0119	0.0121	0.0177	0.0088
0.0084	0.0297	0.0084	0.008	0.019	0.0135
0.0204	0.0319	0.0104	0.0092	0.0193	0.0246
0.0325	0.0231	0.0141	0.0156	0.0225	0.0372
0.0415	0.0071	0.0155	0.0235	0.0304	0.0476
0.0483	0.0204	0.0135	0.0301	0.0405	0.0522
0.0564	0.04	0.0125	0.0339	0.0474	0.0479
0.0653	0.0531	0.0171	0.0358	0.047	0.0338
0.0713	0.061	0.0218	0.0387	0.0398	0.0138
0.0731	0.0686	0.023	0.0431	0.0291	0.0292
0.0719	0.0783	0.0233	0.0455	0.0202	0.0648
0.0655	0.0867	0.028	0.0432	0.0256	0.0954
0.05	0.0892	0.0381	0.0352	0.0409	0.1085
0.0386	0.0851	0.0501	0.0239	0.0522	0.0988
0.068	0.0771	0.0616	0.0183	0.0539	0.0734
0.1141	0.0661	0.0733	0.0196	0.0471	0.0473
0.1495	0.0503	0.087	0.0166	0.0392	0.031
0.1603	0.0312	0.1028	0.0156	0.0407	0.0257
0.1432	0.0199	0.118	0.0349	0.053	0.031
0.1064	0.026	0.1312	0.0717	0.0708	0.0509
0.0648	0.0356	0.1419	0.1229	0.0926	0.0823
0.0306	0.0491	0.1478	0.1796	0.1198	0.1159
0.0077	0.0683	0.1443	0.2256	0.1506	0.1414
0.0164	0.0832	0.1291	0.2461	0.1768	0.1505
0.0349	0.0835	0.1066	0.2366	0.1875	0.1394
0.0532	0.0693	0.0869	0.2057	0.177	0.1122
0.067	0.0554	0.0763	0.1692	0.1489	0.0826
0.0705	0.0537	0.0717	0.1408	0.1129	0.0683
0.0629	0.0509	0.0687	0.1255	0.0785	0.0693
0.0508	0.038	0.0666	0.1209	0.0521	0.0718
0.0481	0.0186	0.0629	0.1209	0.0411	0.0721
0.0712	0.0082	0.0529	0.1223	0.0526	0.0726
0.1244	0.0366	0.0348	0.129	0.0792	0.0729
0.2042	0.07	0.0158	0.1486	0.1113	0.0705
0.3006	0.0994	0.0396	0.1795	0.141	0.0638
0.393	0.1163	0.0944	0.2137	0.161	0.0506

0.4505	0.117	0.1708	0.2481	0.1693	0.0258
0.4376	0.1078	0.2548	0.284	0.1719	0.0366
0.3273	0.1084	0.3245	0.3311	0.1755	0.1285
0.1291	0.1407	0.3686	0.4112	0.1794	0.2603
0.2067	0.2114	0.3968	0.5299	0.1827	0.4048
0.4859	0.3147	0.4285	0.6599	0.1881	0.5215
0.6902	0.4293	0.4636	0.7606	0.1911	0.5799
0.76	0.5181	0.4752	0.7969	0.1838	0.5771
0.6993	0.5459	0.4399	0.7517	0.1676	0.5338
0.5648	0.502	0.3631	0.6336	0.1486	0.4733
0.4277	0.4074	0.2718	0.4752	0.1266	0.4043
0.3296	0.2981	0.1906	0.3182	0.0995	0.3255
0.2633	0.2023	0.1299	0.1953	0.0711	0.241
0.2053	0.1292	0.0935	0.1198	0.048	0.1652
0.1487	0.0787	0.077	0.0845	0.0338	0.1145
0.0994	0.0562	0.066	0.07	0.028	0.0882
0.0621	0.0593	0.0528	0.0605	0.0268	0.0681
0.0348	0.0658	0.0396	0.0502	0.0267	0.0465
0.0138	0.0651	0.0299	0.0389	0.0257	0.0303
0.0123	0.0573	0.0241	0.0289	0.0235	0.0246
0.0255	0.0448	0.0209	0.0218	0.0213	0.0214
0.0355	0.0312	0.0191	0.0176	0.0198	0.0161
0.0408	0.0199	0.0176	0.0162	0.0188	0.0137
0.0404	0.0126	0.0152	0.0185	0.0173	0.0164
0.0341	0.0084	0.0121	0.0226	0.0147	0.0174
0.0244	0.006	0.0105	0.0246	0.0113	0.0143
0.0175	0.0071	0.0121	0.0225	0.0084	0.0131
0.0197	0.0129	0.0151	0.0172	0.0069	0.0195
0.0267	0.0196	0.0168	0.011	0.0068	0.0256
0.0314	0.0236	0.0158	0.0073	0.0064	0.0261
0.0309	0.0227	0.0125	0.0078	0.005	0.0206
0.0253	0.0174	0.0092	0.009	0.0029	0.0123
0.0176	0.0103	0.0079	0.0097	0.001	0.0069
0.0117	0.004	0.0084	0.0104	0.0012	0.009
0.0094	0.001	0.0099	0.0114	0.001	0.0107
0.0097	0.0027	0.0109	0.0121	0.0007	0.0089
0.0106	0.0026	0.0109	0.0119	0.003	0.0046
0.0108	0.0024	0.0095	0.0105	0.005	0.0051
0.0096	0.0043	0.0073	0.0079	0.0057	0.0098
0.0064	0.0072	0.005	0.0045	0.0049	0.0126
0.0018	0.0101	0.0034	0.0017	0.0043	0.0122
0.0032	0.0123	0.003	0.0034	0.0056	0.0091
0.0066	0.013	0.0037	0.0047	0.0074	0.0041
0.0068	0.012	0.0048	0.0038	0.009	0.0019
0.0037	0.0105	0.0057	0.0015	0.0101	0.0079
0.0026	0.0097	0.0056	0.0029	0.01	0.0126
0.0072	0.0092	0.0044	0.0057	0.0084	0.0147
0.0097	0.0076	0.0027	0.0072	0.0057	0.0136
0.0088	0.0051	0.0012	0.0074	0.0031	0.0101
0.0056	0.0026	0.0006	0.0066	0.0054	0.0057
0.0022	0.0027	0.0011	0.0061	0.0097	0.0023
0.003	0.0048	0.0016	0.0061	0.0128	0.0001
0.0042	0.0069	0.0013	0.0057	0.0134	0.0012

0.0039	0.0083	0.0009	0.0047	0.0114	0.0017
0.0033	0.009	0.0029	0.004	0.0077	0.0022
0.0028	0.0089	0.0057	0.005	0.0045	0.0039
0.0014	0.008	0.0081	0.0071	0.0058	0.0064
0.0017	0.0059	0.0092	0.0087	0.0094	0.0095
0.0053	0.0028	0.0088	0.009	0.0125	0.0132
0.008	0.003	0.0069	0.0079	0.0139	0.0171
0.009	0.0068	0.004	0.0059	0.0132	0.0198
0.0087	0.0098	0.002	0.0037	0.0103	0.0203
0.0082	0.0106	0.0033	0.0021	0.0062	0.0186
0.0083	0.0093	0.0047	0.0023	0.0024	0.0152
0.009	0.0065	0.005	0.0035	0.0014	0.011
0.0101	0.0037	0.0044	0.0048	0.0015	0.0069
0.0115	0.0018	0.0039	0.0062	0.0015	0.0041
0.0131	0.0011	0.0046	0.0077	0.0033	0.0032
0.0146	0.0017	0.0061	0.0092	0.005	0.0045
0.0155	0.0025	0.0077	0.0111	0.0057	0.009
0.0154	0.0034	0.0089	0.0132	0.005	0.0147
0.0144	0.0043	0.0096	0.0147	0.0034	0.0195
0.0131	0.005	0.0099	0.0145	0.0018	0.0219
0.0121	0.0061	0.0104	0.0126	0.001	0.0215
0.0114	0.0084	0.011	0.0096	0.0015	0.0185
0.0104	0.0105	0.011	0.0067	0.0032	0.0134
0.0087	0.0106	0.01	0.0043	0.0047	0.0076
0.0062	0.008	0.0079	0.0024	0.0055	0.0077
0.0038	0.0038	0.005	0.0021	0.0055	0.0139
0.0037	0.0023	0.0029	0.0037	0.0048	0.0194
0.0048	0.0073	0.0025	0.0049	0.0035	0.0225
0.0054	0.012	0.0035	0.005	0.0023	0.0231
0.0056	0.015	0.0057	0.0044	0.0031	0.0218
0.0064	0.0153	0.0076	0.0042	0.0057	0.019
0.0079	0.0138	0.0081	0.0048	0.0082	0.0155
0.0097	0.0121	0.0073	0.0058	0.0098	0.0121
0.011	0.0112	0.0055	0.0064	0.0099	0.0097
0.0112	0.011	0.0034	0.006	0.0084	0.0081
0.0102	0.0103	0.0014	0.0047	0.006	0.007
0.0082	0.0086	0.0007	0.0029	0.0036	0.0063
0.0057	0.0065	0.0018	0.0019	0.0025	0.0058
0.0034	0.0054	0.003	0.003	0.0027	0.005
0.0021	0.0061	0.0045	0.0044	0.0029	0.0039
0.0024	0.0074	0.0059	0.0051	0.003	0.0026
0.0038	0.0085	0.0065	0.0046	0.0033	0.0013
0.0053	0.0095	0.0062	0.0038	0.0042	0.0008
0.0062	0.0102	0.0053	0.0047	0.005	0.0024
0.006	0.0101	0.0044	0.0063	0.0051	0.0039
0.0048	0.0089	0.0042	0.0069	0.0045	0.005
0.0032	0.0067	0.0046	0.0062	0.0034	0.0053
0.0019	0.0045	0.005	0.0045	0.0024	0.0052
0.0017	0.0039	0.005	0.0028	0.0018	0.0047
0.0023	0.0043	0.0046	0.0021	0.0016	0.0038
0.0028	0.0043	0.004	0.0022	0.0014	0.0024
0.003	0.0038	0.0032	0.0021	0.0014	0.0013
0.0028	0.0036	0.0024	0.0017	0.0016	0.0008

0.0025	0.0038	0.0023	0.0018	0.0019	0.0009
0.0022	0.0041	0.0031	0.0026	0.002	0.0015
0.0021	0.0041	0.0039	0.0036	0.0018	0.002
0.0021	0.0039	0.0042	0.0043	0.0014	0.0019
0.0021	0.0036	0.0041	0.0044	0.0008	0.0011
0.002	0.0034	0.0035	0.0037	0.0003	0.0005
0.0017	0.0032	0.0028	0.0023	0.0005	0.0017
0.0012	0.0029	0.0024	0.001	0.001	0.0026
0.0008	0.0024	0.0021	0.0001	0.0014	0.0028
0.0005	0.0016	0.0017	0.0006	0.0017	0.0025
0.0008	0.0009	0.0011	0.0009	0.0019	0.002
0.0012	0.0008	0.0007	0.0008	0.0017	0.0015
0.0015	0.0012	0.0008	0.0007	0.0012	0.0012
0.0016	0.0016	0.0011	0.001	0.0005	0.001
0.0016	0.0018	0.0014	0.0018	0.0014	0.0009
0.0012	0.0021	0.0016	0.0022	0.0026	0.001
0.0008	0.0024	0.0018	0.002	0.0034	0.0015
0.001	0.0026	0.002	0.0014	0.0036	0.002
0.0018	0.0028	0.0022	0.0011	0.0033	0.0023
0.0025	0.0031	0.0023	0.0015	0.0029	0.0024
0.0029	0.0032	0.0023	0.0022	0.0025	0.0027
0.003	0.0029	0.0021	0.0026	0.0023	0.0029
0.0027	0.0021	0.0018	0.0028	0.0021	0.003
0.0023	0.0009	0.0014	0.0028	0.0019	0.0027
0.0019	0.0004	0.001	0.0025	0.0019	0.0027
0.0017	0.0012	0.0006	0.0021	0.0018	0.0035
0.0015	0.0015	0.0006	0.0017	0.0018	0.0042
0.0013	0.0018	0.0008	0.0014	0.0017	0.0041
0.001	0.0023	0.001	0.0014	0.0016	0.0032
0.0006	0.0032	0.0013	0.0015	0.0015	0.0019
0.0006	0.0038	0.0014	0.0015	0.0014	0.0018
0.001	0.0039	0.0015	0.0012	0.0013	0.0025
0.0013	0.0034	0.0013	0.0008	0.0013	0.0027
0.0012	0.0026	0.001	0.0005	0.0014	0.002
0.0009	0.0016	0.0008	0.0004	0.0014	0.001

AE example of no burn phenomenon (0.02 mm depth cut):

Test6_0.02/part1	part2	part3	part4	part5	part6
0.0473	0.04	0.0485	0.0185	0.0491	0.0496
0.0421	0.0369	0.0436	0.0169	0.0444	0.0455
0.0294	0.0292	0.0314	0.0131	0.0327	0.0357
0.0153	0.0203	0.0176	0.0096	0.0194	0.0258
0.0052	0.0123	0.0071	0.0084	0.0097	0.0211
0.0019	0.0053	0.0019	0.0091	0.0062	0.0214
0.0055	0.002	0.0014	0.0101	0.0059	0.0234
0.0108	0.0091	0.0027	0.0111	0.0052	0.0271
0.0151	0.0162	0.005	0.013	0.0046	0.034
0.017	0.0222	0.0065	0.0172	0.0077	0.0432
0.0169	0.0268	0.0056	0.0227	0.0143	0.0505

0.0163	0.0318	0.0091	0.0247	0.0236	0.051
0.0192	0.041	0.0332	0.0171	0.0385	0.0485
0.0339	0.0596	0.0827	0.028	0.0673	0.0658
0.0594	0.0914	0.1604	0.0851	0.1152	0.1094
0.0872	0.1338	0.254	0.1649	0.1747	0.1622
0.1094	0.1754	0.3328	0.2462	0.2258	0.2139
0.1225	0.2001	0.3617	0.3016	0.2472	0.2577
0.1281	0.1977	0.3247	0.3103	0.2304	0.2825
0.1265	0.1702	0.2379	0.2699	0.1837	0.2764
0.1147	0.1295	0.1384	0.1968	0.1254	0.2391
0.0922	0.0897	0.0599	0.1163	0.0739	0.1845
0.064	0.0593	0.0167	0.0499	0.0453	0.1322
0.0383	0.0393	0.0084	0.0163	0.0436	0.095
0.0212	0.0266	0.0088	0.0254	0.047	0.0728
0.0134	0.0178	0.0076	0.0294	0.0432	0.058
0.0114	0.0108	0.0068	0.0252	0.0322	0.046
0.0118	0.0067	0.0055	0.0193	0.0182	0.0362
0.0146	0.0081	0.0042	0.0186	0.0095	0.0288
0.0228	0.013	0.0062	0.0209	0.0123	0.0231
0.0396	0.0209	0.0105	0.02	0.013	0.0181
0.0688	0.0344	0.0156	0.0159	0.0075	0.0181
0.1099	0.0546	0.0213	0.0149	0.0098	0.03
0.1519	0.0781	0.0282	0.021	0.0247	0.0475
0.1773	0.0962	0.0345	0.0277	0.0383	0.0604
0.1748	0.1	0.0362	0.0306	0.0449	0.0608
0.1471	0.0867	0.0314	0.028	0.0423	0.0483
0.1076	0.0624	0.0221	0.0211	0.0326	0.0308
0.0689	0.0371	0.0128	0.0123	0.0209	0.0198
0.038	0.0179	0.0068	0.0038	0.0118	0.0162
0.0188	0.0065	0.0045	0.0042	0.0067	0.0144
0.0154	0.0014	0.0044	0.0107	0.0047	0.0178
0.0168	0.0016	0.0049	0.016	0.0041	0.0237
0.0134	0.0021	0.0057	0.0194	0.0036	0.0259
0.0058	0.0027	0.0069	0.02	0.003	0.0235
0.0056	0.003	0.0086	0.0169	0.0022	0.0195
0.0114	0.0029	0.0106	0.0096	0.0012	0.0188
0.0112	0.003	0.0147	0.003	0.0015	0.021
0.0081	0.0037	0.0226	0.0148	0.0063	0.0226
0.015	0.0064	0.0324	0.0267	0.0141	0.0231
0.0252	0.0117	0.04	0.0358	0.0231	0.0238
0.0306	0.0174	0.041	0.0404	0.0305	0.0242
0.0292	0.0204	0.0343	0.0397	0.0329	0.0226
0.0228	0.019	0.0228	0.0344	0.0298	0.0195
0.0155	0.0139	0.013	0.027	0.0233	0.0173
0.0102	0.0082	0.0122	0.0209	0.0168	0.0168
0.0077	0.0067	0.0146	0.0183	0.0126	0.0164
0.0079	0.0085	0.0146	0.0187	0.0118	0.0151
0.0086	0.009	0.0122	0.0198	0.0133	0.0134
0.0078	0.008	0.0084	0.0198	0.0149	0.0117
0.0053	0.0068	0.0041	0.0183	0.0148	0.0101
0.0054	0.0058	0.0026	0.0166	0.0126	0.0087
0.0079	0.005	0.0061	0.016	0.0089	0.0081
0.0086	0.0048	0.0091	0.0176	0.0058	0.0089

0.0065	0.0046	0.0103	0.0209	0.0044	0.0097
0.0041	0.0038	0.0096	0.0247	0.0031	0.0092
0.0071	0.0028	0.0084	0.0276	0.003	0.0086
0.0115	0.0018	0.0084	0.0286	0.0088	0.0104
0.014	0.0007	0.0086	0.027	0.015	0.0134
0.0142	0.0011	0.0075	0.0226	0.0189	0.0155
0.0119	0.0035	0.0051	0.0161	0.0195	0.0161
0.0082	0.0063	0.0035	0.0096	0.0177	0.0158
0.0056	0.0088	0.0034	0.0047	0.0153	0.0154
0.0074	0.0102	0.0049	0.0021	0.0131	0.0153
0.01	0.0099	0.0091	0.0012	0.0111	0.0153
0.0104	0.0079	0.014	0.0021	0.0095	0.0154
0.0084	0.0049	0.0172	0.0039	0.0115	0.0159
0.0056	0.004	0.018	0.0057	0.0185	0.0167
0.004	0.0083	0.0171	0.0078	0.0265	0.0173
0.004	0.0145	0.0163	0.0111	0.0318	0.0165
0.004	0.0211	0.0164	0.0156	0.0325	0.0131
0.0035	0.0267	0.0164	0.0203	0.0292	0.0073
0.0034	0.03	0.0151	0.0238	0.0243	0.0006
0.0053	0.0307	0.0126	0.026	0.0194	0.0053
0.0077	0.0292	0.0109	0.0277	0.0144	0.0084
0.0101	0.0262	0.0121	0.029	0.0085	0.0103
0.0127	0.0232	0.0159	0.0276	0.0071	0.0154
0.0135	0.0236	0.0212	0.0209	0.0153	0.0252
0.0114	0.0309	0.027	0.0103	0.0237	0.0381
0.012	0.0426	0.0318	0.016	0.027	0.0513
0.0218	0.0535	0.0339	0.0353	0.0228	0.0612
0.0344	0.0597	0.0331	0.0528	0.0184	0.0645
0.0437	0.0596	0.031	0.0608	0.0297	0.0615
0.0457	0.0545	0.0291	0.0555	0.044	0.0583
0.0386	0.0477	0.027	0.04	0.0492	0.0623
0.0245	0.042	0.0238	0.024	0.045	0.07
0.008	0.0357	0.0208	0.0171	0.0371	0.072
0.0062	0.0247	0.0269	0.0205	0.0302	0.0649
0.0157	0.0129	0.0467	0.03	0.0251	0.0549
0.0212	0.0315	0.0725	0.0419	0.0212	0.0535
0.0257	0.0602	0.0956	0.0524	0.0181	0.0605
0.0322	0.0834	0.1081	0.0594	0.0155	0.0632
0.0404	0.093	0.106	0.0619	0.0147	0.0545
0.0465	0.0861	0.0909	0.0585	0.0158	0.037
0.0478	0.0668	0.0694	0.0485	0.0184	0.0249
0.0445	0.0443	0.0477	0.034	0.025	0.0281
0.038	0.0271	0.0301	0.0223	0.0363	0.0296
0.0295	0.0183	0.0196	0.019	0.0486	0.021
0.0204	0.0155	0.0188	0.0155	0.0576	0.0051
0.0158	0.0162	0.0263	0.007	0.061	0.0117
0.0193	0.0197	0.0373	0.0098	0.0593	0.0241
0.0252	0.0256	0.0485	0.0174	0.0545	0.0293
0.0329	0.0333	0.057	0.0187	0.0496	0.0285
0.0441	0.0408	0.062	0.0165	0.0474	0.0259
0.0547	0.0457	0.0655	0.0161	0.0487	0.0269
0.059	0.0473	0.0748	0.0158	0.0497	0.0339
0.0541	0.048	0.0969	0.0161	0.0447	0.0479

0.0414	0.0508	0.1292	0.0228	0.0326	0.071
0.0265	0.056	0.1606	0.029	0.0344	0.1004
0.0199	0.0612	0.1774	0.0271	0.063	0.128
0.0253	0.0637	0.1691	0.0236	0.0909	0.1458
0.0333	0.0623	0.1341	0.0373	0.1018	0.1517
0.041	0.0564	0.0825	0.0555	0.0905	0.1493
0.0478	0.0456	0.0332	0.0614	0.0607	0.1432
0.0527	0.0309	0.0201	0.05	0.0231	0.1353
0.0547	0.015	0.0319	0.0267	0.0208	0.1251
0.0529	0.0044	0.0328	0.0076	0.0438	0.1108
0.0461	0.0116	0.0274	0.0194	0.0518	0.0918
0.0345	0.0174	0.0209	0.0249	0.0467	0.0696
0.0208	0.0193	0.0151	0.0213	0.0366	0.0469
0.0092	0.0177	0.0109	0.0162	0.0283	0.0267
0.0088	0.0137	0.0083	0.0162	0.0227	0.0114
0.0141	0.0085	0.0068	0.0168	0.017	0.0083
0.0165	0.0036	0.006	0.0139	0.0103	0.0133
0.0156	0.003	0.0055	0.0089	0.0036	0.015
0.0124	0.006	0.0044	0.0048	0.0023	0.0136
0.0089	0.0082	0.004	0.0036	0.0074	0.0115
0.0063	0.0092	0.0065	0.0052	0.0119	0.0096
0.0045	0.0091	0.0095	0.008	0.0153	0.0068
0.0029	0.0081	0.0112	0.0096	0.017	0.0031
0.0023	0.0066	0.0112	0.0087	0.0171	0.0038
0.0035	0.0049	0.01	0.0059	0.016	0.0073
0.0042	0.0037	0.0081	0.0045	0.0141	0.0089
0.0036	0.0035	0.0059	0.0067	0.0118	0.0081
0.0021	0.0036	0.0039	0.0085	0.0092	0.0056
0.001	0.003	0.0026	0.0083	0.0071	0.0031
0.0019	0.0017	0.0022	0.0067	0.0058	0.0031
0.0031	0.0017	0.002	0.0052	0.005	0.004
0.0036	0.0033	0.002	0.0047	0.0041	0.0041
0.0031	0.0047	0.0021	0.0047	0.003	0.0035
0.0019	0.0053	0.0024	0.0039	0.0019	0.0027
0.0016	0.005	0.0026	0.0023	0.0015	0.0028
0.0028	0.0041	0.0027	0.0009	0.0017	0.0037
0.004	0.0029	0.0028	0.0012	0.0019	0.0044
0.0054	0.0015	0.0029	0.0022	0.0027	0.0044
0.0073	0.0004	0.003	0.0034	0.0051	0.0035
0.0094	0.0017	0.0031	0.0048	0.0077	0.002
0.0108	0.0031	0.0034	0.0062	0.0093	0.0007
0.0107	0.0039	0.0038	0.0072	0.0093	0.0015
0.0092	0.0038	0.0042	0.0076	0.0082	0.0022
0.0071	0.0027	0.0046	0.0071	0.0072	0.0025
0.0056	0.0011	0.0051	0.0057	0.0069	0.003
0.0051	0.0005	0.0057	0.0035	0.007	0.0036
0.0042	0.0015	0.0063	0.0014	0.0063	0.0039
0.0025	0.0019	0.0068	0.0017	0.0045	0.004
0.0011	0.0019	0.0074	0.0034	0.0026	0.0042
0.0034	0.0018	0.0079	0.0048	0.0026	0.0042
0.0058	0.0017	0.0079	0.0054	0.0035	0.004
0.0071	0.0016	0.0073	0.0053	0.0037	0.0032
0.0071	0.0023	0.006	0.0046	0.0034	0.0017

0.006	0.0038	0.0047	0.0037	0.0038	0.0014
0.0041	0.0051	0.004	0.0025	0.0048	0.0033
0.002	0.0057	0.004	0.0015	0.0058	0.005
0.0009	0.0054	0.0039	0.0018	0.0064	0.0058
0.0023	0.0045	0.0031	0.0022	0.0063	0.0061
0.0032	0.0036	0.0014	0.0016	0.0059	0.0064
0.0032	0.0027	0.0007	0.0007	0.0054	0.0063
0.0025	0.0016	0.0022	0.0009	0.005	0.0059
0.0019	0.0005	0.0026	0.0007	0.0048	0.0049
0.0018	0.0009	0.0024	0.0003	0.0045	0.0037
0.0017	0.0018	0.0026	0.0014	0.0041	0.0025
0.0012	0.0023	0.0034	0.0019	0.0034	0.0015
0.0007	0.0024	0.0045	0.0017	0.0026	0.0016
0.0017	0.0025	0.0058	0.0012	0.0026	0.0022
0.0032	0.0027	0.0068	0.0013	0.0036	0.0028
0.0045	0.0032	0.0073	0.0024	0.0047	0.0033
0.0053	0.0036	0.0069	0.0035	0.0051	0.0038
0.0057	0.0035	0.0056	0.0041	0.005	0.0047
0.0058	0.0027	0.0045	0.0039	0.0046	0.0058
0.0059	0.0014	0.0042	0.0031	0.0042	0.0065
0.0058	0.0006	0.0046	0.0019	0.004	0.0065
0.0051	0.0019	0.0046	0.0012	0.0037	0.0056
0.0037	0.003	0.0042	0.0013	0.0034	0.0041
0.0019	0.0038	0.0034	0.0022	0.003	0.0024
0.0016	0.0041	0.0024	0.0033	0.0029	0.0013
0.0029	0.0041	0.002	0.0034	0.003	0.0016
0.0035	0.004	0.0031	0.0024	0.0032	0.002
0.0031	0.004	0.0045	0.0007	0.0036	0.0017
0.0022	0.004	0.0055	0.0008	0.004	0.0007
0.0021	0.0039	0.0055	0.0014	0.0043	0.0009
0.0025	0.0033	0.0049	0.001	0.0044	0.0027
0.0021	0.0023	0.0039	0.0004	0.0041	0.0041
0.0016	0.0014	0.0028	0.0015	0.0032	0.0047
0.0025	0.0009	0.0018	0.0022	0.0022	0.0045
0.0039	0.0006	0.0008	0.0022	0.0013	0.0039
0.0047	0.0013	0.0002	0.0014	0.0006	0.0035
0.0047	0.0022	0.0007	0.0003	0.0005	0.0033
0.0041	0.0026	0.0009	0.0007	0.001	0.0031
0.0036	0.0023	0.0007	0.0009	0.0015	0.0026
0.0033	0.0017	0.0009	0.0012	0.0017	0.0018
0.0035	0.0011	0.0018	0.0022	0.0016	0.0015
0.0041	0.0009	0.0028	0.0033	0.0015	0.002
0.0045	0.001	0.0035	0.004	0.0015	0.0022
0.0042	0.0012	0.0039	0.0042	0.0016	0.0017
0.0031	0.0011	0.0038	0.004	0.0018	0.0006
0.0017	0.0008	0.0034	0.0035	0.0021	0.0014
0.0009	0.0006	0.0025	0.0028	0.0022	0.0027
0.002	0.001	0.0015	0.0021	0.0023	0.0037
0.0028	0.0016	0.0008	0.0016	0.0022	0.0042
0.003	0.0021	0.001	0.0015	0.0022	0.0043
0.0025	0.0022	0.0012	0.0014	0.0023	0.0041
0.0018	0.002	0.0011	0.0014	0.0024	0.0036
0.0009	0.0016	0.0011	0.0013	0.0023	0.0029

0.0004	0.0012	0.0013	0.001	0.0022	0.002
0.0007	0.0013	0.0015	0.0005	0.0024	0.0012
0.0011	0.0015	0.0014	0.0004	0.0025	0.0007
0.0012	0.0019	0.0012	0.0012	0.0023	0.001
0.0011	0.0021	0.0011	0.0017	0.0018	0.0015
0.0009	0.0022	0.0015	0.0017	0.0012	0.002
0.001	0.0022	0.0017	0.0013	0.0009	0.0023
0.0015	0.0021	0.0016	0.001	0.0013	0.0024
0.0023	0.002	0.0012	0.0013	0.0018	0.002
0.0032	0.002	0.0007	0.0014	0.0022	0.0014
0.0036	0.002	0.0004	0.0012	0.0022	0.0013
0.0034	0.0019	0.0004	0.001	0.002	0.0022
0.0027	0.0018	0.0003	0.0012	0.0015	0.0031
0.0018	0.0017	0.0004	0.0016	0.0008	0.0037
0.001	0.0018	0.0004	0.0017	0.0003	0.0037
0.0007	0.0019	0.0003	0.0013	0.0001	0.0035
0.0011	0.002	0.0002	0.0009	0.0002	0.0032
0.0017	0.002	0.0003	0.001	0.0005	0.0028
0.0021	0.0019	0.0004	0.0011	0.0009	0.0023
0.002	0.0016	0.0005	0.0009	0.0011	0.0017
0.0014	0.0014	0.0004	0.0006	0.0011	0.0011
0.0008	0.0011	0.0004	0.0007	0.0008	0.0011
0.0007	0.0011	0.0005	0.001	0.0005	0.0015
0.0012	0.0013	0.0006	0.0009	0.0004	0.0019
0.0017	0.0016	0.0008	0.0007	0.0003	0.0021
0.0019	0.0017	0.001	0.0003	0.0003	0.0024
0.0015	0.0015	0.0012	0.0001	0.0008	0.0028
0.0007	0.0011	0.0014	0.0004	0.0014	0.0035
0.0009	0.0008	0.0014	0.0006	0.0016	0.004
0.0018	0.0011	0.0013	0.0008	0.0016	0.0043
0.0024	0.0016	0.0013	0.0007	0.0013	0.0044
0.0025	0.0019	0.0012	0.0004	0.0009	0.0043
0.0022	0.002	0.0011	0.0002	0.0004	0.0039